Order Number 1356274

Fluid flow modeling for pneumatically fractured formations

Nautiyal, Deepak, M.S.

New Jersey Institute of Technology, 1994

U·M·I
300 N. Zeeb Rd.
Ann Arbor, MI 48106

ABSTRACT

This thesis investigates the flow of compressible fluids in pneumatically fractured formations. Pneumatic fracturing is a recently developed technique for increasing permeability in geologic formations by the controlled injection of high pressure air. The artificially induced fractures enhance the flow rate of liquids and vapors in the subsurface, and can be applied to in situ remediation of hazardous waste sites, and for other hydrogeological applications.

A flow model for discrete fractures is derived based on the assumptions of viscous, laminar fluid flow through planar fractures (Poiseuille type flow). The model takes into account non-linearity introduced by gas compressibility effects. Provision is also made for turbulent conditions which can result from high flow velocity and/or surface roughness of fractures. The model is presented in both linear and radial flow formats.

Model validation is accomplished by analyzing pressure and flow data from a siltstone formation which had been pneumatically fractured in the vadose zone. Air flows were observed to increase from a baseline of 0.3-0.4 SCFM before fracturing, to 4.0-71 SCFM after fracturing. Using this model, the total equivalent (single) aperture for the 8.4 ft. test zone was found to increase from 86 microns in the prefracture condition, to 516 microns in the postfracture condition. Analysis of fracture flow velocities and associated Reynolds numbers indicated that although laminar flow conditions exist in natural fracture networks, some degree of turbulence may be encountered in pneumatically induced fractures owing to aperture enlargement.

Detailed study of borehole video tapes of the fracture well indicated the principal mechanism of flow enhancement was aperture dilation of existing natural fractures, and improvement of fracture connectivity. A minor amount of new

horizontal and vertical fractures were also noted. Statistical analysis of the video also indicated an improvement in flow uniformity along the borehole profile, as a result of fracturing. A physical model of the fracture zone is presented which is useful for analysis of contaminant mass transport in the formation, especially applications involving molecular diffusion, heat transfer, and biodegradation processes.

FLUID FLOW MODELING
FOR
PNEUMATICALLY FRACTURED FORMATIONS

by
Deepak Nautiyal

A Thesis
Submitted to the Faculty of the Graduate Division of
New Jersey Institute of Technology
in Partial Fulfillment of the Requirements for the Degree of
Master of Science in Environmental Engineering

Department of Civil and Environmental Engineering

January 1994

APPROVAL PAGE

A GIS BASED MULTI-MODAL MULTIPLE OPTIMAL PATH TRANSIT ADVANCED TRAVELER INFORMATION SYSTEM

Nicholas A. Koncz

Dr. Kyriacos Mouskos, Thesis Co-Adviser — Date
Assistant Professor, Civil and Environmental Engineering,
Institute for Transportation, NJIT

Dr. Joshua Greenfeld, Thesis Co-Adviser — Date
Associate Professor, Civil and Environmental Engineering

Dr. Louis J. Pignataro, Committee Member — Date
Distinguished Professor, Transportation Engineering and
Director, Institute for Transportation, NJIT

BIOGRAPHICAL SKETCH

Author: Nicholas A. Koncz

Degree: Master of Science in Transportation

Date: October 1994

Undergraduate and Graduate Education:

- Master of Science in Transportation,
  New Jersey Institute of Technology, Newark, NJ, 1994
- Bachelor of Science in Civil Engineering, Summa Cum Laude
  New Jersey Institute of Technology, Newark, NJ, 1987

Major: Transportation

Professional Positions:

- Design Engineer, Boswell Engineering,
  South Hackensack, NJ, 1987-1993
- Research Assistant, New Jersey Institute of
  Technology, Newark, NJ 1993-1994

This thesis is dedicated
to my parents
Prema and Bishwambhar Datt Nautiyal

ACKNOWLEDGMENT

I wish to express my sincere gratitude to my advisor, Dr. John Schuring. By his valuable help, guidance and patience throughout the writing of this thesis, I have been able to improve my research, technical, analytical and writing skills.

I thank Dr. Paul Chan and Dr. Henry Shaw for serving as members of the committee and for their careful review and helpful suggestions.

I also recognize my colleagues and friends, Tom Boland, Suresh Puppala, Firoz Ahmed, Yuan Ding, Trevor King and Conan Fitzgerald, for their constant cooperation, useful suggestions and encouragement throughout this study.

And finally, I acknowledge my wife and helpmate, Preeti, for her love and patience during the last few months.

TABLE OF CONTENTS

TABLE OF CONTENTS
(Continued)

TABLE OF CONTENTS
(Continued)

LIST OF TABLES

Table **Page**

LIST OF FIGURES

LIST OF FIGURES
(Continued)

LIST OF SYMBOLS

a	= degree of non linearity
b	= fracture aperture (L)
β	= compressibility of fluid
D	= Diameter of tube (L)
e	= exponential power used as b^e
e_{max}	= maximum-error for neglecting Klinkenberg effect
ε	= coefficient to define roughness
g	= acceleration due to gravity (L/T^2)
$i = \frac{dp}{dx}$	= hydraulic gradient (L/L)
k	= intrinsic permeability (L^2)
K'	= turbulent coefficient of hydraulic conductivity
K"	= Poiseuille's function
L	= tube length (L)
m	= mach number to define compressibility of gases
μ	= dynamic viscosity of fluid ($F\text{-}T/L^2$ or $M/L\text{-}T$)
ν	= kinematic viscosity of fluid (L^2/T)
ρ	= unit weight of fluid (F/L^3)
ρ_o	= fluid density at unit pressure
P_e	= pressure at extraction well

LIST OF SYMBOLS
(Continued)

P_o	= hydrostatic pressure
P_w	= pressure at monitoring well
ΔP	= driving pressure differential
Q	= volumetric flow rate (L^3/T)
Q_m	= rate of mass flow (M/T)
R	= radial distance from an extraction well (L)
R_e	= Reynolds number
R_w	= radius of extraction well
t_a	= apparent tensile strength
u	= flow velocity(L/T)
y'	= effective unit wt
ψ	= friction factor
∇^2	= La place operator

CHAPTER 1

INTRODUCTION

1.1 General Information

The remediation of subsurface contamination caused by chemical releases from spills or so-called uncontrolled waste disposal sites is a national priority. Prior to 1980, remedial efforts focused largely on containment of contaminated materials and/or removal and off-site disposal in approved hazardous waste facilities. Ultimately then, containment was typically the solution, and the only reduction in toxic properties of these materials occurred through natural "degradation" processes. Methods for cleaning up hazardous waste sites have changed since 1980 when the Comprehensive Environmental Response, Compensation, and Liability Act (CERCLA), or Superfund, was enacted. Congress has recently enacted legislation that prohibits the land disposal of hazardous wastes unless the United States Environmental Protection Agency (U.S.EPA) determines otherwise [i.e., Hazardous and Solid Waste Amendments (HSWA)] and encourages permanent treatment of contaminated substances [i.e., Superfund Amendment and Reauthorization Act (SARA)].

To date, the Superfund National Priority List (NPL) developed by U.S.EPA contains over 1255 sites, and current estimates for cleanup costs average in excess of $25 million per site. The 1992 Site Remediation Program Status Report, prepared by the New Jersey Department of Environmental Protection and Energy (N.J.DEPE), describes 638 environmentally complex sites being cleaned up under New Jersey's site remediation program. These listings represent only the major sites in the state, and there are numerous other medium and smaller sites that will require remediation or corrective actions as well. Of these sites, most include contamination of the soil and almost all have produced some sort of ground water pollution. Remedial technologies which are both environmentally sound and cost effective are needed. In many cases, in situ treatment of contaminated soils and hazardous waste can affect permanent and significant reductions in the volume, toxicity, and mobility of hazardous substances. Also, the costs which are typically associated with in situ approaches are much lower than the cost associated with ex-situ approaches.

Currently available in situ technologies include vapor extraction, bioremediation, thermal treatment, pump and treat, air sparging, and soil washing. The ability of these technologies to remediate hazardous waste sites is highly dependent on the permeability of the soil and rock underlying the site and the ability to move air and/or water through the contaminated formation. A key problem in New Jersey, particularly in the northern portion, is the relative low permeability of the Brunswick geologic formation, which underlies nine counties in a wide band extending across the northern and central portion of the state (including Bergen, Essex, Huntertown, Hudson, Mercer, Middlesex, Passaic, Somerset, and Union Counties). It is significant that the limits of the Brunswick Formation corresponds closely with New Jersey's principal industrial belt. In addition, geological formations similar to the Brunswick formation exist throughout the United States.

In response to the problem of low permeability formations, a new technology known as pneumatic fracturing (PF) was developed at the Hazardous Substance Management Research Center (HSMRC) at New Jersey Institute of Technology, which can significantly speed up the clean-up of hazardous waste sites, and yet is relatively inexpensive to apply. Pneumatic fracturing can be integrated with a number of other in situ remediation processes to treat difficult sites containing low permeable geologic formations, where available technologies are ineffective and clean-up efforts have become paralyzed. To date, most applications of pneumatic fracturing have focused on enhancement of in situ remediation of contaminated sites, although it may be applied to other uses such as water well enhancement and dewatering.

The pneumatic fracturing process consists of injecting high pressure air or other gas into geologic formations. If the injection is performed at a pressure which exceeds the natural in situ stresses, and at a flow rate which exceeds the permeability of the formation, failure of the geologic medium will result. In rock formations, the principal effect of pneumatic fracturing is dilation and extension of existing discontinuities, thereby increasing fluid conductivity and improving interconnection of existing fractures. Pneumatic fracturing has also been applied to low permeability soil formations to create new fracture networks, which enhance the permeability of the formation.

Pneumatic fracturing is similar in concept to the hydraulic fracturing techniques applied in the petroleum industry and civil engineering for decades (Howard and Fast (1970); and Gidley, et al. (1989)). The principal difference is that pneumatic fracturing uses a gas to create the fractures, while hydraulic fracturing uses water, slurry, or other liquid agent. An advantage of using gas as a fracture injection fluid is its lower viscosity, which reduces friction loss and greatly increases the velocity of fracture propagation. For example, pneumatic fractures obtain their maximum radius in 30 seconds or less in most geologic formations. Also, pneumatic fracturing does not add any liquid to the formation, which may be detrimental when treating contaminated zones above the water table. In fact, many contaminated formations can benefit from the aeration provided by pneumatic injections which enhance sparging, volatilization, and biodegradation.

1.2 Objective and Scope

The efficiency of in situ remediation in the vadose zone is dependent on the amount of air flow which can be developed in the formation. The higher the air flow, the more rapid the contaminants can be removed and/or treated. The time required to remediate a site therefore depends on the flow and mass transport characteristics of the geologic formation.

Experiences from ten major projects performed to date in the vadose zone have shown that pneumatic fracturing consistently increases the air permeability of the formation. This is the result of an artificially created network of fractures which permits a high rate of convective air flow through the fractures.

Prediction of the time required to treat the contaminants within a fractured formation requires a thorough understanding of the air flow characteristics of both the open fracture, and the unfractured porous matrix between fractures. While a number of investigators have analyzed the problem of this dual porosity system, most previous studies have focused on saturated systems. Also, previous studies have addressed natural fractures, and not artificially induced open fractures like those created by pneumatic fracturing, which can differ significantly in their geometry, aperture and other characteristics.

This research study describes the effect of pneumatic fracturing on the flow and mass transport characteristics of a contaminated siltstone formation. The study begins with review of the theory of fluid flow in open planar fractures, which is extended to the present problem. A discrete fracture flow model is then developed taking into account the effects of gas compressibility and turbulence. Next, the model is used to analyze the results of soil gas extraction tests performed at a test site where pneumatic fracturing was applied. By regressive analysis of the flow and the differential pressure data, the effective aperture (or thickness) of the pneumatically induced fractures are determined and mapped throughout the well field. These are compared with borehole video records to examine the enhancement mechanisms, and to develop a physical model of the pneumatically fractured formation.

The objectives of this thesis are therefore to :

(1) Summarize the work of previous investigators studying flow through discrete fractures.

(2) Develop a model defining the relationship between extracted air flow and aperture for open, artificially induced fractures. The compressible nature of air will be considered in the relationship. Turbulence effects will also be included.

(3) Use field test data from a contaminated siltstone formation which was pneumatically fractured to validate the flow relationship.

(4) Establish a physical model of the artificially fractured formation for use in contaminant transport analysis, including an estimate of average fracture aperture and spacing.

CHAPTER 2

BACKGROUND OF PNEUMATIC FRACTURING

2.1 Project History

Initial work on pneumatic fracturing began in the Spring of 1988 at the Hazardous Substance Management Research Center (HSMRC) of the New Jersey Institute of Technology (NJIT). The research started with bench scale investigations of contaminant removal from fractured and unfractured test vats using a vapor extraction process (Papanicolaou, 1989; Shah, 1991). Experiments were performed using three Plexiglas vats filled up with soil containing a surrogate contaminant of known concentration and density . Using vapor extraction as the treatment method, the contaminant removal rates of fractured and unfractured vats were studied. The results of this study conducted on two different test soils consistently indicated that pneumatic fracturing increased contaminant removal rate by 170% to 360%, compared with standard vapor extraction of the unfractured soil.

A second series of experiments investigated the flow characteristics and mass transport rate of a single fracture with known dimensions (Ng, 1991). Experiments were performed using a custom fabricated horizontal infiltrometer. Results from this series of experiments proved that the improved mass flow rate in fractured soils was attributable to enhanced subsurface air-flow rate. In addition, this experiment confirmed that the flow rate through a fracture is proportional to the cube of the aperture (thickness) of the fracture.

The transition of pneumatic fracturing from lab study to field demonstration began in 1989. Since then, the technology has been successfully demonstrated at a number of "clean" and contaminated sites (Schuring, Jurka, and Chan (1991); Pisciotta, et al., (1991); and Schuring, et al., (1992)). These field studies and demonstrations have yielded critical data for evaluating various theoretical aspects of pneumatic fracturing, and have also provided a feedback for continual improvements in the equipment systems.

In July 1991, the technology received a U.S. Patent, and in August 1992 it was evaluated by U.S. Environmental Protection Agency (EPA) under its Superfund Innovative Technology Evaluation (SITE) program. The first commercial version of the pneumatic fracturing technology was built by Accutech Remedial Systems (ARS) of Keyport, New Jersey, in Spring 1993.

Current major ongoing activities are demonstration of the pneumatic fracturing technology integrated with bioremediation under the U.S. EPA Emerging Technologies SITE Program at a petroleum refinery in Pennsylvania, and also a demonstration of pneumatic fracturing for the U.S. Department of Energy (DOE) at a Superfund site in Oklahoma.

Future research emphasis of the pneumatic fracturing group will be investigation of various aspects of pneumatic fracturing process related to enhancement of other remediation technologies, and also investigation of the theoretical aspects of pneumatic fracturing including development of models to predict fracture propagation and dimensions (length and aperture), as well as contaminant removal rates from various geologic formations and subsurface conditions.

2.2 Methodology of Pneumatic Fracturing

The pneumatic fracturing process consists of injecting high pressure air or any other gas into a geologic formation at a pressure which exceeds the natural in situ stresses of the formation, and at a flow rate which exceeds the permeability of the formation. This causes failure of the medium and creates a network of fractures radiating outwards from the injection point. The fracture network increases the flow rate of vapors or liquids through the formation, and makes the contaminants more accessible for removal and/or treatment. Fig. 1 shows a schematic of the pneumatic fracturing system.

The first step in applying the technology consists of drilling boreholes to predetermined depths in the contaminated area of the site. The location of the boreholes is determined by investigating the hydrogeology of the site, as well as the distribution of the contaminant.

Next, a patented device known as an "HQ injector" is lowered into the fracture borehole to a predetermined elevation, and then the seals of the HQ injector are inflated using compressed nitrogen gas. The HQ injector isolates an approximate two feet section of the borehole for each injection.

The HQ injector is next connected to the source of pressurized air through a system of hoses and a high pressure injection manifold. A fracture injection is then made for a short duration which is usually 30 seconds or less. The pressures and flows during injection are controlled through a system of precision switches, ball valves, and regulators.

The actual process of pneumatic fracturing is relatively rapid, and good field productivity is achievable. A typical single pneumatic injection cycle takes between 10 and 15 minutes, depending on the time to move the injector vertically within the same hole, and horizontally from hole to hole. A production rate of 15 to 20 fractures per day is considered attainable with one rig.

The response of geologic formations to pneumatic fracturing and the potential benefits depend on the nature and composition of the deposit. In fine-grained soils, which normally have low permeability values, pneumatic injections create conductive channels which increase the permeability and expose additional surface area in the formation (see Fig. 2a). For coarse grained soils, the process provides a means for rapidly aerating the formation (see Fig. 2b). For sedimentary rocks, such as shale and

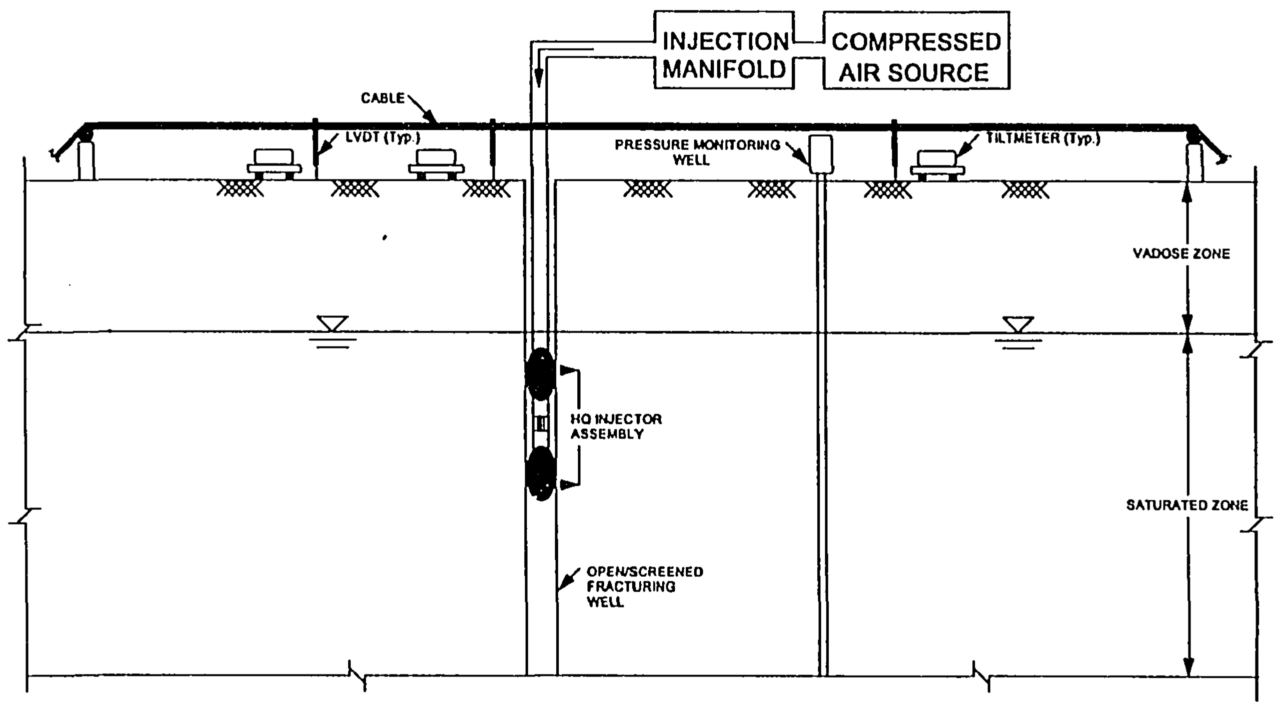

Figure 1 Schematic of pneumatic fracturing

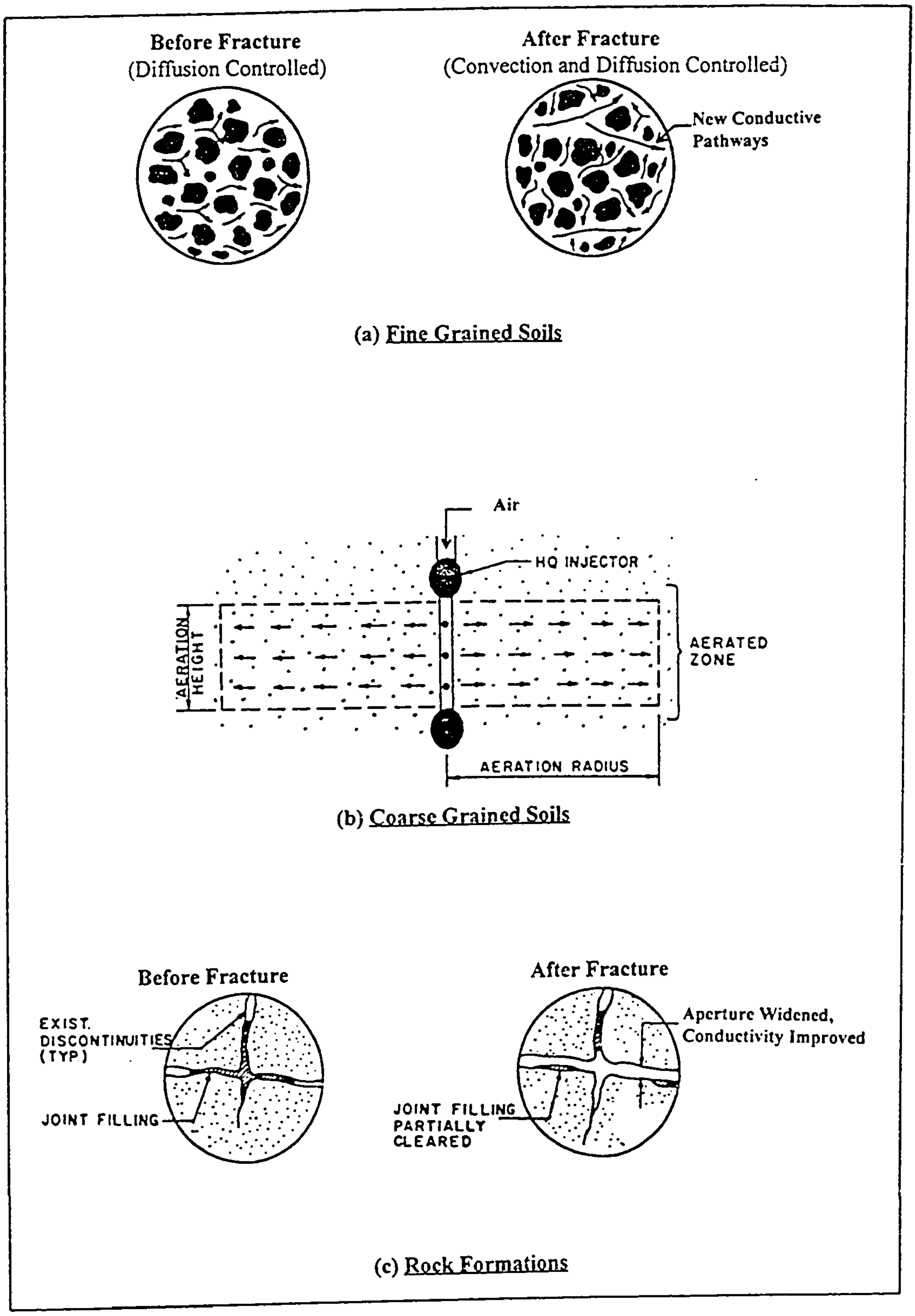

Figure 2 Effect of pneumatic fracturing on geologic micro structure.

sandstone, the process can enhance the permeability of the formation by widening the apertures of the existing discontinuities and/ improving their interconnectivity (see Fig. 2c). It may also create a minor amount of new fractures in rock formations. Pneumatic fracturing is also being used to inject supplements (e.g. nutrients, buffers, innoculum) into formations to enhance in situ bioremediation.

The actual reduction in remediation time using pneumatic fracturing will be dependent on the amount of permeability enhancement observed after fracturing, which is typically in the range of 10 to 100 times for fine grained soils. The actual proportion of time saved will also depend on the time required for diffusion of contaminants from the unfractured media between the fractures. As a result, the overall time saved by pneumatic fracturing will not be as dramatic as the increase in formation permeability, but the remediation time will nevertheless be reduced.

Since pneumatic fracturing is a new and currently developing technology, the theory of pneumatic fracturing is presently under development using the principles of soil mechanics, rock mechanics, fluid mechanics, and hydrogeology. By combining the results of various lab experiments and field demonstrations with the ongoing analytical studies, a firm theoretical understanding of pneumatic fracturing is emerging. The following is a brief overview of two main theoretical considerations: (1) mechanics of pneumatic fracturing; and (2) fractured media flow and mass transport.

2.3 General Theoretical Considerations of Pneumatic Fracturing

2.3.1 Mechanics of Pneumatic Fracturing

Pneumatic fractures can be generated in geologic formations if air or any other gas is injected at a pressure which exceeds the natural strength, as well as the in situ stresses present in the formation. It must also be injected at a flow rate that exceeds the natural permeability of the formation so that sufficient "back" pressure can be developed. Pneumatic fractures will tend to propagate in the direction normal to the least principal stress in the formation in accordance with the findings of Hubbert and Willis (1956) in their study of hydraulic fracturing. It follows that in overconsolidated formations where the least principal stress is vertical, fractures will tend to propagate horizontally. Conversely, in normally consolidated or underconsolidated formations, fractures will tend to propagate vertically. Since most contaminated sites have overconsolidated formations due to past geologic events (e.g. overburden stress relief, desiccation, tectonic forces), it is expected that pneumatic fracture propagation will be predominantly horizontal. In stratified formations, which has natural weakness along the bedding planes, the tendency towards horizontal fracture patterns is even more accentuated.

Field observations are generally consistent with these theoretical considerations, since pneumatic fracture propagation has been predominantly horizontal. However, in shallow recent fills, some upward inclination of the fractures has been observed the reason for which is attributed to the lack of stratification and consolidation in these formations.

The amount of pressure required to initiate pneumatic fractures is dependent on the cohesive or tensile strength of the formation, as well as the overburden pressure (depth and density of the formation). An expression for predicting pneumatic fracture initiation pressure has been developed (King, 1993) by assuming the geologic material to be brittle, elastic, and overconsolidated. Assuming the formation has an effective unit weight, γ', and an apparent tensile strength, t_a, the fracture initiation pressure, P_i may be estimated by :

$$P_i = C\gamma' z + t_a + P_o \tag{2.1}$$

where C is a coefficient (ranging from 2.0 to 2.5), z is the overburden depth and P_o is the hydrostatic pressure. Substituting typical values for clay soil and shale bedrock at a depth of 20 ft, the above expression yields initiation pressures of 50 psi and 150 psi respectively. Fracture initiation pressures are therefore relatively modest at shallow depths (where most of the contamination occurs).

The most important system parameter for efficient pneumatic fracturing is injection flow rate, as it largely determines the dimensions of a pneumatic fracture. Once a fracture has been initiated, it is the high volume air flow which propagates the fracture and supports the formation. The design goal of a pneumatic fracturing system therefore becomes one of providing the highest possible flowrate. Field observations indicate that pneumatic fractures reach their maximum dimension in less than 20 seconds, after which continued injection simply maintains the fracture network in a dilated state (in essence, the formation is "floating" on a cushion of injected air). Apparently, pneumatically induced fractures continue to propagate until they intersect a sufficient number of pores and existing discontinuities, so that fluid loss rate (leak-off) into the formation exactly equals the injection flow rate. In general, injection rates of 1000 to 2000 SCFM are sufficient to create satisfactory fracture networks in low permeability formations. To date, the radii of pneumatic fractures have ranged from 10 to 25+ feet from the injection point.

2.3.2 Fractured Media Flow and Transport

In a pneumatically fractured formation, the ability to treat and/or remove contaminants depends on the flow and transport characteristics of the fractured medium. The open, self-propped fractures resulting from pneumatic fracturing process are capable of transmitting significant amounts of fluid flow. An approach for investigating the flow potential of individual fractures is the "parallel plate analogy" (e.g., Harr, 1962 and Ziegler, 1976). Using this approach, the functional relationship between flow, Q, and fracture aperture or thickness, b, can be represented by

$$Q \propto b^3 \tag{2.2}$$

This relationship is known as "cubic law". It emphasizes the high flow potential for even small fractures, since flow rate is proportional to the cube of the aperture. This accounts for the significant permeability increases which have been observed in pneumatically fractured formations.

Once a fracture network is established in a low permeability formation, aqueous and residual products in the vicinity of the fracture are more easily accessed, and in the case of vapor extraction, they are removed rapidly through volatilization. Due to the heterogeneity's present in all geologic formations, it is expected that fracture distribution will not be uniform and unfractured matrix blocks will remain between adjacent fractures. These unfractured matrix blocks will contain residual and adsorbed contaminant which can only be removed by the process of diffusion. Since diffusive distances are shortened by the creation of fractures by pneumatic fracturing, contaminant removal will occur faster compared with an unfractured formation. Contaminant transport out of the matrix blocks will continue as long as air flow is maintained through the fracture network, and the vapor concentrations at the fracture/matrix interface are kept low enough to cause outward diffusive gradients. The spacing of the pneumatically induced fractures within a fracture interval will vary according to the geology, but a fracture spacing of one foot can usually be achieved.

It is noted that the highest contaminant concentration usually occur within and adjacent to existing structural discontinuities in the formation (e.g., joints, cracks, bedding planes). Since pneumatic fracturing dilates and interconnects existing discontinuities, direct access is provided to a majority of the contaminant mass. In these situations, the diffusive processes in the matrix blocks becomes less important, and it may be possible to meet target concentrations without cleaning the blocks completely, thereby reducing the time required for cleanup.

2.4 Monitoring Methods for Pneumatic Fracturing

Successful application of the pneumatic fracturing technology depends not only on the fracture injection procedure, but also on thorough characterization and evaluation of prefracture and postfracture condition of the formation. Over the years a number of methods and monitoring techniques have been developed to evaluate the pneumatic fracturing process and its impact on the geologic formation. The monitoring equipment pertinent to the study include flow measuring manifold, pressure indicators, tiltmeters, and borehole video camera. Each of these systems will now be described.

2.4.1 Flow Manifold

Flow measurements for the air permeability tests are made using variable area flow meters, also known as rotameters. Since air flow in the formation typically varies by one or more orders of magnitude, a manifold of rotameters is required. Rotameters are selected with overlapping ranges, so reading over a continuous scale is possible. Generally the rotameters are used for the low flow ranges which correspond to the prefracture stage extraction from the formation. For the postfracture stage extraction, when the flow range is generally high, a combination of pitot tubes, magnehelics, manometers, and massflowmeters are used in parallel to quantify and double check the flow. This system is preferred above 5 to 10 ACFM (actual cubic feet per minute) flow range, because excessive flow restrictions and pressure drops caused by rotameters will underestimate the actual flow. A schematic diagram of the flow manifold used for the field demonstrations is shown in Fig. 3. This system has an effective range of 0.001 to 100 ACFM.

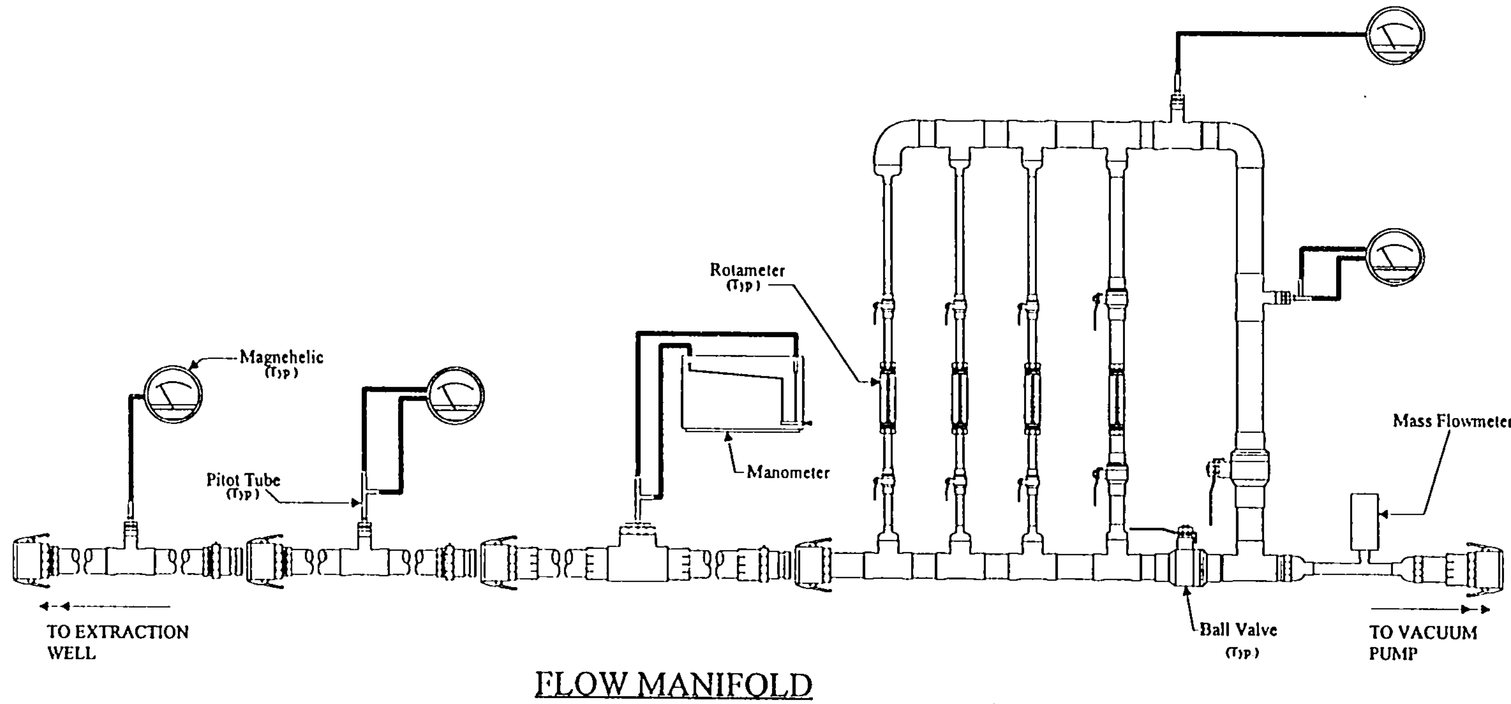

Figure 3 Flow manifold system.

2.4.2 Pressure-Flow Indicators

Pressure-flow indicators are used at monitoring wells for estimating the horizontal extent of the fractures as they establish air communication with outlying monitoring wells. During fracture injection, evidence of direct communication is often observed in the form of air rushing out of the monitoring wells. Additional evidence is also observed during vacuum extraction in the form of negative pressure recorded at outlying wells. Air communication measurements through pressure-flow indicators are valuable since they not only provide absolute confirmation whether or not fractures have intersected a particular well, but also these pressure and flow data can be used for analyzing the prefracture and postfracture permeability of the formation.

The pressure-flow indicator uses a combination of flow gauges and/or pressure gauges. A detail of a typical pressure-flow indicator is shown in Fig. 4

2.4.3 Heave Monitoring with Tiltmeters

Ground surface heave detection has been one of the methods for estimating the dimensions (both aperture and length) of the fractures. In the initial stage of development of pneumatic fracturing, heave was measured with an engineering level and graduated rods driven in the ground. Heave was observed visually as direct displacement during the fracture event. Later, as the technology progressed, more accurate and comprehensive determination were necessary so a custom fabricated reference beam system was utilized. The reference beam provided more data points, and less visual observers were required.

A limitation of these early methods of surface heave measurement is the magnitude of the observed surface effects becomes smaller, as the depth of injection increases, since heave is absorbed by the formation as elastic strain. A second limitation is the inability to record the time history of the fracture propagation, since reference beam system recorded only maximum movement.

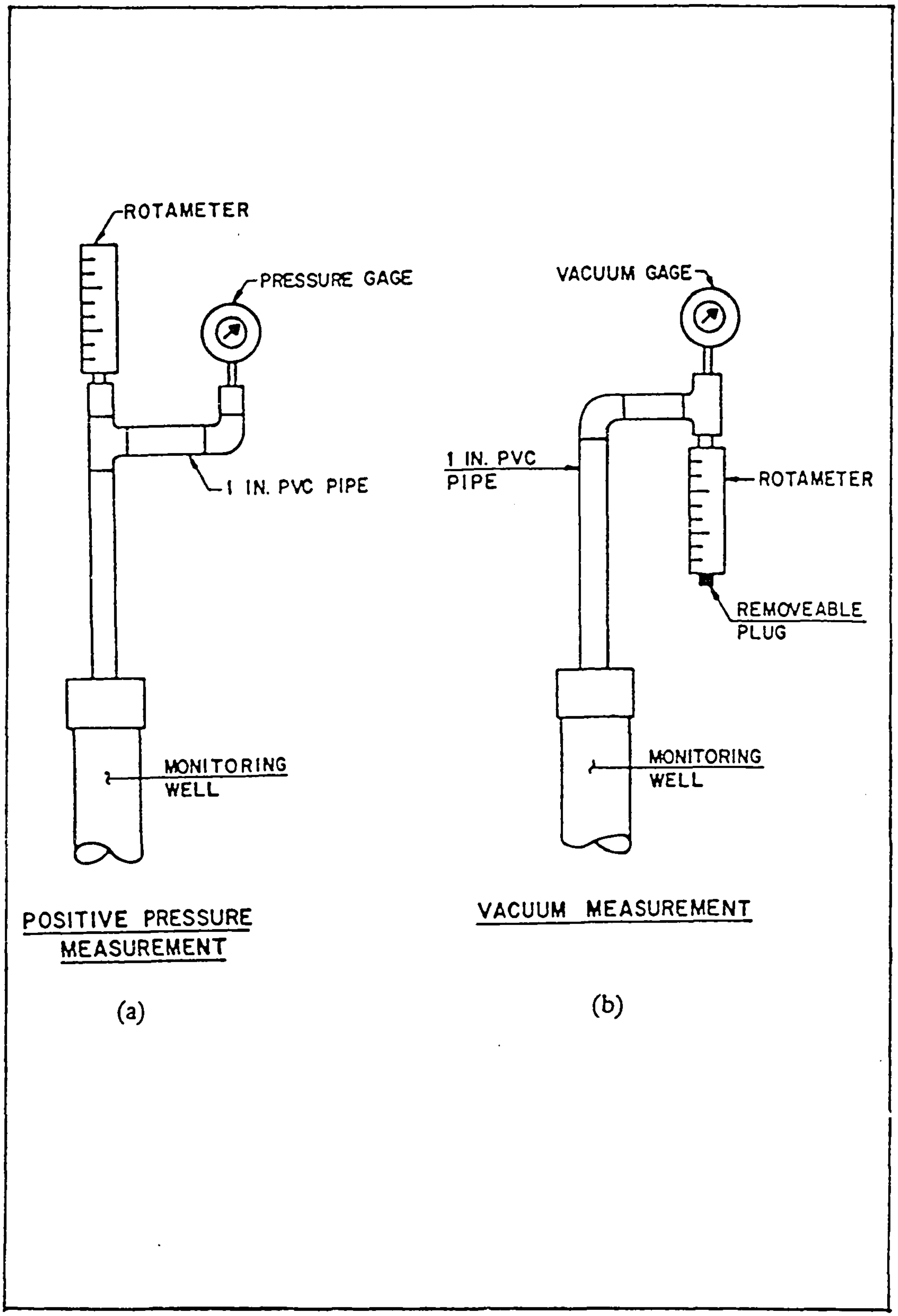

Figure 4 Pressure flow (PF) indicator.

In order to refine the system of fracture detection, a state-of-the-art electronic tiltmeter system is currently used to provide a dynamic time history of fracture propagation. Since a tiltmeter only senses the tilting of the surface and not the displacement, heave rods and optical levels are still used to calibrate and "truth" the tiltmeter data. Tiltmeters are run during pneumatic injection to observe fracture propagation, and also afterwards to record the settling of the formation to measure the residual heave.

A typical application of tiltmeters for heave detection involves an array of twelve biaxial tiltmeters positioned in a cross-pattern with injection well located at the center. A typical arrangement of tiltmeters is shown in Fig. 5. The tiltmeters are placed on rigid pads which are founded on tamped sand bedding to assure intimate contact with the ground surface.

Each biaxial tiltmeter contains two electrolytic sensors, which provide tilt sensing in the X- and Y- axes, respectively. The tiltmeters are connected in a common electronic network which downloads to an automatic data logger. This can then be accessed and controlled by a laptop microcomputer. The combined data acquisition system has the capability to sample each tiltmeter every 0.5 seconds during the injection. A slower 5 minute sampling run is made before and after each fracture to establish baseline behavior, and to check for sensor stability.

Tiltmeters measure differential tilt, i.e. they measure the change in angular deformation of the ground surface. The tiltmeters have a sensitivity range of 0.6 arc seconds to 3 degrees (high gain), and a noise level of approximately 2 arc seconds. The digital tilt values recorded during injections are "curve fitted" to generate the deformation surface using a computer. The deformation surface is then converted to contours of ground surface heave. These contour maps represent an approximation of the surface movement. A typical ground surface heave contour is shown in Fig. 6.

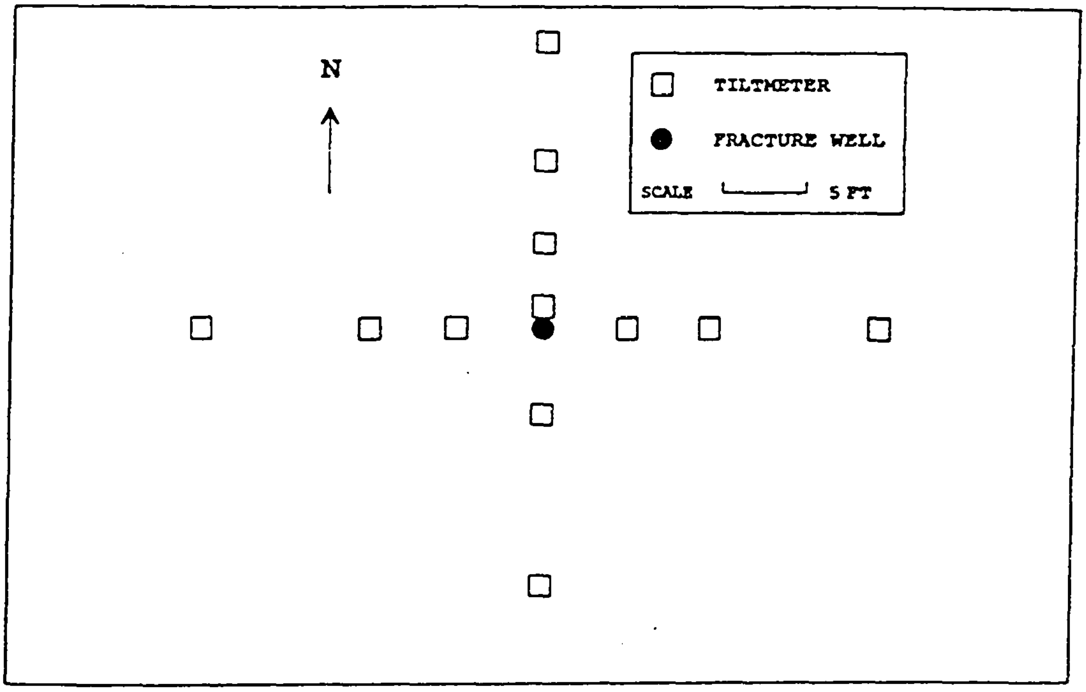

Figure 5 Typical tiltmeter array for fracture monitoring during fracture injection

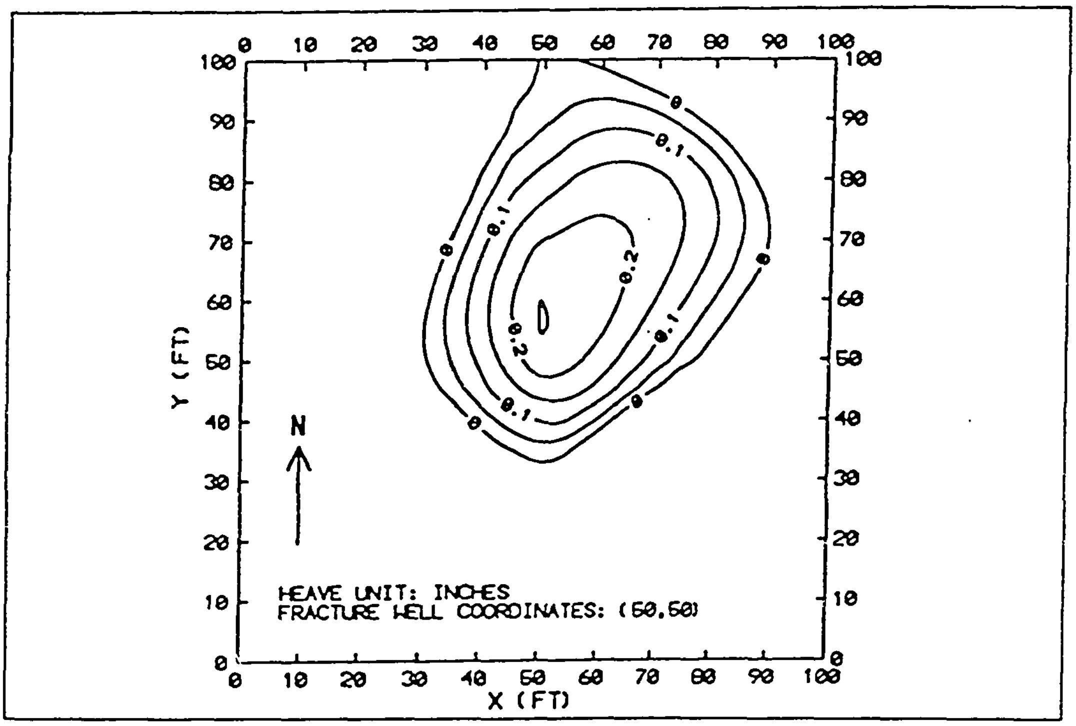

Figure 6 Typical tiltmeter ground surface heave contour

2.4.4 Borehole Camera

A high resolution borehole video camera has been used on a limited basis for direct examination of pneumatically induced fractures. The camera is lowered into the borehole via an armored support cable. The camera height is controlled with a winch system, and a CRT monitor. A video record of the borehole walls is made for future analysis.

Prior to any fracture injections, a baseline record of the borehole is established. The condition of the borehole is again examined after completion of the fracture injection. Comparison of the "before" and "after" videos provide insight into the effects of pneumatic fracturing on the formation.

2.5 Applications of Pneumatic Fracturing

As defined earlier, pneumatic fracturing is simply an enhancement process which "opens up" geologic formations to increase permeability. Once the formation has been fractured, several other proven clean-up technologies can be applied to facilitate in situ contaminant removal and/or treatment. Presently, the technologies which are being integrated with pneumatic fracturing are vapor extraction, bioremediation, hot gas injection, and pump and treat.

2.5.1 Vapor Extraction

Pneumatic fracturing was originally conceived for augmenting the vapor extraction (VE) process in low permeability formations. Vapor extraction is an in situ process for removing volatile organic compounds (VOC's) from the formation under the application of vacuum pressure. A vapor extraction system involves a motor driven vacuum pump, a venturi scrubber (to extract liquids and/or solids), a gas treatment unit (e.g., vapor phase carbon or catalytic oxidation), controls to regulate the vacuum, and various instruments to measure air flow, vacuum pressure, and gas temperature.

An important element of VE is the installation of vent wells to let surface air enter the subsurface. Normally, when vapor extraction is applied to high-permeability formations, air migrates from the surface through the formation to replenish air removed by VE. However, in low permeability formations, where there usually is inadequate surface recharge, vent wells must be installed. An added benefit is that by opening and closing selected vent wells, subsurface air flow and pressure can be controlled to enhance vapor removal.

One possible variation to the conventional VE approach is pulsing. Pulsing involves building up the vacuum in the subsurface with the vent wells capped. This process serves to enhance volatilization by reducing vapor pressure. After the vacuum has reached sufficient levels, selected vent well caps are opened to create a "flush" effect. Following this flush, the procedure is repeated.

2.5.2 Bioremediation

Pneumatic fracturing seems to provide excellent means for the enhancement of in situ bioremediation of contaminated sites. In addition to providing the much needed subsurface oxygen, the integrated bioremediation/pneumatic fracturing system can also inject microbes, nutrients, and buffers into the contaminated formation. The pressurized gas injects the nutrients and microbes deep into the formation through the fracture networks created by pneumatic fracturing.

A pilot test integrating pneumatic fracturing with bioremediation is currently ongoing at a refinery in Eastern Pennsylvania. At this site, a field prototype equipment for injecting nutrients and microbes into the pneumatic injection stream is being used for the first time. Various bench scale tests have been carried out to investigate the ability of microbes to survive pneumatic injection at high pressure (Fitzgerald, 1993)

2.5.3 Hot Gas Injection (HGI)

Hot gas injection (HGI) was integrated with pneumatic fracturing process at the Superfund Innovative Technology Evaluation(SITE) demonstration at Hillsborough, NJ. HGI involves heating of the formation to enhance volatilization of VOC's, thereby increasing the removal rates. The effectiveness of the HGI process is enhanced by pneumatic fracturing since the hot gases travel through the artificially created fracture network.

Equipment needs are modest and include a blower pump, pressure gauges, air flow meters and temperature meters. HGI is often operated in a "closed loop" mode, which recirculates the heated air through the formation. Injection temperatures average 175 °F to 250 °F when using a blower to compress and heat the air. If VOC mass removal is sufficiently high, carbon treatment may be replaced with a catalytic oxidizer, and the waste heat from the oxidizer can be used to increase injection air temperature.

HGI may be used to build up formation temperatures with vent wells capped and minimal VE. When the formation is sufficiently heated, HGI can be stopped, and VE can be used to build up vacuum with capped vent wells. The vent wells can then be uncapped and VE be used to flush the formation.

2.5.4 Pump and Treat

The pump and treat process is the most commonly used groundwater remediation technology at hazardous waste sites. The objectives of this technology are to reduce the concentration of contaminants to an acceptable level during cleanup and/or to contain contaminants in order to protect the subsurface from further contamination (plume control).

Pneumatic fracturing can also be integrated with pump and treat process, since it is extremely difficult to apply pump and treat to formations of low hydraulic conductivity. Pneumatic fractures created by the pneumatic fracturing process not only enhance the permeability of formation to provide greater flow rate and dewatering capability, but also enhance absorption potential for the reinjection of treated ground water, thereby speeding up the entire process of pump and treat remediation.

Pneumatic fracturing was first successfully used with the pump and treat process in a siltstone formation in New Jersey where the objective was to enhance absorption potential for the reinjection of treated ground water. At a recent demonstration of saturated zone pneumatic fracturing at a Superfund site in Oklahoma, the objective was to enhance product recovery from the formation. It should be noted that the pneumatically induced fractures at this site enhanced the product recovery from the formation from 87 gallons per month to 1450 gallons per month.

CHAPTER 3

THEORETICAL REVIEW OF FLUID FLOW IN DISCRETE FRACTURES

3.1 General

After a geologic formation has been pneumatically fractured, the ability to treat and/or remove contaminants will depend on the flow and transport characteristics of the artificially fractured medium. It is therefore useful to review the work of previous investigators studying the hydrogeology of fractured media. Unlike studies of porous media, flow in fractured systems has only come under scrutiny within the last two to three decades.

The two general approaches for analyzing flow in fractured media include the equivalent porous medium and the dual porosity approaches. As the name implies, the equivalent porous medium approach assumes that the fractures are distributed sufficiently throughout the formation, so that it can be analyzed with standard porous media methods. The applicability of this approach largely depends on the scale of the domain under study. For example, if the fractures are very closely spaced and/or the area under study is very large, the porous media method will yield satisfactory results.

However, in many hydrogeologic situations of smaller scale, say for a single well or for a small site, the local hetrogenities introduced by the presence of fractures cannot be ignored. Streltsova - Adams (1978) stated the problem well: "Permeability to fluid flow of original dense bedrock is usually very low ranging from 0.001 to 0.5 milli-darcy (1 darcy equal to 0.85 m/day or 0.001 cm/sec), while the fracture permeability ranges from a few milli-darcys to many darcys. The inter granular porosity of the original rock ranges from 2 to 27%, while the fracture porosity is typically less than 0.1%."

It is clear then, that many situations require the use of the dual porosity approach to analyze flow and transport in the fractured media. In the dual porosity approach, the fractured media is assumed to be the superposition of two flow systems over the same volume, consisting of a porous matrix and the open fracture network. As a special case of the dual porosity method, it is often useful to analyze the discrete fracture only, and ignore the flow and storage characteristics of the porous matrix blocks. This is the approach which has been adopted for the present research study. This is based on field experiences to date which have consistently shown large increases in formation permeability as a result of fracturing. It can therefore be concluded that the vast majority of the flow in a pneumatically fractured formation is occurring as discrete fracture flow.

3.2 General Definitions and Terminology for Fractured Rock Formations

Fracture/ Discontinuities : A general term for any break in a rock, whether or not it causes displacement, due to mechanical failure by stress. Fractures or discontinuities include cracks, joints and faults (AGI, 1987).

Crack : A partial or incomplete fracture (AGI, 1987).

Joints : A surface of a fracture or a parting in a rock, without displacement; the surface is usually planar and often occurs with parallel joints to form part of a joint set (AGI, 1987).

A group of parallel joints is called a set and joint sets intersect to form a joint system. Joints can be open, filled or healed. Joints frequently form parallel to bedding planes, foliation and cleavage and may be termed bedding joints, foliation joints and cleavage joints, accordingly.

Fault : A fracture or zone of fractures along which there has been displacement of the sides relative to one another parallel to the fracture (AGI, 1987).

The walls of a fault are often striated and polished as a result of the shear displacement. Frequently rock on both sides of a fault is shattered and altered or weathered, resulting in fillings such as breccia and gouge. Fault widths may vary from millimeters to hundred of meters.

Microfractures : Microscopic fractures in rocks on the order of a millimeter or less in length.

Bedding : The arrangement of a sedimentary rock in beds or layers of varying thickness and character; the general physical and structural character or pattern of beds and their contacts with the rock mass. The term may be applied to the layered arrangement and structure of an igneous or metamorphic rock (AGI, 1987).

Lineation : A general, nongenitic term for any linear structure in a rock, of whatever scale, e.g. flow lines, slickensides, or axes of folds. Lineation in metamorphic rocks includes mineral streaking and stretching, crinkles and minute folds parallel to fold axes, and lines of intersection between bedding and cleavage, or of variously oriented cleavages (AGI, 1987).

Filling : Any material that separates the adjacent rock walls of a discontinuity. It is usually weaker than the parent rock. Typical filling materials are sand, silt, clay, breccia, gouge and mylonite, but also included are thin mineral coatings and healed discontinuities such as quartz and calcite veins.

3.3 Aspects of Fracture Affecting Fluid Flow

3.3.1 Fracture Aperture (width)

Fracture aperture is the perpendicular distance between the adjacent walls of a discontinuity, in which the intervening space is air or water filled. Fracture aperture is the major controlling factor for fluid flow through a fractured media, as flow through a single fracture is a function of some exponential power of the fracture aperture. Direct measurement of fracture apertures in outcrops (Bianchi and Snow,

1969) suggests that the variation in fracture apertures with depth can be approximated by a log-normal distribution. In general, fracture apertures follow a log-normal distribution, although the mean and variance change with depth. Actual measurements in boreholes at relatively shallow depths, as reported by Snow (1968), indicate that typically fractures vary in width from 0.004 in. (102 microns) at a depth of 50 ft. to 0.002 in. (51 microns) at 200 ft. Snow's (1968) study concluded that fracture spacing generally increases with depth while fracture aperture generally decreases.

It is very difficult to define apertures in terms of true width, since the asperities which create fracture surface roughness also affect the fracture aperture opening size. In rock mechanics, fracture apertures are usually classified by size as in Table 1.

Table 1 Aperture Classification (after Barton, 1973)

Aperture, mm (microns)	Class
<0.1 (100)	Very tight
0.10 - 0.25 (100 - 250)	Tight
0.25 - 0.50 (250 - 500)	Partly open
0.50 - 2.50 (500 - 2,500)	Open
2.50 - 10.0 (2,500 - 10,000)	Moderately
>10 (> 10,000)	Wide

Field measurement of fracture aperture is most commonly done indirectly, using borehole hydraulic tests. Assuming only one fracture intersects the test interval, a packer test will yield an aperture as a function of the hydraulic conductivity by using the "cubic law" (see Section 3.4). If more than one fracture actually intersects the test interval, then this method will overestimate the aperture of either fracture (Gale 1982). It is noted that in the following chapter of this thesis, an attempt has been made to confirm this usual method to estimate fracture aperture by using a borehole camera and ground surface heave measurements.

3.3.2 Fracture Spacing

Fracture spacing is the perpendicular distance between adjacent discontinuities. The term normally refers to the mean or modal spacing of a set of joints. Fracture spacing is influenced by the rock composition, texture, structural position, and bed thickness. A thin bed contains more fractures than a thick bed under similar conditions. Brittle rocks, like silicified carbonates, cherts, micrites, and dolomites, fracture more intensely than do ductile rocks with a high percentage of clay and organic matter, such as shale or argillaceous dolomites. As a general trend, fracture density decreases with depth, as does fracture porosity. Average fracture spacing as measured by Snow has been reported as 4 ft. near the surface and 14 ft. at depths of 950 ft. The average near-surface fracture porosity was estimated to be 0.05% and was found to decrease by an order of magnitude for each increase in depth of 200 ft.

3.3.3 Fracture Orientation

Fracture orientation is the attitude of a discontinuity in space. The orientation of a fracture is usually expressed by its strike and dip. The strike is the trace of the intersection of the fracture with a horizontal plane, and its direction can be specified by its azimuth counted in degrees clockwise from the north. For example, an azimuth 300° corresponds to the direction N60W. The dip (or inclination, or plunge) is the magnitude of the angle between the fracture and a horizontal plane expressed in degrees.

The orientations of fractures, though not regular, is not purely random. Usually, many of the fractures observed in a single outcrop are approximately parallel to one or several planes. These fractures, which have approximately the same orientation, constitute a fracture set. The existence of sets is due to the fact that the orientations of fractures is related to tectonic history. The first tectonic event usually creates two or more conjugate sets of fractures, whereas the last event has usually reactivates previous fractures.

Natural fracture systems that are oriented consistently throughout a large volume of rock are subdivided by Stearns and Friedman (1972) into two major classes: regional orthogonal fractures and structure-related fractures. Regional orthogonal fractures are typically uniformly developed and laterally continuous over large areas. Price (1959) considers orthogonal fracture patterns the result of regional uplift and subsequent faulting. Fractures associated with faults usually contain a dominant fracture set parallel to fault plane. However, fracture density may be highly variable, being generally greater in the vicinity of the fault. Fold related fractures are diverse both in their orientation and in their size, and several types of these fracture sets are usually distinguished by their relationship to bedding. Fractures in domes usually have a radial pattern and no clearly dominant direction.

Orientation of artificially induced fractures has been extensively studied in the petroleum industry. In rock, the orientation of these fractures appears to be depth dependent; at depths less than roughly 300 m, artificially induced fractures are typically sub-horizontal, whereas at greater depths they are typically sub-vertical.,

For soils, the loading history, and thus the degree of consolidation of a soil are assumed to govern the orientation of these artificial fractures. These fractures are assumed to be vertical in normally consolidated soil, whereas they are assumed to be horizontal in overconsolidated deposits.

3.3.4 Fracture Connectivity

Fractures that intersect a borehole and are continuous within the well's drainage area make an "ideal" fractured system with uniform effective permeability. In such a fractured formation, the fracture and matrix blocks constitute a fracture-and-porous (double-porosity) medium, to which a continuum approach can be applied. However, a naturally fractured formation may also consist of meshes of discontinuous fractures whose geometry and orientations are random functions of position. Such a formation may be viewed as consisting of localized networks, or clusters, of fractures, with limited to poor interconnectivity. Both the effective permeability and the pressure behavior of a formation with a discontinuous system of fractures can depart radically from those of an equivalent porous medium or an ideal formation with uniform fracture permeability.

The fluid-flow behavior of a fractured rock mass with an impermeable matrix is determined entirely by the geometry of the fracture system. The effective permeability is dependent on the density of fracture intersections. As the fracture density increases, the behavior of the fractured medium becomes more like that of a homogeneous, anisotropic medium. Fracture permeability increases linearly with increasing fracture length, since the probability of fracture intersections increases.

3.3.5 Fracture Asperities

In fractures at depth under compressional stress, the walls are pressed together, with a finite fraction of fracture surfaces in contact, such contacts being known as asperities. The aperture of a fracture is likely to be smaller near the asperities and larger in the open channels within the fracture plane. Since the wall separation in the immediate vicinity of the asperities is very small, the contact points remain wetted for a long period of time and hydrochemical alterations will tend to occur, thereby forming fracture coatings. These fracture coatings are therefore long-term processes relating to mechanical deformation and stability, chemical dissolution and precipitation, and hydrological flow and transport under partially saturated conditions. In general, asperities are considered to be a function of the lithology, the degree of weathering or chemical alteration, and the number of contact points.

Because of the reduced area of the fracture at the contact zones, there is a reduction in the amount of net fluid flow through the fracture. This causes the flow lines to converge toward and then diverge away from the contact zones, resulting in somewhat tortuous flow paths in a fractured porous medium.

3.3.6 Surface Roughness

Fracture roughness is the inherent surface roughness and waviness relative to the mean plane of a discontinuity. Both roughness and waviness contribute to the shear strength. Large scale waviness may also alter the dip locally.

In conventional rock mechanics surface roughness is usually considered solely in relation to the angle of sliding friction, ϕ, along a discontinuity. Barton (1973) describes various type of surface roughness (refer Fig. 7) in three general categories as stepped, undulating, and planar, with each category further subdivided into rough, smooth, and slickensided. Barton also proposed a joint roughness coefficient (JRC) concept to define the surface roughness of a discontinuity.

3.4 Investigation of Flow Through Fractured Formations: Chronological History

The fundamental governing equations for fluid mechanics are the Navier-Stokes (1845) equations. This inherently nonlinear set of partial differential equations has no general solution, and only a small number of exact solutions have been found. Exact solutions of Navier-Stokes equation include the Poiseuille flow in a circular tube, and

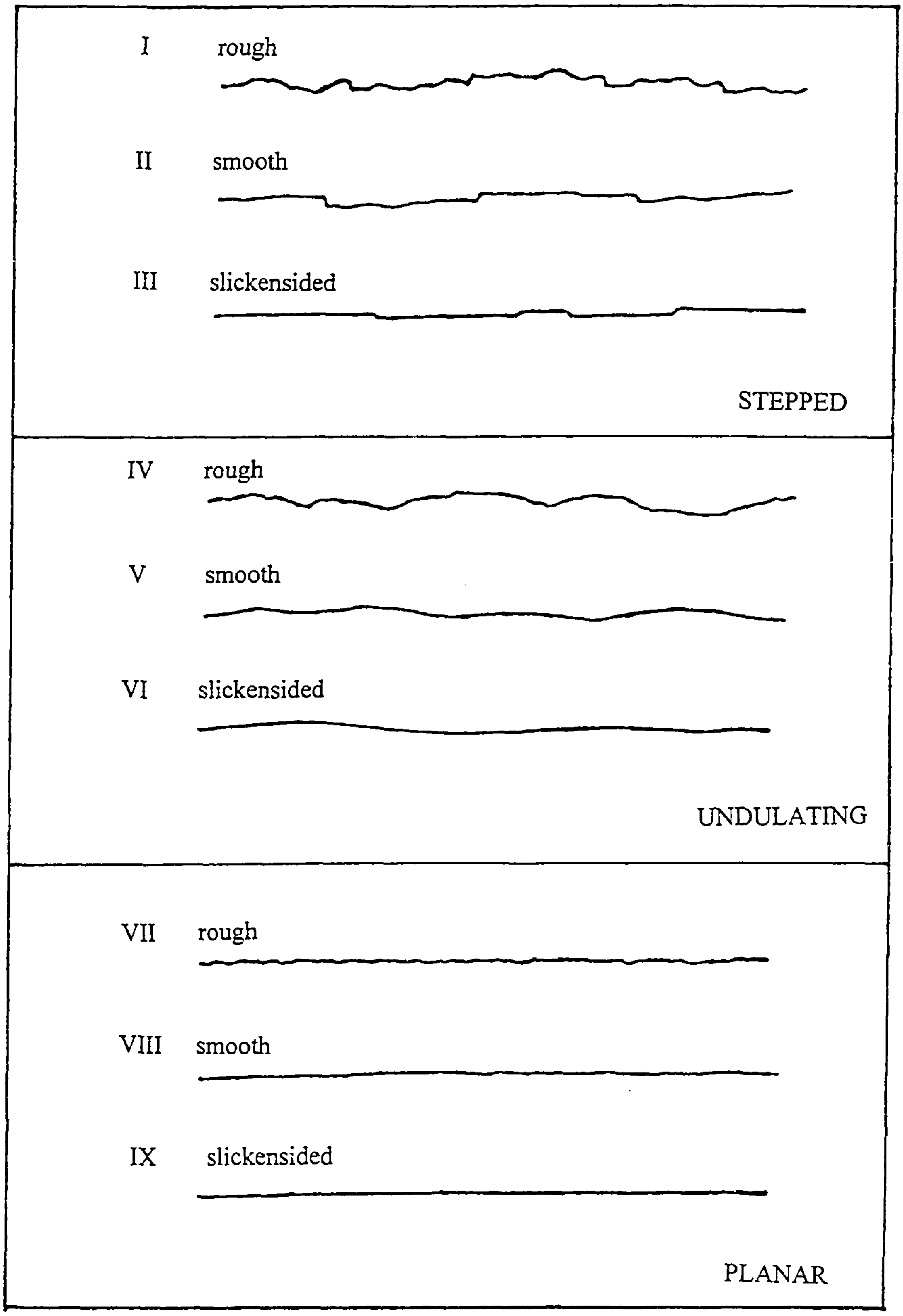

Figure 7 Typical roughness profiles : classified according to surface properties, lengths 1-10 m (after Barton, 1973)

other cross-sectional geometry's, such as parallel plates, annuli, eccentric circles, ellipses, confocal ellipse, and equilateral triangles.

As scientists were researching the fluid flow through thin cross sections, interest in the area of study of fluid flow through porous media was also concurrently developing in the scientific community. In 1856, a French Hydraulic Engineer named Henry Darcy carried out a laboratory experiment to analyze the flow of water through sand. The result of his experiment can be generalized into the empirical law that now bears his name. From his investigations of the flow through horizontally stratified beds of sand, Darcy concluded that the flow velocity was proportional to the hydraulic gradient. Darcy's law may be expressed as

$$u = Ki \tag{3.1}$$

where

u = flow velocity (L/T)

K = hydraulic conductivity (L/T)

i = hydraulic gradient (L/L)

Darcy's law is not only of fundamental importance in the analysis of ground water flow, but it is equally important in many other applications of porous-media flow. It describes the flow of soil moisture and is used by soil physicists, agricultural engineers, and soil mechanics specialists. It also describes the flow of oil and gas in deep geological formations, and is used by petroleum and natural gas reservoir analysts.

Darcy's law is only valid for the laminar flow conditions; however Misbach (1937) proposed a velocity-hydraulic gradient relationship which could be used for turbulent flow conditions. The Misbach Law can be expressed as

$$u^a = K'i \tag{3.2}$$

where,

K' = turbulent coefficient of hydraulic conductivity, and a = degree of nonlinearity

Poiseuille can be regarded as one of the pioneer researchers of fluid flow through thin cross-sections. Poiseuille's fundamental objective was to find out functional relationship among four variables: the volumetric efflux rate of distilled water from a tube Q, the driving pressure differential ΔP, the tube length L, and the tube diameter D. From his experiments, Poiseuille was able to discern that the efflux volume varied directly as the fourth power of the average diameter. His findings can be expressed mathematically as

$$Q = K'' \Delta P D^4 / L \tag{3.3}$$

where constant K" was explained by Poiseuille as a function of temperature and the type of liquid flowing.

It is still a mystery as to who first solved the problem of unidirectional flow between two parallel plates commonly called two-dimensional Poiseuille flow, as Poiseuille never mentioned flow between parallel plates in his scientific works. Sutera, et al., (1993) states that such flows between parallel plates were well known to Stokes (1898), and were probably derived earlier.

For the steady-state flow of viscous, incompressible fluids (at small Reynolds numbers), the Navier-Stokes's equation of motion, the most general equations governing fluid flow, reduce in form to a generalized statement of Darcy's law. Recognizing this relationship, Hele-Shaw (1897) devised an apparatus (which bears his name) whereby two-dimensional ground water flow could be investigated experimentally for structures with complex boundaries. Essentially, the model consists of two closely spaced glass plates containing completely the shape of the structure to be investigated. A viscous fluid such as glycerin is then allowed to flow between inlet and outlet levels until steady-state flow is reached. Then, by injecting colored dyes along the upstream edge, the patterns of streamline can be observed.

Open, self propped fractures resulting from pneumatic injection are capable of transmitting significant amounts of fluid. Fracture flow is most often modeled by analyzing the flow of a viscous liquid between two smooth parallel plates. This basic equation describing fluid flow in a fracture has been derived by a number of investigators based on Navier-Stokes equation for single phase laminar flow of a viscous incompressible fluid, and is commonly known as Poiseuille's Equation for flow between parallel plates, or the "parallel plate analogy". The derivation of this equation follows.

For Poiseuille flow between two infinite smooth parallel plates, the mean velocity, u, of the flowing fluid is expressed by the following formula

$$u = -\frac{\rho}{12\mu} b^2 \frac{dP}{dx} \tag{3.4a}$$

or

$$u = -\frac{g}{12\upsilon} b^2 \frac{dP}{dx} \tag{3.4b}$$

where,

u = mean velocity (L/T)

ρ = unit weight of fluid (F/L^3)

μ = dynamic viscosity of fluid ($F\text{-}T/L^2$)

ν = kinematic viscosity of fluid (L^2/T) = $\frac{g\mu}{\rho}$

b = aperture between smooth plates (L)

g = acceleration due to gravity (L/T^2)

dP/dx = hydraulic gradient (L/L)

If the flow is laminar and one adopts the analogy of parallel planar plates to represent the fracture surfaces, the hydraulic conductivity K_f of a fracture having an aperture b is given by or $$K_f = \frac{gb^2}{12\nu} \tag{3.5}$$

If it is assumed that the flow in the fracture is Darcian, an expression for volumetric flowrate occurring radially towards a well can be derived :

or $$Q = -\frac{\pi g b^3 (P_2 - P_1)}{6\nu \ln(R_2/R_1)} \tag{3.6}$$

where, P_1 and P_2 are pressures measured at radial distance R_1 and R_2, respectively, from the center of the well. In practical application, R_1 and P_1 are commonly the radius and pressure of the well.

This relationship is known as the "cubic law", since flow in the fracture, Q, is proportional to the cube of the aperture, b. Inspection of the equation emphasizes the high flow potential for even small fractures, and accounts for the significant permeability often observed in fractured formations.

It is instructive to compare potential fluid flows through an open smooth fracture controlled by the cubic law, and a layer of porous media which follows Darcy's Law. As indicated in Fig. 8, the radial flow towards a well intersecting a fracture with an aperture of 1 mm is equivalent to the radial flow from a layer of medium sand 70 cm thick. In this case, the flow computation for the sand layer was made using familiar Theim Equation for confined aquifer flow. Pressure gradients and radius of influence were assumed equal for this comparison.

While the cubic law concept is applicable to real fractured rock formations, various investigators have shown that deviations may be expected from this ideal model. An anomaly that could arise in an ideal fracture flow system is development of turbulence. Thus, the flow of a fluid in a fracture may be of either viscous or turbulent type, depending upon the fluid properties and the conditions prevailing in the fracture. Fluid flow in the vicinity of a well bore is especially susceptible to turbulence, due to the higher gradients caused by converging radial flow. Huitt

CUBIC LAW
(FLOW IN DISCRETE FRACTURE)

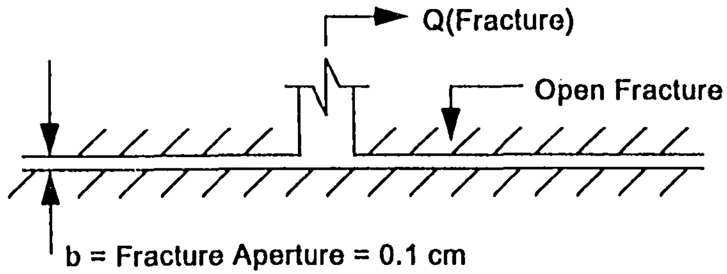

Cubic Law : $Q_F = \dfrac{6\pi g b^3 \Delta P_F}{\nu Ln(R_1/R_2)}$ [Eq. 1]

POROUS MEDIUM
(FLOW IN CONFINED LAYER)

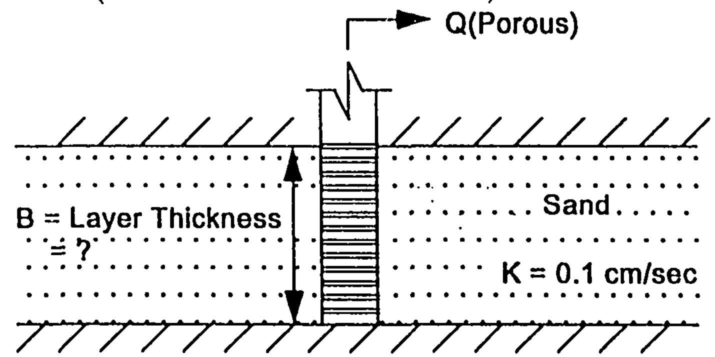

Theim Equation : $Q_F = \dfrac{2\pi K B \Delta P_P}{Ln(R_1/R_2)}$ [Eq.2]

Assume Equivalent Parameters :

Flow :	$Q_F = Q_P$
Pressure Gradient :	$\Delta P_F = \Delta P_P$
Influence Radii :	R_1, R_2 (Fracture) = R_1, R_2 (Porous)

Analysis Of Equivalent Flow :Equating Eq. 1 and Eq.2 $Q_F = Q_P = \dfrac{\pi g b^3 \Delta P_F}{6\nu Ln(R_1/R_2)} = \dfrac{2\pi B K \Delta P_P}{Ln(R_1/R_2)}$, $\Leftrightarrow$ $\boxed{B = \dfrac{g b^3}{12\nu K}}$ [Eq.3]

Substituting : g = 981 cm/ sq. sec, ν = 0.0114 sq. cms/ sec @ 15 °C, K = 0.1 cms/ sec., b = 0.1 cms in Eq.3 yields B = 71.7 cms

Therefore, b = 0.1 cm $\Leftrightarrow$ B = 71.7 cm (Say 70 cm)

Figure 8 Comparison of fracture flow and porous media flow (for water as a fluid)

(1956) categorized ranges of steady state and unsteady state flow of single phase Newtonian fluids through fractures. Prior to Huitt, Lamb (1945) had stated that the flow through a fracture would be viscous as long as the proportion of width to overall length of the fracture is small.

Many researchers have also described fluid flow behavior in fractures in terms of a Manning-type friction factor plot, in which the Reynolds number, R_e

$$\mathrm{Re} = \frac{b'u\rho}{\mu} \tag{3.7}$$

is correlated with the friction factor, ψ, as

$$\psi = \frac{b'}{\left(u^2/2g\right)}\Delta P \tag{3.8}$$

where

b' = twice the fracture aperture = 2b (L)

The cubic law for laminar flow in an open ideal fracture then reduces to the following simple relationship between the friction factor and Reynolds number

$$\psi = \frac{96}{R_e} \tag{3.9}$$

In general, various studies have shown that fluid flow in smooth fractures can be treated similarly to fluid flow in circular conduits. Huitt (1956) concluded that flow in planar fractures departs from viscous flow at a Reynolds number of about 1800, but the flow does not become completely turbulent until a Reynolds number of about 4000 is exceeded.

Many researchers such as Mises (1914) and Nikuradase (1940) investigated the effect of surface roughness on flow through a pipe. Huitt (1956) states that in the turbulent flow region, the effects of surface roughness become prominent. The extent to which the friction factor is controlled by the surface roughness is dependent on the relative surface roughness (which is the ratio of arithmetic mean elevation of surface roughness to the radius of the pipe) and the Reynolds number.

The first comprehensive work on flow through open fractures was by Lomize (1951). He used parallel glass plates and demonstrated the validity of the cubic law as long as the flow was laminar. He also investigated the effects of changing the fracture walls from smooth to rough and, finally, to models with different fracture shapes. He introduced the concept of defining the roughness, ε, in terms of the absolute height of the asperities and developed the empirical equation

$$\psi = \frac{96}{R_e}\left[1 + 6(\varepsilon/2b)^{1.5}\right] \tag{3.10}$$

which is valid for $\varepsilon/2b > 0.065$.

Equation 3.10 can be rewritten as

$$\psi = \frac{96}{R_e} f \tag{3.11}$$

where f is a factor that accounts for deviations from the ideal conditions that were assumed in deriving equation 3.9. For smooth walls, $f = 1$, whereas for rough walls, $f > 1$. Lomize (1951) also considered the effect of flow through fractures with planar but non-parallel (converging or diverging) sides.

Wilson and Witherspoon (1970) conducted laboratory studies on flow channels of varying shape and roughness. They concluded that flow will be laminar if the Reynolds number is less than 200. The surface roughness has no appreciable effect upon the resistance to flow when the flow is of a viscous nature.

Studies by Louis (1969 & 1974) suggested that the Reynolds number at which transition from laminar to turbulent flow occurs is influenced by the surface roughness of the fracture. While laboratory investigations of flow between smooth parallel plates generally indicate a critical value of 2300 to 2400, Louis points out that for very rough fractures this transition can occur at a Reynolds number as low as 300.

This study suggests that when turbulent flow occurs in fractures, the cubic law is no longer valid and the proportionality of aperture to flow reduces from an exponent of 3 down to 1.5. The results of this study are shown in Fig. 9.

Sharp and Maini (1972) also investigated flow characteristics of a discontinuity in terms of laminar and non-laminar flow. They found that the flow rate through a discontinuity does not always follow cubic law. Their results, expressed as $Q \propto b^e$, gives exponent values, e, as given in Table 2.

Table 2 Exponential power corresponding to various flow regimes (after Sharp and Maini, 1972)

	Rough Discontinuity	Parallel Plate
Linear Laminar Flow	$e = 2$	$e = 3$
Non - Linear Laminar	$1.2 < e < 2$	—
Fully Turbulent Flow	$e = 1.2$	$e = 1.5$

Wilson and Witherspoon (1970) studied the effect of fracture intersections by monitoring flow across a 90° intersection of two circular pipes. Maini (1971) also conducted similar experiments using intersecting parallel plates. Both these tests indicated measurable losses in velocity and pressure because of the abrupt change in flow directions and mixing at the intersection. From these tests, it was inferred that intersection losses can be ignored as long as the Reynolds number is less than 100, but if the flow through a significant section of fracture is turbulent, then intersection losses should be considered.

Wilson and Witherspoon (1970) also studied the effects of fracture orientation and anisotropy on flow of fluid through fractured formation. They used finite element techniques to analyze two-dimensional flow through fracture networks of different fracture orientations and degrees of anisotropy. Their study results indicated that flow rate was primarily controlled by the degree of anisotropy. However, both

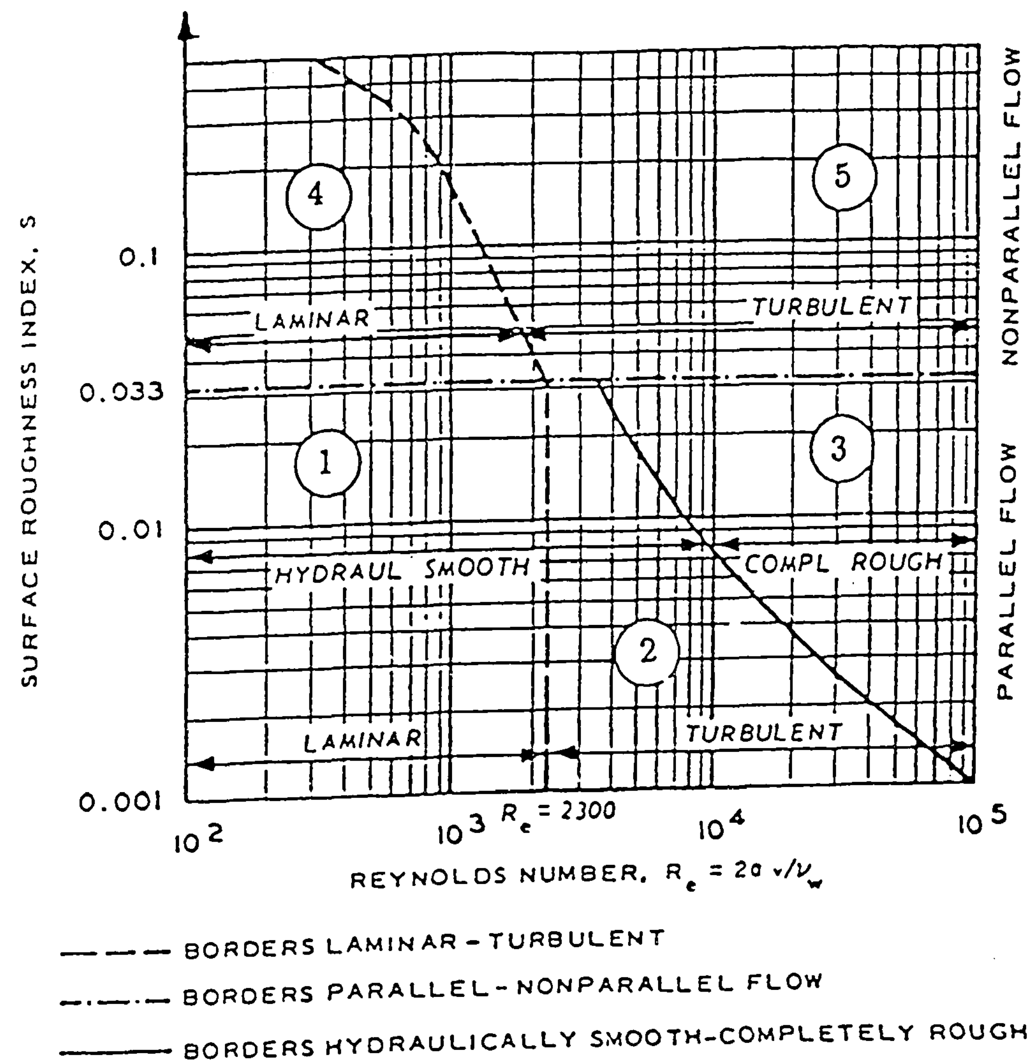

Figure 9 Range of validity of fracture flow laws (after Louis, 1969)

fracture network orientation and degree of anisotropy had a significant effect on the flow pattern and pressure distribution.

Another deviation of fracture flow in real formations is the fact that fracture surfaces are not exactly parallel. Moreover, at points and aerial segments within a fracture, the aperture may disappear altogether, as adjacent blocks come into direct contact. By expressing a fracture as a series of "n" discrete segments of different aperture, Wilson and Witherspoon (1974) defined the effective aperture, b_{eff}, as

$$b_{eff}^3 = \frac{\sum_{i=1}^{n} l_i}{\sum_{i=1}^{n} \left(l_i / b_i^3 \right)} \tag{3.12}$$

where l_i is the length of a fracture segment which has an aperture b_i.

The flow of fluid through fractures and their conductivities are directly related to stress applied to the fractured block, since with changing normal stress, the aperture, the relative contact surface area and the degree of asperity contact of a fracture are changed. Thus it could be inferred that both fracture aperture and flow through a fracture will decrease as we go deeper in the subsurface, due to increased overburden stress.

Though there are significant number of research studies to substantiate that the average discontinuity apertures decrease with depth, it does not mean that conducting discontinuities with significant apertures do not persist at depth. In the laboratory experiments (Witherspoon et al.,, 1980) at normal stress in excess of 20 MPa corresponding to a depth of 1000 m, it was not possible to affect either hydraulic or acoustic closure of comparatively smooth discontinuities (refer to Fig. 10). Similarly tests conducted in the field led Snow (1965) to observe that, once formed and opened, a fracture is never completely hydraulically closed.

Furthermore Gale and Raven (1980) demonstrated through laboratory experiments that the relationship between normal stress and normal deformation of

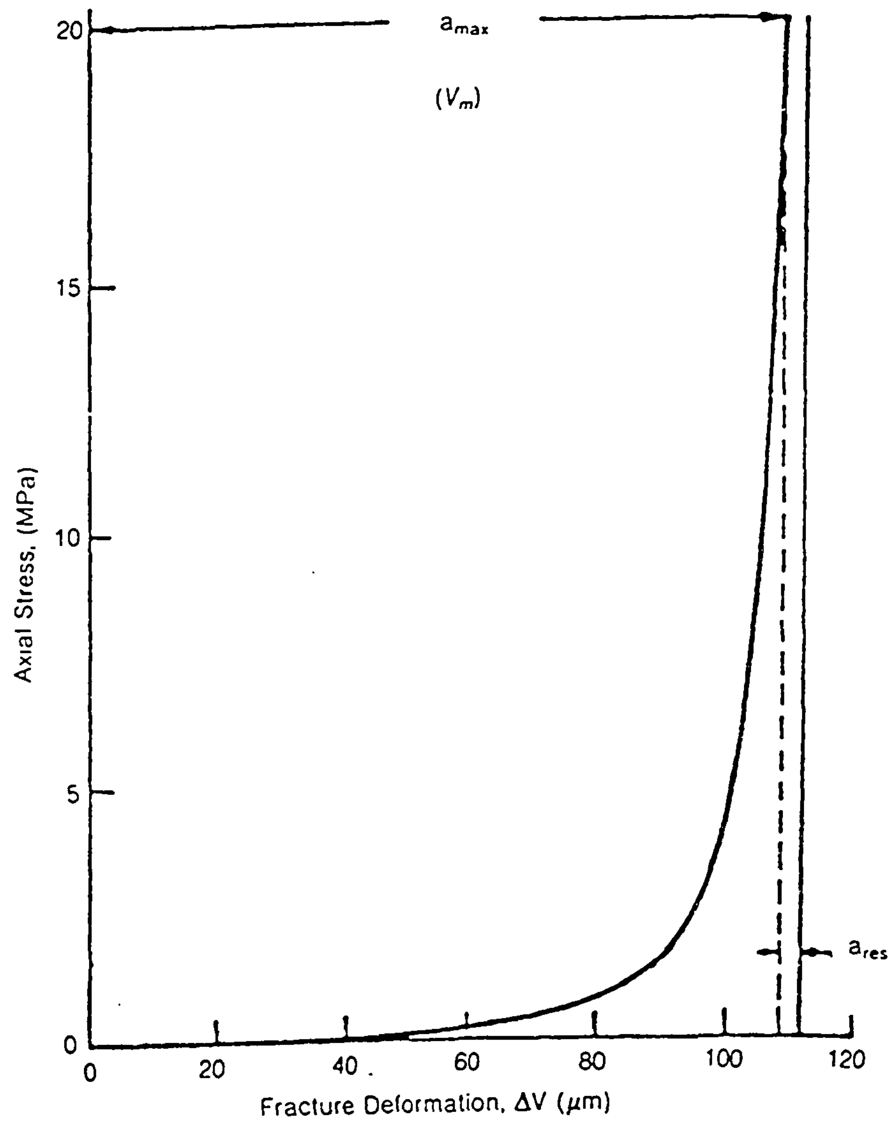

Figure 10 Maximum and residual aperture under normal stress (after Witherspoon et al., 1980)

natural, open fractures is invariably non-linear, involving hysterisic behavior during cycles of loading and unloading. Cumulative, permanent deformation was also observed in these experiments. Results of a typical hysterisis loading cycle are shown in Fig. 11.

Sharp and Maini (1972), in their study of permeability of a fractured sample subjected to various shear displacements under negligible normal stress, found changes in permeability of two orders of magnitude at a shear displacement of 7 mm and an overall dilation of only 2 mm. In general, it has been observed for fractured rock blocks subjected to direct shear stress, that the change of permeability will depend on the rock type, fracture aperture, roughness, normal stress, and displacement history.

Tsang and Witherspoon (1983) studied the relationship between flow rate and applied normal stress for mated and unmated joints. They indicated that when normal stress was applied to a joint sample, the resultant "soft" mechanical behavior gave rise to a sharp drop in flow under initial normal stress. Hence the more well-mated the discontinuity, the sharper the decline in flow with stress at a low level of applied normal load. This implies that conductivity decreases more rapidly for well - mated joints during initial loading.

Bandis et al., (1985) proposed that for larger aperture "open" fractures, the largest reduction in permeability would be predicted for smooth joints and least reduction for very rough joints if the same initial aperture and increasing normal stress were assumed.

Because the stress field in a rock mass is highly anisotropic, and because fractures have highly non-linear deformation characteristics, the change in aperture per unit change in effective stress is highly dependent on the initial effective stress acting along the fracture plane. Thus fractures at the same depth below the ground

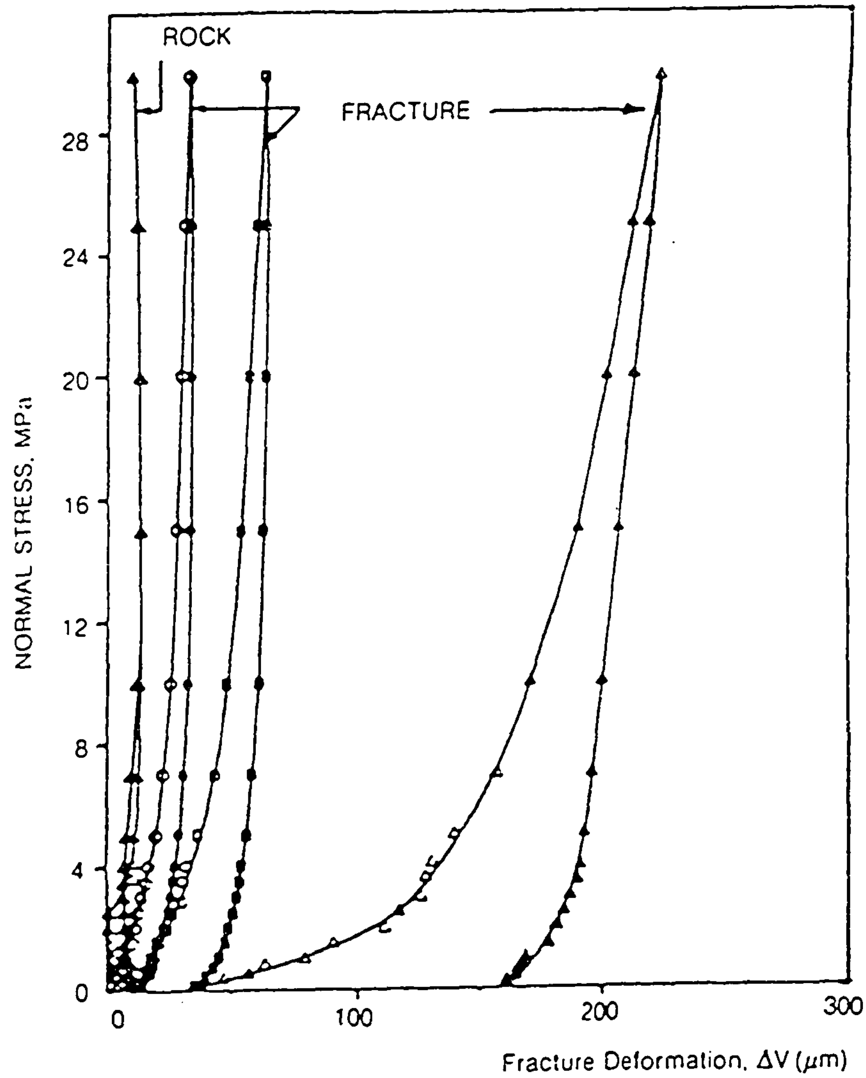

Figure 11 Discontinuity and rock deformation as a function of normal stress under cyclic loading (after Gale and Raven, 1980).

surface but with different orientations may be subjected to different effective normal stresses, and hence have different fracture permeabilities.

It is also clear that natural fractures are not necessarily continuous, and zones may occur where the fracture surfaces are in contact and not open. In conjunction with this hypothesis, investigators have also addressed the effect of normal stress on fracture flow. Laboratory experiments performed by the Witherspoon, et al., (1980) on test specimens of granite, basalt, and marble showed that apertures still transmitted flow in general proportion to the cubic law through fractures with an aperture of four micrometers under a normal stress of 20 MPa.

3.5 Flow of Gases Through Porous Media

The mechanism of fluid flow through a porous medium is governed by the physical properties of the matrix, geometry of flow, pressure, volume, and temperature (PVT) properties of the fluid, and pressure distributions within the flow system. Though pneumatic fracturing has potential for use for ground water treatment and for enhancement of pumping rates for water well systems, it has so far predominantly been integrated with vacuum extraction for vadose zone remediation. Since the vacuum extraction process involves flow of air through the formation, it is important to investigate the flow of air through the pneumatically fractured formation, and to modify the cubic law relationship to account for the difference of property of gases over liquids such as water. It should be noted that air flow is more complicated than ground water flow because of compressibility effects, the Klinkenberg effect, variations in air density and viscosity that results from temperature fluctuations in the unsaturated zone, and the possibility of inducing water movement during the pneumatic test.

3.5.1 Viscosity and Pressure Effects

The effect of variation of pressure dependent viscosity and gas law deviation factor has been a problem area in the analysis of flow through porous media. The earliest attempt to solve this problem was the method of successions of steady-state proposed by Muskat (1946). Approximate analytical solutions were obtained by linearizing the flow equation for ideal gas to yield a diffusivity type equation. Such solutions, though widely used and easy to apply to indirect problems, are of limited value because of idealized assumptions and restrictions imposed upon the flow equation.

To understand the mechanism of flow of gases through a porous medium, it important to understand gases and the effect of pressure (or vacuum) on their flow through a porous medium.

The state of a gas in which molecules behave most independently of each other is called an ideal gas. This is a theoretical concept which corresponds to the assumption that : (a) the molecules are minute spheres; (b) their volume is very small compared with that actually occupied by the gas; (c) the molecules do not exert forces upon each other; (d) they travel along rectilinear paths in a perfectly random fashion; and (e) the molecules make perfectly elastic collisions. By an ideal gas or perfect gas we mean one which obeys Boyle's law at all temperatures. Boyle's law states that the product of the pressure P and volume V remains a constant. That is :

$$PV = \text{constant} \tag{3.13}$$

or considering two different points between a system the relationship between them is written as

$$P_1V_1 = P_2V_2 \tag{3.14}$$

describing an isothermal compression.

Darcy's law can be applied to the flow of gases through the porous medium. It can be written as

$$u = -\frac{k}{\mu}\Delta P \tag{3.15}$$

where k is the intrinsic permeability of the medium and (μ) is the dynamic or absolute viscosity of the fluid.

Muskat (1946) defines the density-pressure interdependencies of various fluids for viscous flow as

$$\rho = \rho_0 P^m e^{\beta P} \tag{3.16}$$

where ρ = density of the fluid

ρ_0 = fluid density at zero pressure

β = compressibility of the fluid, and

P = pressure of the fluid

The particular fluid of significance can be classified as :

<u>Liquids</u> : m=0

Incompressible Liquids : $\beta = 0$

Compressible liquids : $\beta \neq 0$

<u>Gases</u> : β =0

<u>Isothermal expansion</u> : m = 1

<u>Adiabatic expansion</u> :

m = (specific heat at constant vol.)/ (specific heat at constant pressure)

Therefore, for gases, the density-pressure relationship defined by Eq. (3.16) can be written as

$$\rho = \rho_0 P^m \tag{3.17}$$

Furthermore, Muskat (1946) describes that on applying the equation of continuity to the Darcy's expression for mean velocity, the density, ρ, of a gas flowing in a homogenous porous medium must obey the fundamental equation

$$\nabla^2 \rho^{\frac{1+m}{m}} = \frac{\partial^2 \rho^{\frac{1+m}{m}}}{\partial x^2} + \frac{\partial^2 \rho^{\frac{1+m}{m}}}{\partial y^2} + \frac{\partial^2 \rho^{\frac{1+m}{m}}}{\partial z^2} = \frac{(1+m) f \mu \rho_0^{1/m}}{k} \frac{\partial \rho}{\partial t} \qquad (3.18)$$

where k and f denote the intrinsic permeability and porosity of the porous medium, respectively.

3.5.2 The Steady-State flow of Gases in Porous Medium

3.5.2.1 Linear system

For the flow of gases through linear system, an example of which would be a laboratory air permeability experiment, the gas flow analysis can be done in the following manner as derived in Muskat (1946). As steady-state flow conditions are expected, the right side of Eq. 3.18 could be set to zero. That is

$$\nabla^2 \rho^{\frac{1+m}{m}} = \nabla^2 P^{1+m} = 0 \qquad (3.19)$$

The pressure distribution in a linear system (refer Fig. 12a) at any distance x is given by

$$P^{1+m} = (P_1^{1+m} - P_2^{1+m}) \frac{x}{L} + P_2^{1+m} \qquad (3.20)$$

where P_2 and P_1 are the boundary values of the pressure at x=0 and x=L, respectively. The rate of mass flow, Q_m, for the system is therefore

$$Q_m = -\frac{kA\rho}{\mu} \frac{\partial P}{\partial x} = -\frac{kA\rho_0}{(1+m)\mu} \frac{\partial P^{1+m}}{\partial x} \qquad (3.21)$$

but differentiating Eq. (3.20) with respect to x the following is obtained

$$\frac{\partial P^{1+m}}{\partial x} = \frac{(P_1^{1+m} - P_2^{1+m})}{L} \qquad (3.22)$$

Substituting Eq. (3.22) to Eq. (3.21) results in

$$Q_m = -\frac{kA\rho_0}{\mu(1+m)L} (P_1^{1+m} - P_2^{1+m}) \qquad (3.23)$$

for isothermal flow, i.e. m=1, the above Equation can be written as :

$$Q_m = -\frac{kA\rho_0}{2\mu L}(P_1^2 - P_2^2) \tag{3.24}$$

Substituting Eq. 3.17 into Eq. 3.24 the volumetric flowrate, Q, can be derived as

$$Q = -\frac{kA\rho}{2\mu P_1 L}(P_1^2 - P_2^2) \tag{3.25}$$

The derivation of this expression has been substantiated elsewhere, e.g. Sullivan and Hertel (1940), Langfelder (1968), and Zeigler (1976).

3.5.2.2 Radial System

For radial systems, the pressure distribution (Fig. 12b) is given by Muskat (1946) as

$$P^{1+m} = \frac{(P_1^{1+m} - P_2^{1+m})\log(R/R_1)}{\log(R_2/R_1)} + P_2^{1+m} \tag{3.26}$$

The associated mass flux through a system of thickness, h, will be

$$Q_m = -\frac{2\pi rhk\rho}{\mu}\frac{\partial P}{\partial r} = -\frac{2\pi rhk\rho_0}{(1+m)\mu}\frac{\partial P^{1+m}}{\partial r} = -\frac{2\pi hk\rho_0(P_1^{1+m} - P_2^{1+m})}{(1+m)\mu\log(R_2/R_1)} \tag{3.27}$$

which is similar in form to the Theim Equation.

Again substituting Eq. 3.17 into Eq. 3.27, the volumetric radial flowrate will be

$$Q = -\frac{2\pi hk\rho(P_1^{1+m} - P_2^{1+m})}{(1+m)\mu P_1\log(R_2/R_1)} \tag{3.28}$$

In view of the fact that the steady-state flow of gases is governed by Laplace's equation in the dependent variable P^{1+m}, where m determines the thermodynamic character of the flow, the analytical expressions for the solutions for various problems

(a) LINEAR SYSTEM

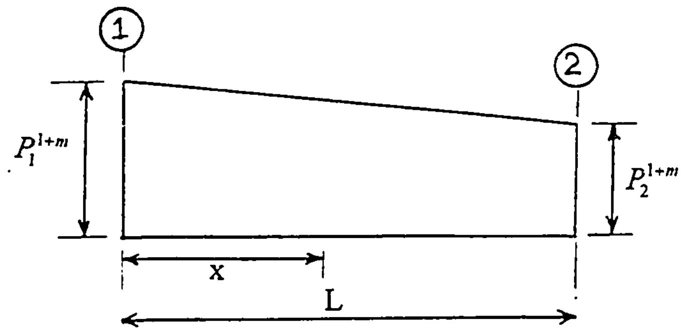

at any point at a distance x from point 1, the pressure is given as

$$P^{1+m} = \left(P_1^{1+m} - P_2^{1+m}\right)\frac{x}{L} + P_2^{1+m}$$

(b) RADIAL SYSTEM

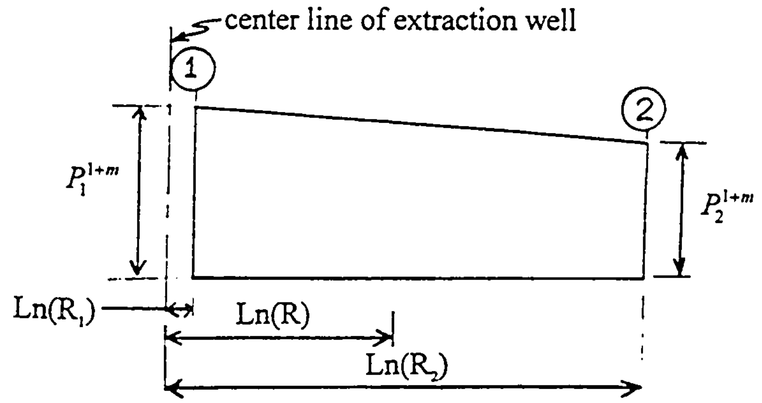

pressure at any point at radial distance R from the extraction well is given by

$$P^{1+m} = \left(P_1^{1+m} - P_2^{1+m}\right)\frac{Ln\left(\frac{R}{R_1}\right)}{Ln\left(\frac{R_2}{R_1}\right)} + P_2^{1+m}$$

Figure 12 Fluid pressure distribution in a linear and a radial system.

can be simply taken as those for the corresponding systems of steady-state liquid flow, also governed by Laplace's equation. The only change that needs to be made with respect to the pressure distributions is the replacement of the pressure, P, in the expressions for the case of the steady-state liquid flow by P^{1+m}. And the values of the mass fluxes and volumetric fluxes for the steady-state solutions for gas flow are to be obtained from those for steady-state liquid systems by replacing the $(P_1 - P_2)$ of the later by $\rho_0 \dfrac{(P_1^{1+m} - P_2^{1+m})}{1+m}$ and $\rho \dfrac{(P_1^{1+m} - P_2^{1+m})}{(1+m)P_1}$, respectively, ρ_0 being the gas density at unit pressure. In the case of most practical interest, that of isothermal flow (m=1), the above change is equivalent to that of multiplying the volume fluxes of the steady-state liquid flow by the mean density in the gas-flow system to get the mass flux in the later.

For linear gas flow, the pressure distribution will be given simply by a linear variation of P^{1+m}, and for radial flow systems, the pressure quantity P^{1+m} varies logarithmically with the radial distance. As to the effect of the thermodynamic character of the flow on the flow of a gas, it is found that the isothermal flow (m = 1) will give the least flow, the flux increasing as the value of m decreases, so that, for example, 16 percent more air will pass adiabatically (m=0.71) through a linear system due to the higher outflow densities when m<1, which more than compensates for the lower outflow-pressure gradients in the latter case.

Johnson et al., (1990) has proposed the use of a form of Eq. 3.28 for analysis of gas flow in the design of vapor extraction systems. For the application, isothermal conditions are assumed and m is set equal to 1.0.

3.5.3 Non-Steady State Considerations

When applying vacuum extraction to pneumatically fractured formations, steady state analysis is valid since pressure equilibrium is reached quite rapidly at most sites. This is illustrated from Fig. 13 which shows that the vacuum pressure at outlying monitoring wells reached maximum values within 2 to 3 minutes and remained relatively stable thereafter. The probable explanation for this rapid response is the substantial increase in formation conductivity caused by the artificially formed fractures. Such behavior has been observed, in dry or moderately wet formations. However, if perched water is present in the formation or if the moisture content of the formation is very high, the subsurface air flow is affected and may exhibit fluctuations due to the presence of water in fractures. For such situations, it is prudent to dewater the site before starting the vacuum extraction process.

Although true non-steady state behavior has rarely been observed at pneumatically fractured sites, it may applicable for prefracture baseline analysis, or at the periphery of the fractured zone. Many researches, such as McWhorter (1990), Massman (1989), Johnson et al.,(1990), have proposed non-steady state methods for calculating air flowrate through unsaturated zones for vacuum extraction systems.

3.5.4 The Klinkenberg Effect

The Klinkenberg effect is an enhancement of air permeability through slippage of air molecules along the boundaries of air-filled pores. This occurs when the mean free path of air molecules approaches the dimensions of the pores. The Klinkenberg (1941) effect is expressed as :

$$k = k_{\infty}(1+\frac{d}{P}) \qquad (3.29)$$

where k is the air-phase permeability at high air-phase pressure and d is a parameter of the porous medium (i.e. k_{∞}). Typical values of d are 0.0086 atmospheres and 0.7660 atmospheres for gravel and silt, respectively.

The Klinkenberg effect introduces non-linear terms into air-flow modeling. Thus, the conditions under which the Klinkenberg effect can be neglected must be

PLEASE NOTE

Page(s) not included with original material
and unavailable from author or university.
Filmed as received.

University Microfilms International

identified. Baehr and Hult (1991) estimate the maximum error, e_{max}, in air permeability calculations for neglecting Klinkenberg effect as following :

$$e_{\max} = 100\left[\frac{k(P_w) - k(P_{atm})}{k(P_{atm})}\right] \tag{3.30}$$

where P_w is air pressure at extraction well and P_{atm} is atmospheric air pressure. Using Eq. 3.29 and Eq. 3.30, the following can be implied :

$$e_{\max} = 100\frac{\left[\frac{P_{atm}}{P_w} - 1\right]}{\left[\frac{P_{atm}}{d} + 1\right]} \tag{3.31}$$

Fig. 14a and Fig. 14b shows contours of e_{max} as a function of P_w/P_{atm} and Klinkenberg parameter, d, for the case of air withdrawal and air injection, respectively. An analysis of these graphs show that consideration of the Klinkenberg effect, especially for the air withdrawal case, would result in a maximum possible error of 10% or less for most standard vacuum extraction systems, as the Pw/Patm values generally range from 0.7 to 0.9 (5 to 15 inches of Hg vacuum). But if higher vacuum levels are used, as in "High Vac." systems or in "Vacuum Enhancement" systems, the error may be significantly greater than 10% and may necessitate consideration of Klinkenberg effect for permeability evaluation of the formation. McWhorter (1990) also stated that the nonlinearity arising from Klinkenberg effect would be of importance only for circumstances that results in large pressure gradients such as will occur for large injection or withdrawal rates in media with low permeability.

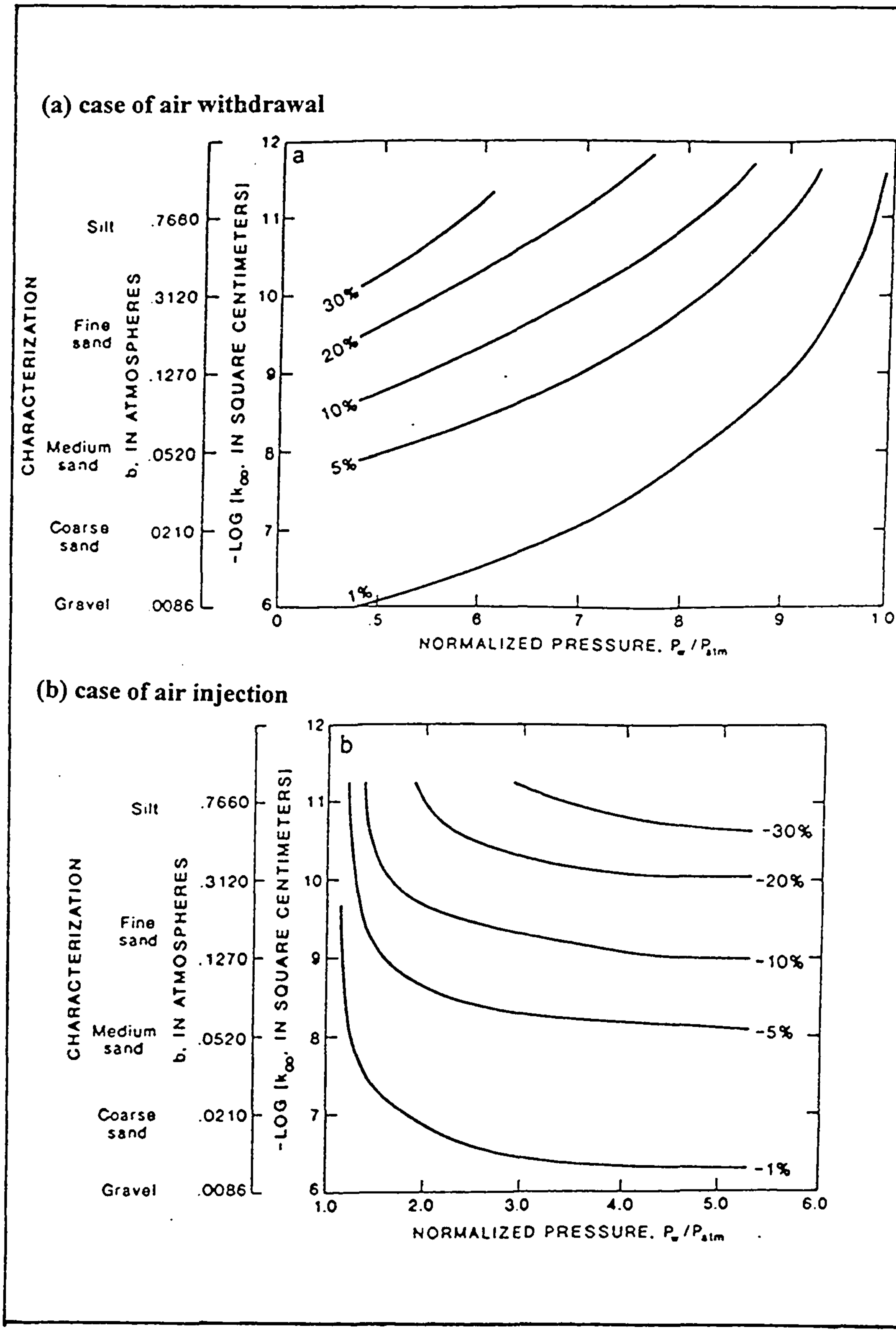

Figure 14 Maximum possible error in obtaining air permeability estimate due to neglecting the Klinkenberg effect (Baehr and Hult, 1991)

CHAPTER 4

DEVELOPMENT OF PNEUMATIC FRACTURING FLUID FLOW MODEL

4.1 Model Approach

The mechanism of fluid flow through a fractured medium is governed by the physical properties of the matrix, geometry of flow, pressure distributions within the flow system and the properties of the fluid. Though pneumatic fracturing has potential for use for groundwater treatment and for enhancement of pumping rates for water well systems, it has so far predominantly been integrated with vacuum extraction for vadose zone remediation. Since the vacuum extraction process involves flow of air through the formation, it is important to investigate the flow of air through the pneumatically fractured formation, and to modify the cubic law relationship to account for the difference in fluid properties. It should be noted that the air flow is more complicated than ground water flow because of compressibility effects, boundary slippage, spatial variations in air density and viscosity, and the possibility of inducing water movement during the pneumatic test.

The importance of developing a new flow model for pneumatically induced fractures is even more acute, since the artificial fractures have apertures which are considerably larger than natural fractures. This results in higher flow velocities and more drastic pressure gradients in the formation. Therefore, it is inappropriate to ignore the effects of gas compressibility and turbulence.

The general approach which will be followed for derivation of the Pneumatic Fracturing Fluid Flow Model (P.F. Flow Model) is outlined below :

1. The derivation will begin with the equation of Poiseuille flow between two parallel plates assuming a viscous, incompressible fluid (this is the "Cubic Law"). The resulting fracture flow equation will be converted into radial coordinates.
2. Gas compressibility effects will be introduced assuming an isothermal condition and constant viscosity. Only gas pressure and density will be varied.
3. The power exponent of aperture in the relationship will be generalized to allow for possible turbulence in the high velocity flow in pneumatically induced fractures.
4. The relationship for flow in a single fracture will be extended to flow in a multiple fracture system.

The derivation of the P.F. Gas Flow Model outlined above is presented in the following section.

4.2 Development of P.F. Fluid Flow Model

Poisseuille Flow and the Cubic Law

The simplest model of the flow through a single fracture is the analogy with Poiseuille flow between two infinite smooth parallel plates. The case considered is a fluid flowing steadily through a slit or fracture of uniform aperture, b. The flow is 1-dimensional in the direction i; that is, the velocity components, u_j and u_k along y and z directions, respectively, are zero. This situation is illustrated in Fig. 15, which shows a section normal to the boundaries and parallel to the flow. The coordinate in the direction of flow is designated as x, and the coordinate orthogonal to both x and the boundaries is y. The origin for y is at one of the solid boundaries.

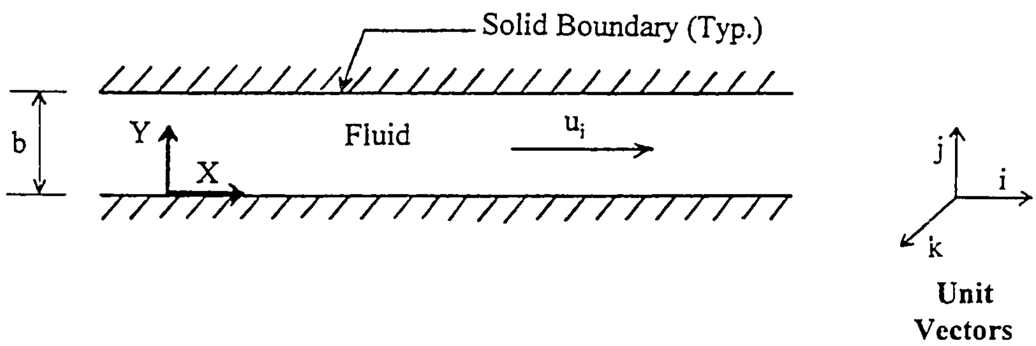

Figure 15 Section showing flow through a single fracture

The general equation of fluid flow for this model (Refer Eq. A9, Appendix "A") can be written in terms of potential function, P, as

$$\frac{\partial P}{\partial x_i} = \frac{\mu}{\rho} \frac{\partial^2 u_i}{\partial x_j \partial x_j} \tag{4.1}$$

which is a valid approximation for flow in porous media under ordinary potential gradients provided the fluid density is constant. In the above equation, μ is the dynamic viscosity, and ρ is the unit weight of the fluid, respectively.

In addition to the assumptions discussed in Appendix "A", which were accepted for the derivation of Eq. 4.1, additional assumptions are made in describing the boundary conditions for the flow in a fracture. These are :

1. At boundaries where a fluid is in contact with a solid, the fluid velocity relative to the boundary is zero. This implies that there is infinite shear at the boundary.
2. At boundaries where a liquid is in contact with a gas, the shear is assumed to be negligible. This is based on the fact that viscosity of gases are less than that of common liquids by about three order of magnitude.
3. Symmetry of velocity distribution is assumed where there is no reason to postulate a lack of symmetry.

Because all components of u orthogonal to u_i are zero, the right side of Eq. 4.1 can be written as an ordinary second derivative, that is

$$\frac{\mu}{\rho} \frac{d}{dy}\left(\frac{du}{dy}\right) \tag{4.2}$$

The subscript, i, is dropped because u has zero components in orthogonal directions. Therefore, the flow equation for this case is

$$\frac{dP}{dx} = \frac{\mu}{\rho} \frac{d}{dy}\left(\frac{du}{dy}\right) \tag{4.3}$$

Integrating Eq. 4.3 with respect to y gives

$$\frac{dP}{dx}y = \frac{\mu}{\rho}\frac{du}{dy} + C_1 \qquad (4.4)$$

noting that at y = b/2, the value of du/dy is zero, which can be substituted into Eq. 4.4 yielding

$$C_1 = \frac{dP}{dx}\frac{b}{2} \qquad (4.5)$$

Therefore Eq. 4.4 can be written as

$$\frac{dP}{dx}\left(y - \frac{b}{2}\right) = \frac{\mu}{\rho}\frac{du}{dy} \qquad (4.6)$$

or

$$du = \frac{\rho}{\mu}\frac{dP}{dx}\left(y - \frac{b}{2}\right)dy \qquad (4.7)$$

Integrating Eq. 4.7 with respect to y again, the following is obtained :

$$u = \frac{\rho}{\mu}\frac{dP}{dx}\left(\frac{y^2}{2} - \frac{b}{2}y\right) + C_2 \qquad (4.8)$$

Recognizing that at y = b, the value of u is zero. Substituting this condition into Eq. 4.8 leads to C_2=0. Therefore Eq. 4.8 reduces to

$$u = \frac{\rho}{\mu}\frac{dP}{dx}\left(\frac{y^2}{2} - \frac{b}{2}y\right) \qquad (4.9)$$

Now computing mean velocity, $\bar{u}$, between two parallel plates gives

$$\bar{u} = \frac{1}{b}\int_0^b u\,dy \qquad (4.10)$$

Substituting Eq. 4.9 in Eq. 4.10, $\bar{u}$ becomes

$$\bar{u} = \frac{1}{b}\int_0^b \frac{\rho}{2\mu}\frac{dP}{dx}\left(y^2 - by\right)dy \qquad (4.11)$$

or,

$$\bar{u} = \frac{\rho}{2\mu b}\frac{dP}{dx}\int_0^b \left(y^2 - by\right)dy \qquad (4.12)$$

Integrating Eq. 4.12 we get, $\bar{u} = -\frac{\rho}{12\mu} b^2 \frac{dP}{dx}$ (4.13)

So it is seen that the mean velocity between two parallel plates is proportional to the square of the aperture of the fracture. This relationship is known as the "cubic law".

This result can be extended to determine radial flow, Q, towards a well (Refer to Fig. 16) through a fracture by

$$Q = \bar{u} \times (area) \quad (4.14)$$

$$Q = \bar{u} \times (2\pi x b) \quad (4.15)$$

Substituting Eq. 4.13 in Eq. 4.15, gives

$$Q = \left(-\frac{\rho}{12\mu} b^2 \frac{dP}{dx} \right) (2\pi x b) \quad (4.16)$$

or,

$$Q = -\frac{\pi \rho b^3}{6\mu} x \frac{dP}{dx} \quad (4.17)$$

Eq. 4.17 can be rewritten as

$$dP = -\frac{6\mu Q}{\pi \rho b^3} \frac{dx}{x} \quad (4.18)$$

Integrating Eq. 4.18 for the boundary conditions of P_1 and P_2, and R_1 and R_2 for x, the following is obtained

$$\int_{P_1}^{P_2} dP = -\frac{6\mu Q}{\pi \rho b^3} \int_{R_1}^{R_2} \frac{dx}{x} \quad (4.19)$$

or

$$P_1 - P_2 = -\frac{6\mu Q}{\pi \rho b^3} \ln\left(R_2 / R_1 \right) \quad (4.20)$$

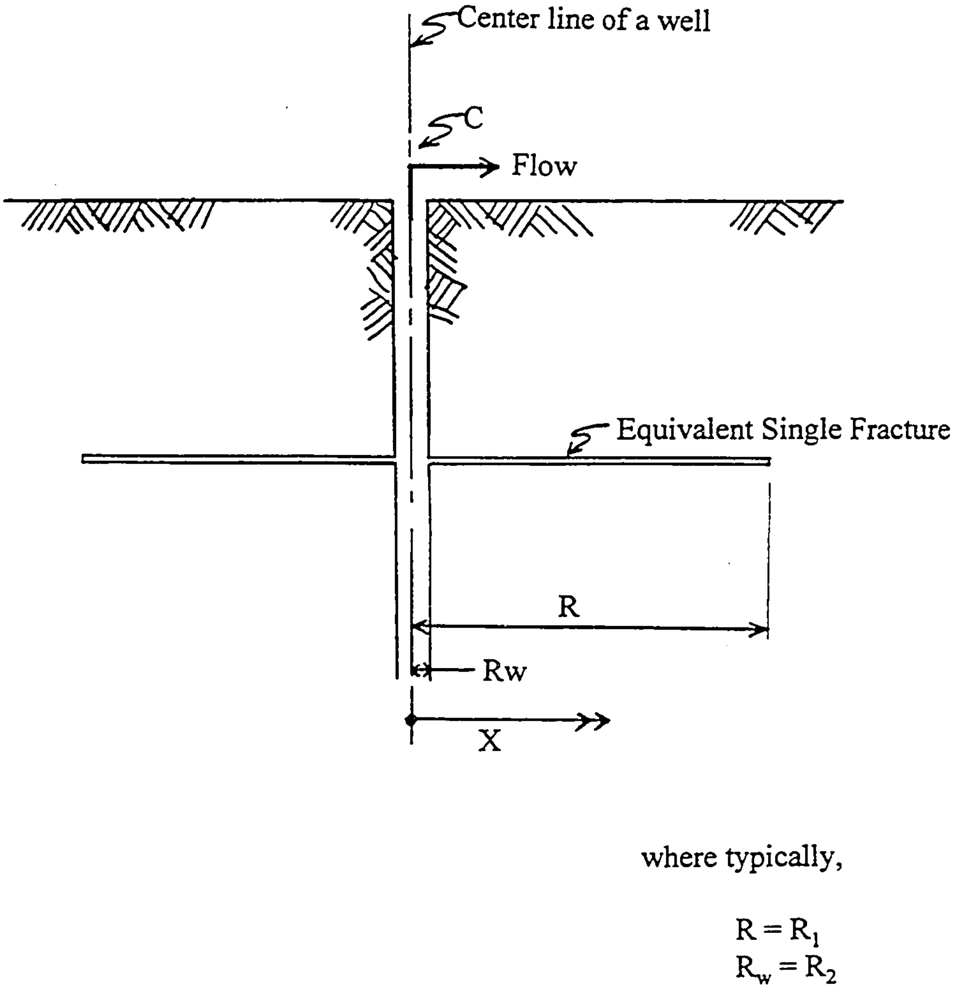

Figure 16 Section Showing radial flow towards an extraction well

If it is assumed that the flow in the fracture is darcian, an expression for volumetric flowrate occurring radially towards a well can be written as

$$Q = -\frac{\pi \rho b^3 (P_1 - P_2)}{6\mu \ln(R_2/R_1)} \tag{4.21}$$

or by

$$Q = -\frac{\pi g b^3 (P_1 - P_2)}{6\nu \ln(R_2/R_1)} \tag{4.22}$$

where, Q= volumetric flowrate (L^3/T)

b= fracture aperture (L)

μ = dynamic viscosity of the fluid ($F\text{-}T/L^2$)

ν = kinematic viscosity of the fluid (L^2/T) = 0.14987 cm^2/sec (for air)

g = acceleration due to gravity (L/T^2) = 981 cm/sec^2

ρ = unit weight of fluid (F/L^3)

P_1, P_2 = pressures at well in height of fluid. (L)

R_1, R_2 = radial distance from extraction well ($R_1 < R_2$) (L)

Gas Compressibility Effects

Further, it was seen in Chapter 3 from Sullivan and Hertel (1940), Muskat (1946), Langfelder (1968), and Zeigler (1976), that for flow of gases, the gradient term P_1-P_2 or ΔP of steady-state fluid systems can be replaced by

$$\frac{(P_1^{1+m} - P_2^{1+m})}{(1+m)P_1^m} \tag{4.23}$$

where m determines the thermodynamic nature of the expansion of a gas as it moves from high to low pressure regions. It is noted m=1 for isothermal expansion of an ideal gas, and for adiabatic expansion m < 1.0.

Substituting Eq. 4.23 in Eq. 4.21 and 4.22, the volumetric flowrate of gas occurring radially towards a well becomes

$$Q = -\frac{\pi g b^3}{6\nu \ln(R_2/R_1)} \frac{\left(P_1^{1+m} - P_2^{1+m}\right)}{(1+m)P_1^m} \tag{4.24}$$

For flow of gas through a fractured formation since there is no significant variation in temperature of the gas, isothermal conditions can be assumed. Therefore volumetric flowrate of gases occurring radially towards a well under isothermal conditions can be written as :

$$Q = -\frac{\pi g b^3 (P_1^2 - P_2^2)}{12\nu P_1 \ln(R_2/R_1)} \tag{4.25}$$

This result is presented as a new expression for analyzing gas flow in fractures. In essence, it is a "cubic law" for radial flow of compressible fluids.

Using the density-pressure relationship defined by Muskat (1934) of $\rho = \rho_0 P^m$ for gases as shown in Eq. 3.17, an alternate form of the above equation can be expressed in terms of the mass flowrate, Q_m, as

$$Q_m = -\frac{\pi \rho b^3 (P_1^2 - P_2^2)}{12\mu P_1 \ln(R_2/R_1)} \tag{4.26}$$

It is interesting to note the amount of error which the omission of compressibility of gaseous fluids introduces in assessment of flow through porous medium. This is summarized in Fig. 17, which compares the percentage error with various pressure differentials. Specifically, this figure was generated by comparing the (P_e - P_w) term for incompressible fluid flow, with $\frac{P_e^2 - P_w^2}{2P_e}$ term for flow of compressible fluids under isothermal conditions. The figure indicates substantial error at high well vacuum and pressure differentials.

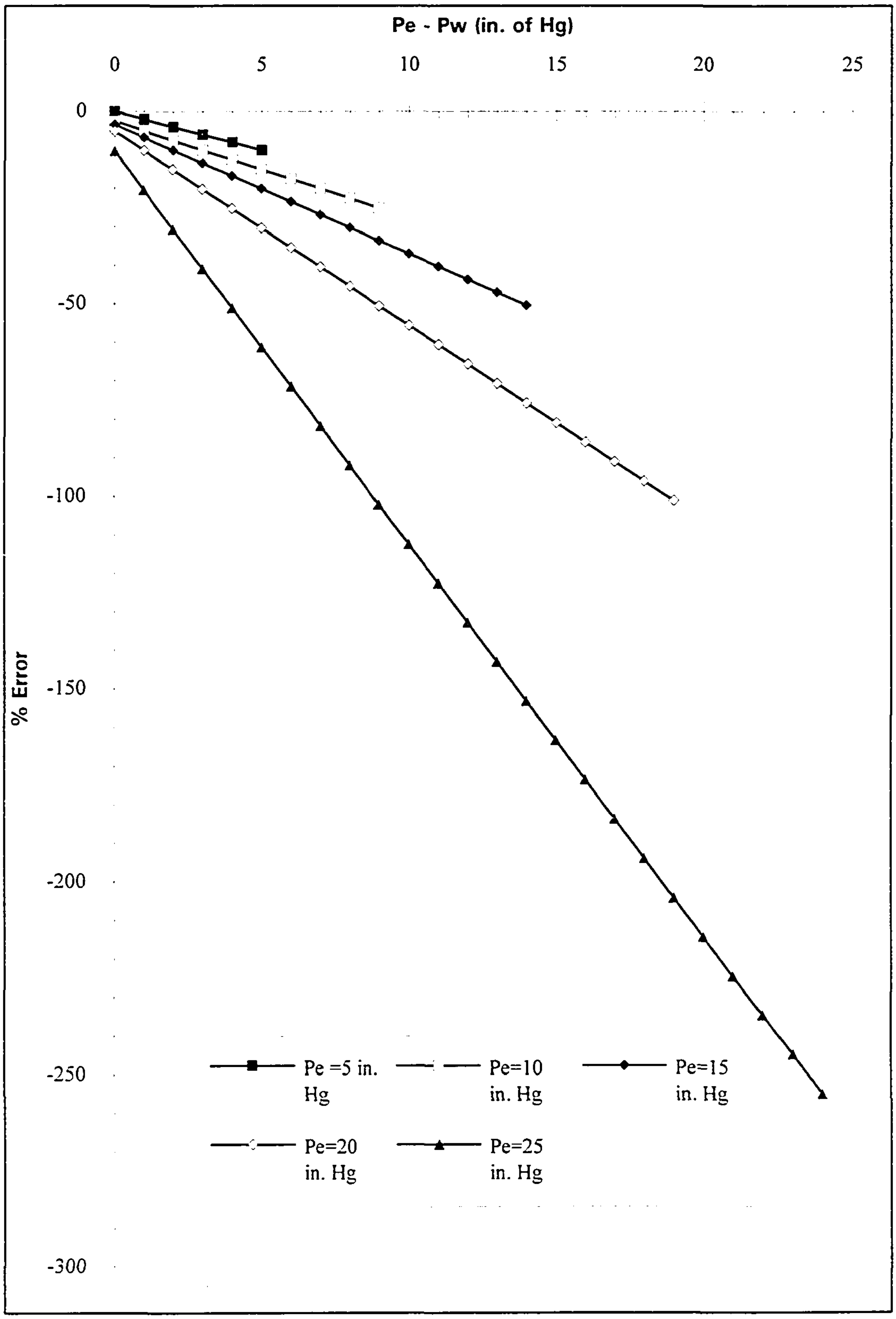

Figure 17 Error in flow computation by neglecting gas compressibilty

Turbulence Effects

While the cubic law is applicable to real fractured rock formations, various investigators [e.g. Huitt (1956), Mises (1914), Nikuradase (1940), Lomize (1951), Wilson and Witherspoon (1970), Louis (1979), Maini (1971). See Chapter 3.] have shown that deviations may be expected from this ideal model. An anomaly that could arise in an ideal fracture flow system is development of turbulence in fluid flow.

Most of these researchers have described fluid flow behavior in fractures in terms of Reynolds number, Re,

$$R_e = \frac{2bu\rho}{\mu} = \frac{2bug}{\nu} \tag{4.27}$$

Studies (e.g. Louis (1969 & 1974), Sharp and Maini (1972), Wilson and Witherspoon (1970). See Chapter-3) shows that for flow between smooth parallel plates, the critical Reynolds number for transition from viscous to turbulent flow may range from 2300 to 2400, but for very rough fractures this transition can occur at a Reynolds number as low as 100 to 300. These studies suggest that when turbulent flow occurs in fractures, the cubic law is no longer valid, and the proportionality of aperture to flow reduces from an exponent of 3 to as low as 1.2. Using these findings, the volumetric flow rate of gases occurring radially towards a well under isothermal conditions can further be modified as

$$Q = -\frac{\pi g b^{e}(P_1^2 - P_2^2)}{12\nu P_1 \ln(R_2/R_1)} \tag{4.28}$$

where e varies from 3 to 1.5 depending on Reynolds number and fracture roughness.

Multiple Fractures

It should be noted that the flowrate discussed above was for volumetric flow assuming a single fracture only. In real applications, multiple fractures typically intersect a borehole. Under such conditions, if say n number of fractures of equal aperture, b_i, intersect a borehole, then the total volumetric flowrate, Q_{Total}, to the well would be

$$Q_{Total} = \sum_{i=1}^{i=n} \left(-\frac{\pi g b_i^e (P_1^2 - P_2^2)}{12 \nu P_1 Ln(R_2/R_1)} \right) \tag{4.29}$$

It is clear from the above equation that for a given flowrate, the cumulative fracture aperture will increase as the number of fractures increase. This effect is illustrated in Table 3, which compares the cumulative apertures for 1, 3, and 6 fractures for the *same* flow.

Table 3 Cumulative aperture vs. number of fractures

Cumulative Aperture (microns)		
1 Fracture	3 Fracture	6 Fracture
516	= (3×357.7) = 1073	= (6×284) = 1704

Klinkenberg Effect

A review of the Klinkenberg effect (Baehr and Hult, 1991), described in Chapter 3, indicates that its omission in estimating air permeability of pneumatically fractured formations would generally result in a maximum error of <10%. This is illustrated in Fig. 18, wherein the region shown corresponds to the zone of most probable error for pneumatically fractured formations. The delineation of this region is based on various site results, which indicate that the permeabilities of a pneumatically fractured formations generally correspond to that of a medium sand, which has a Klinkenberg coefficient of 0.052.

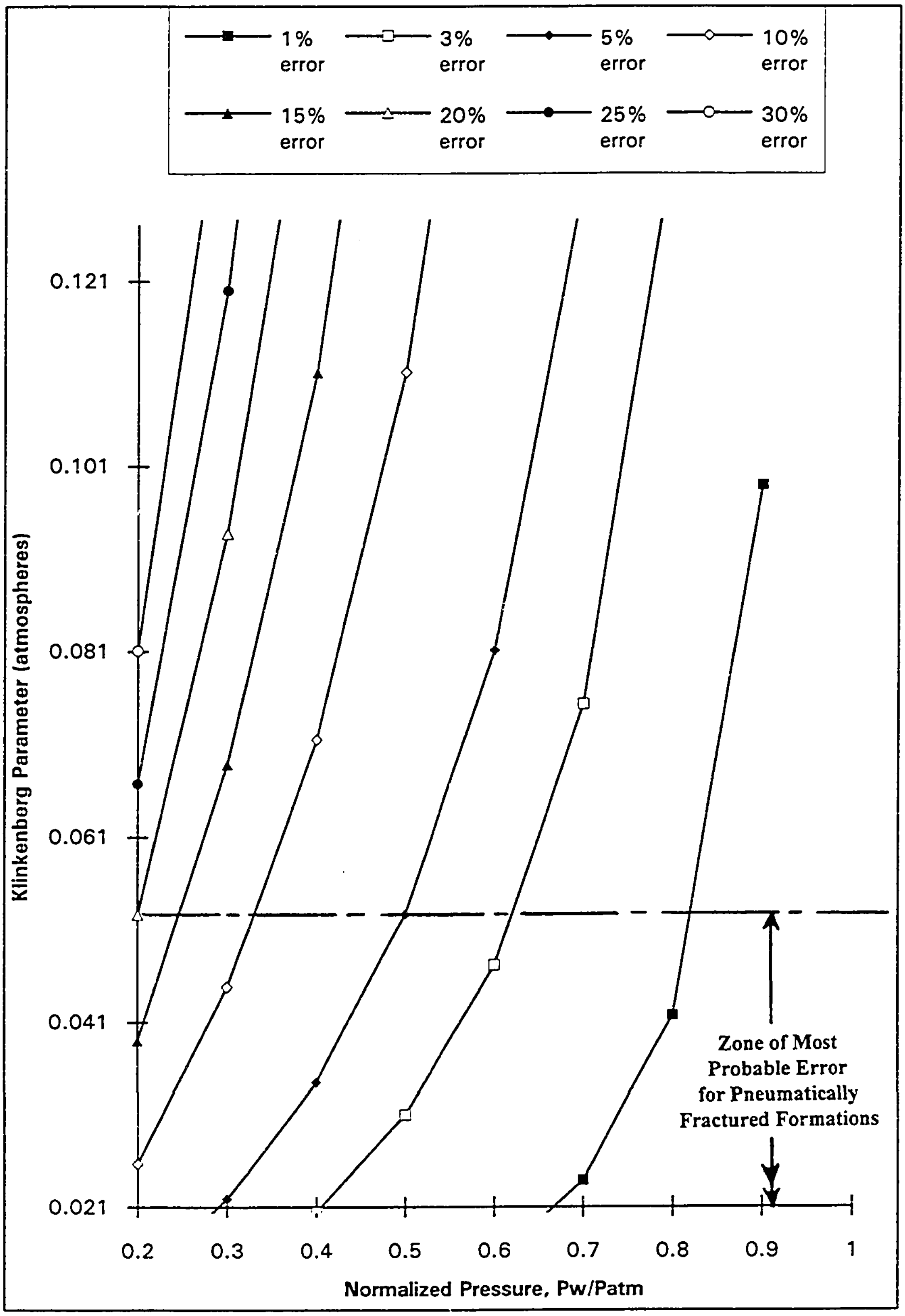

Figure 18 Error resulting in flow computation by neglecting Klinkenberg effect

4.3 Case Study Description

In order to validate the flow model derived in the Section 4.2, the data from a recent field study of pneumatic fracturing was analyzed. This section describes the site characteristics, experimental methodology, and overall field test results. The section which follows, Section 4.4, describes an analysis of the discrete fracture flow for the same case study.

4.3.1 Site Description

The research test site is located in Hillsborough, New Jersey, which is in the west central portion of the state. The test was performed in a consolidated formation of Triassic age which is commonly known as Brunswick formation, although recently it has been renamed the Passaic formation of the Newark Super Group. The stratigraphy of the site can be generally described as three feet of soil fill overlying siltstone. The predominant joint set was nearly horizontal, corresponding to the formation dip which is approximately five degrees west. The rock within the treatment zone was typically only slightly weathered, and core recovery ratios were usually good and exceeded 90%. The rock structure is intensely jointed, however, as indicated by the RQD's which were typically less than 25%. Some of the joints showed evidence of weathered clay products on their surfaces and infrequent vugs and carbonate fillings were also noted.

The phreatic ground water surface was located at a depth of 22 feet below the ground surface during the time of the test. All drilling and fracture operations were limited to the vadose zone, and were carried out above a depth of 18 feet. A perched water zone was encountered during the test from 12 to 18 feet, which necessitated frequent dewatering during the test operations.

The test site was formerly occupied by a manufacturing facility which resulted in contamination of the fractured siltstone and the groundwater with trichloroethylene

(TCE) and other Volatile Organic Compounds (VOC's). From the existing studies, it was clear that TCE was present in both the groundwater and the vadose zone, with concentrations of TCE in the soil gas perhaps reaching several hundred ppmv, and concentrations in the groundwater in the < 100 ppm range. In order to remediate the site, removal of the VOC's in the vadose zone was necessary since they formed a source which gradually leached into the underlying ground water. Site characterization and feasibility tests at the site showed that the formation permeability was too low for conventional vapor extraction to be effective. Prior to the decision to apply pneumatic fracturing at the site, the remediation options under consideration were costly excavation and removal of the source area, or encapsulation of the source area with a slurry wall.

4.3.2 Experimental Methodology

The pneumatic fracturing field test was sponsored by the U.S.EPA under the Superfund Innovative Technology Evaluation Program (SITE). Fig. 19 shows the layout of the wells employed in the tests. A central well FW was installed which served as both the fracture well and the main vapor extraction well. It was surrounded by seven monitoring wells which range from 7.5 to 20 feet from the central well. All wells were cased to a depth of 8 feet (see Fig. 20), but remained uncased in the treatment zone to assure maximum connection with the formation. All wells terminated at a depth of 18 feet which was approximately 4 feet above the ground water table. As indicated on the figure, the wells were oriented along the strike and dip of the formation to examine possible effects of geologic structure on fracturing.

The general experimental approach was to monitor the changes in subsurface airflow and VOC mass removal rate which resulted from the fracturing. Prior to any fracturing activities, baseline behavior was established by extracting air from the

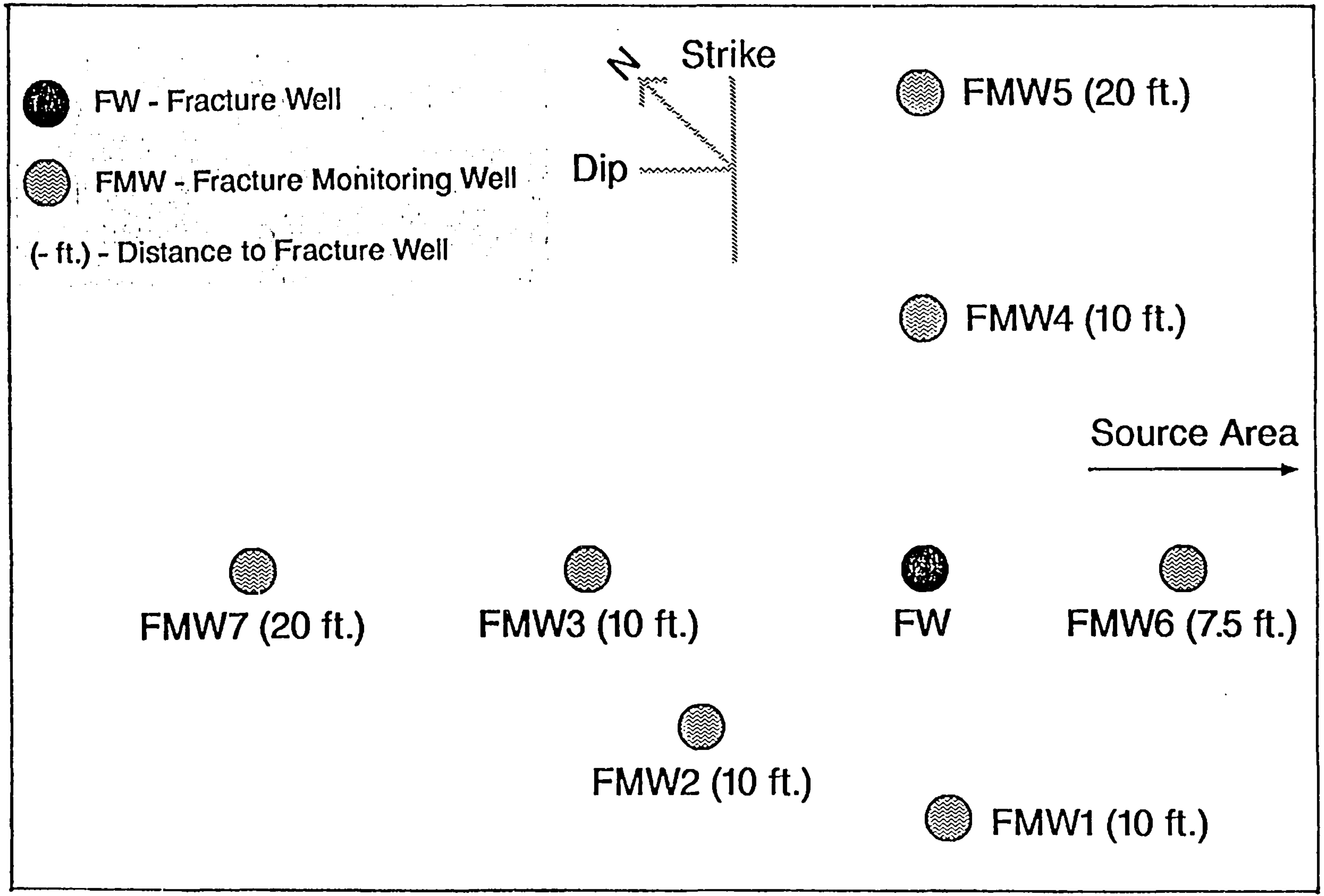

Figure 19 Well layout plan, Hillsborough test site (H.T.S.)

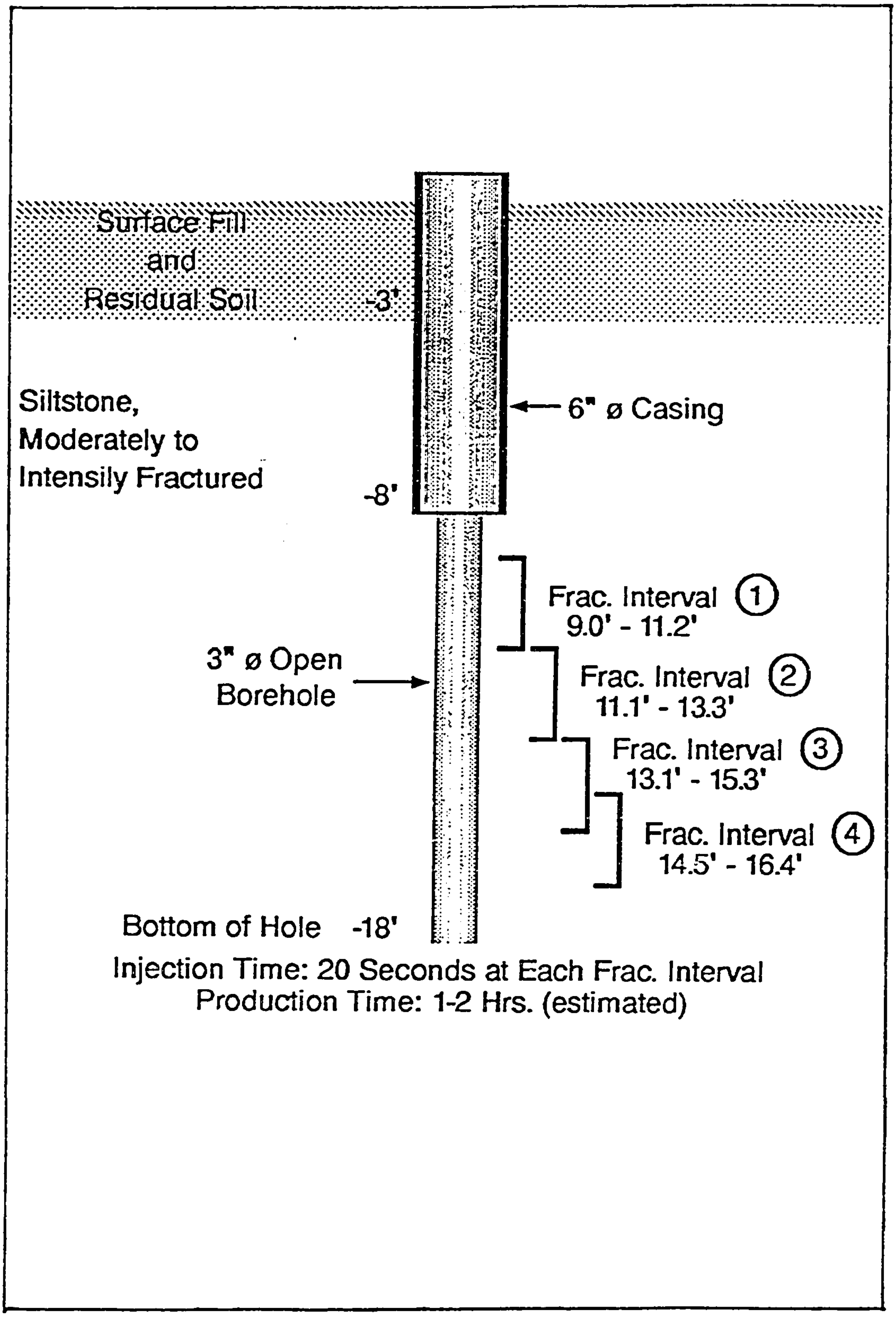

Figure 20 Fracture well detail, H.T.S.

central well as well as each individual monitoring well. Extraction tests were run both with all wells sealed to measure vacuum radius of influence, as also with selected wells uncapped to evaluate the effects of passive air inlet into the formation. To measure VOC removal rate, cumulative samples were collected and analyzed with a field gas chromatograph.

After baseline behavior was established, a series of four pneumatic fracture injections were made at successively deeper intervals ranging from 9.0 to 16.4 feet below grade. Each injection lasted about 20 seconds and was applied to discrete two foot intervals. During injection, pressure gauges were mounted on the outlying monitoring wells to provide an indication of the lateral extent of the pneumatic fractures. Also, a pressure transducer was used to monitor the pressure within the fracture interval in the FW borehole. Another method used to estimate fracture radius was measurement of ground surface heave using electronic tiltmeters and surveyors levels. Direct examination of the effects of the fracture injections on the bedrock formation were made with a borehole video camera. The camera was used to record the condition of the fracture well both before and after the pneumatic injections.

After completion of the pneumatic fracturing, the extraction tests on the fracture well and the monitoring wells were repeated to evaluate change in flow rate and TCE mass removal rate from the formation. The results of these tests were then compared with the baseline values to evaluate the effects of the pneumatic injections.

4.3.4 Analysis of Total Well Air Flows

The time history of air flow from the central extraction well FW is Shown in Fig. 21. This represents the results of test runs performed over a period of several days which are shown in continuous time for convenience. These tests were performed with a source vacuum of 136 inches of water and all outlying monitoring wells were sealed during these tests. Fig. 22 shows the average air flows for each of the tests.

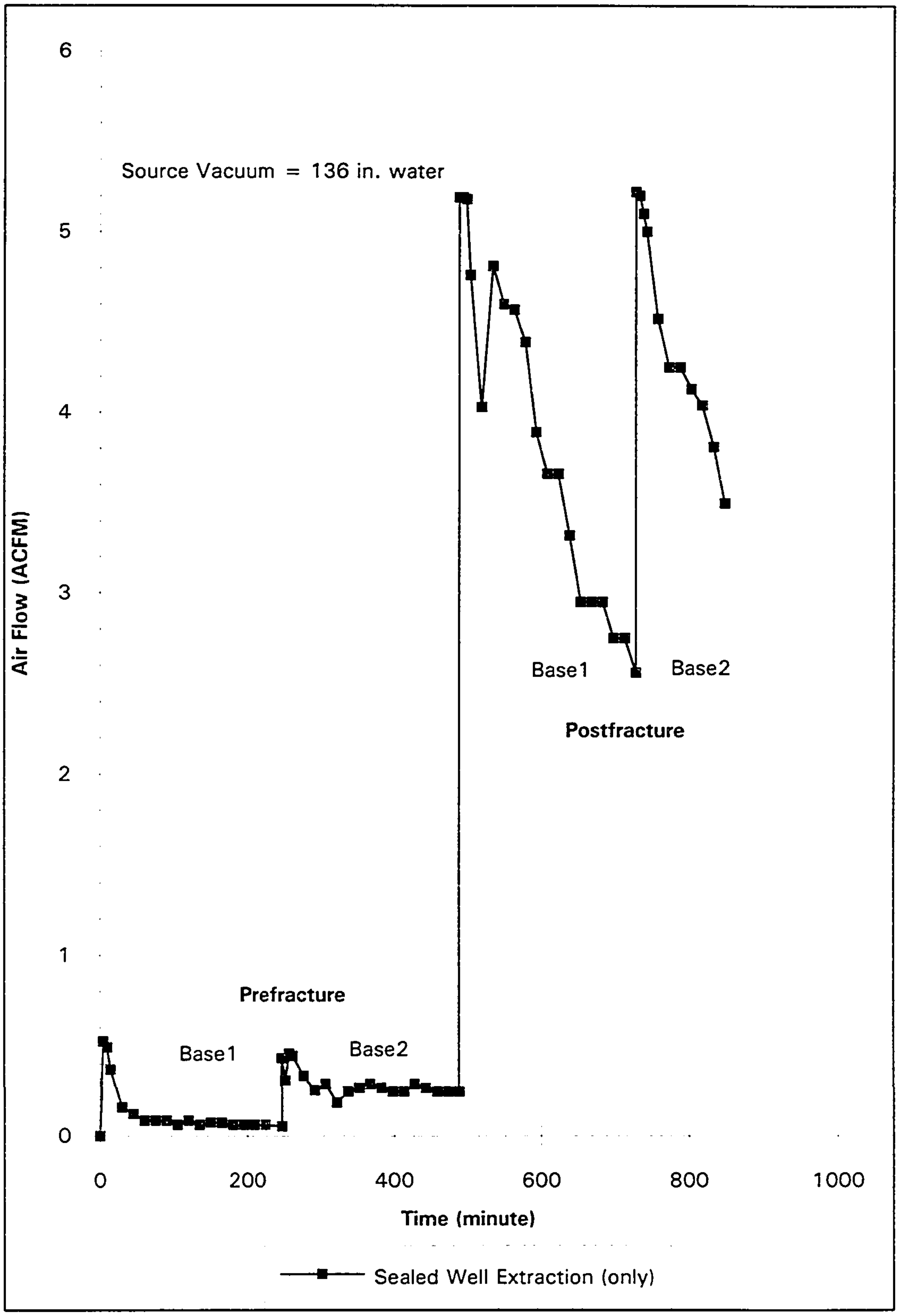

Figure 21 Air flow time history for fracture well (FW), H.T.S.

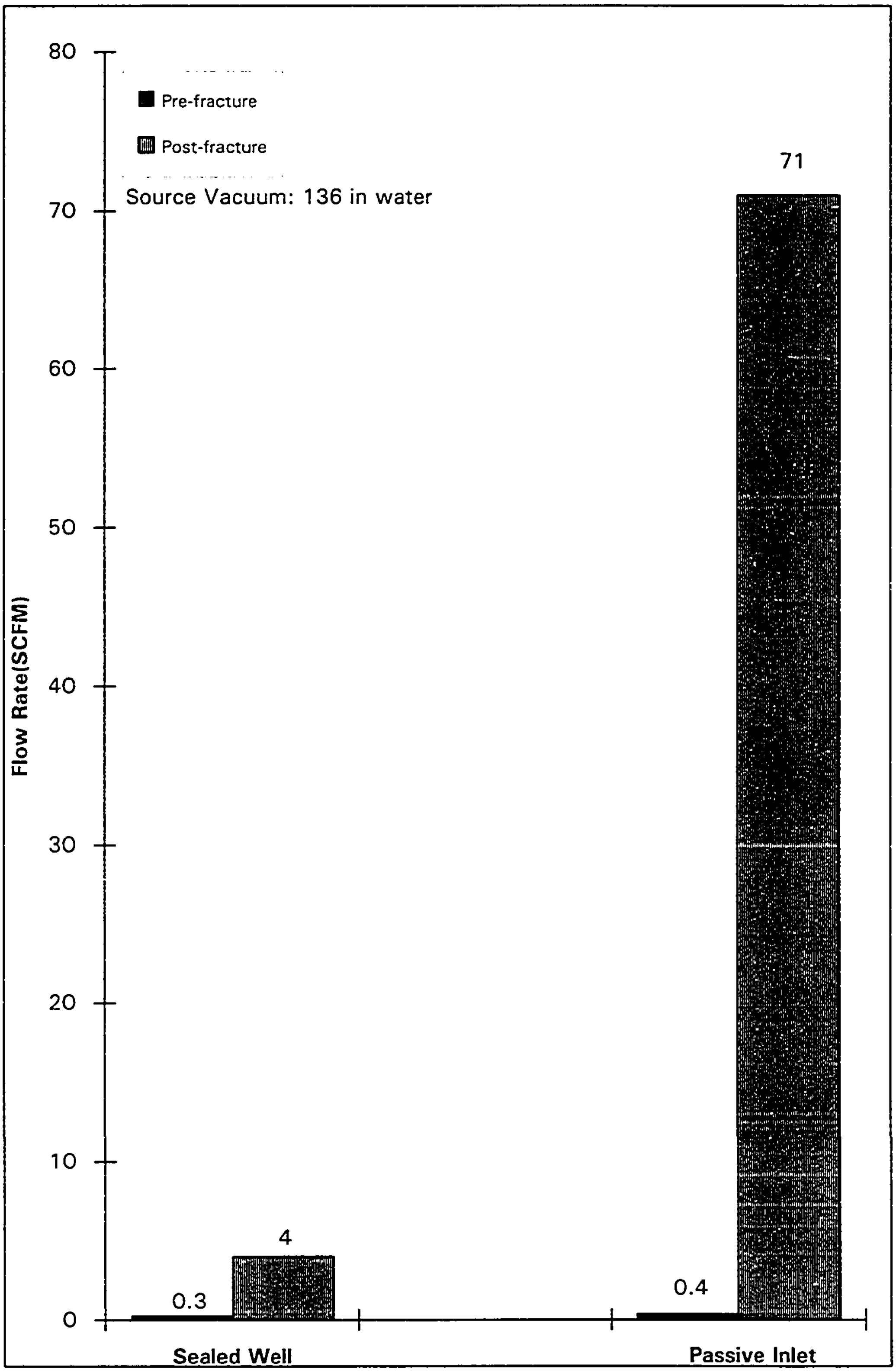

Figure 22 Average extracted air flow from fracture well (FW), H.T.S.

These data show that the pneumatic fracture injections had substantial influence on formation permeability and air flow. On average, the extracted air flow increased 13 to 178 times compared with the prefracture baseline for the sealed well and passive inlet extraction condition, respectively. It is noted that steady state flow conditions were attained relatively rapidly due to the jointed nature of the formation. The slowly declining flow values shown in the time history are attributed to the migration of perched water towards the test area while the system was under vacuum. As indicated, the well flows recovered after each periodic dewatering.

All of the peripheral monitoring wells exhibited improved vacuum pressure communication with a central fracture extraction well. The pressure response of monitoring wells MW5 is shown in Fig. 23. As indicated, sensible vacuum increased substantially. Extraction tests performed on each individual monitoring well further confirm the extent of the pneumatic fractures. As shown in Fig. 24, extracted air flows from the monitoring wells increased substantially from 13.5 to 64 times. These data confirm that the increase in formation permeability resulting from the pneumatic fracture injections extended over the entire test area. It is noted that surface heave data recorded by the electronic tilt meters showed that the pneumatic fractures propagated up to 35 feet from the injection point, but these larger radii could not be confirmed with flow and vacuum measurements since the farthest monitoring well was 20 feet.

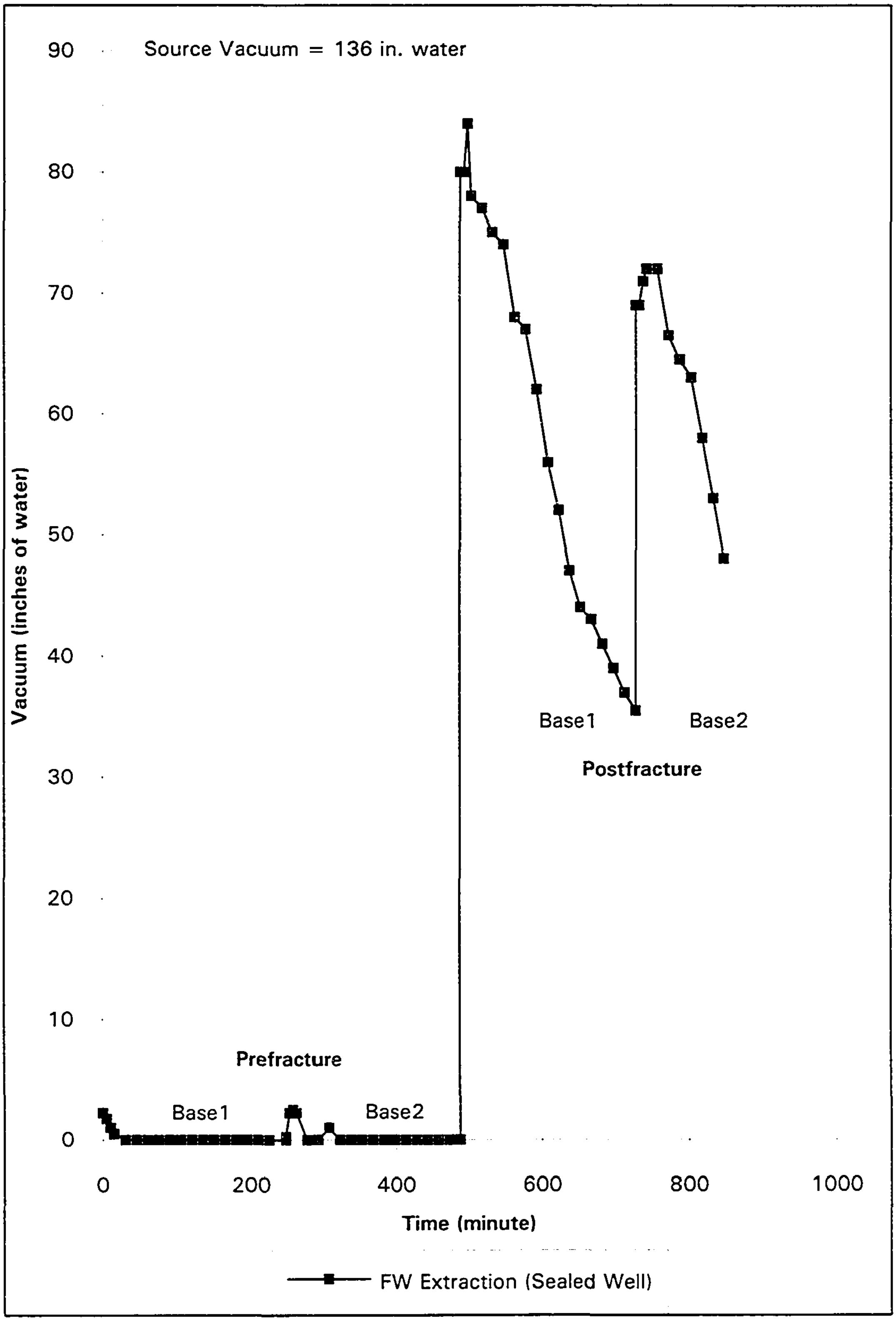

Figure 23 Pressure time history at MW5, H.T.S.

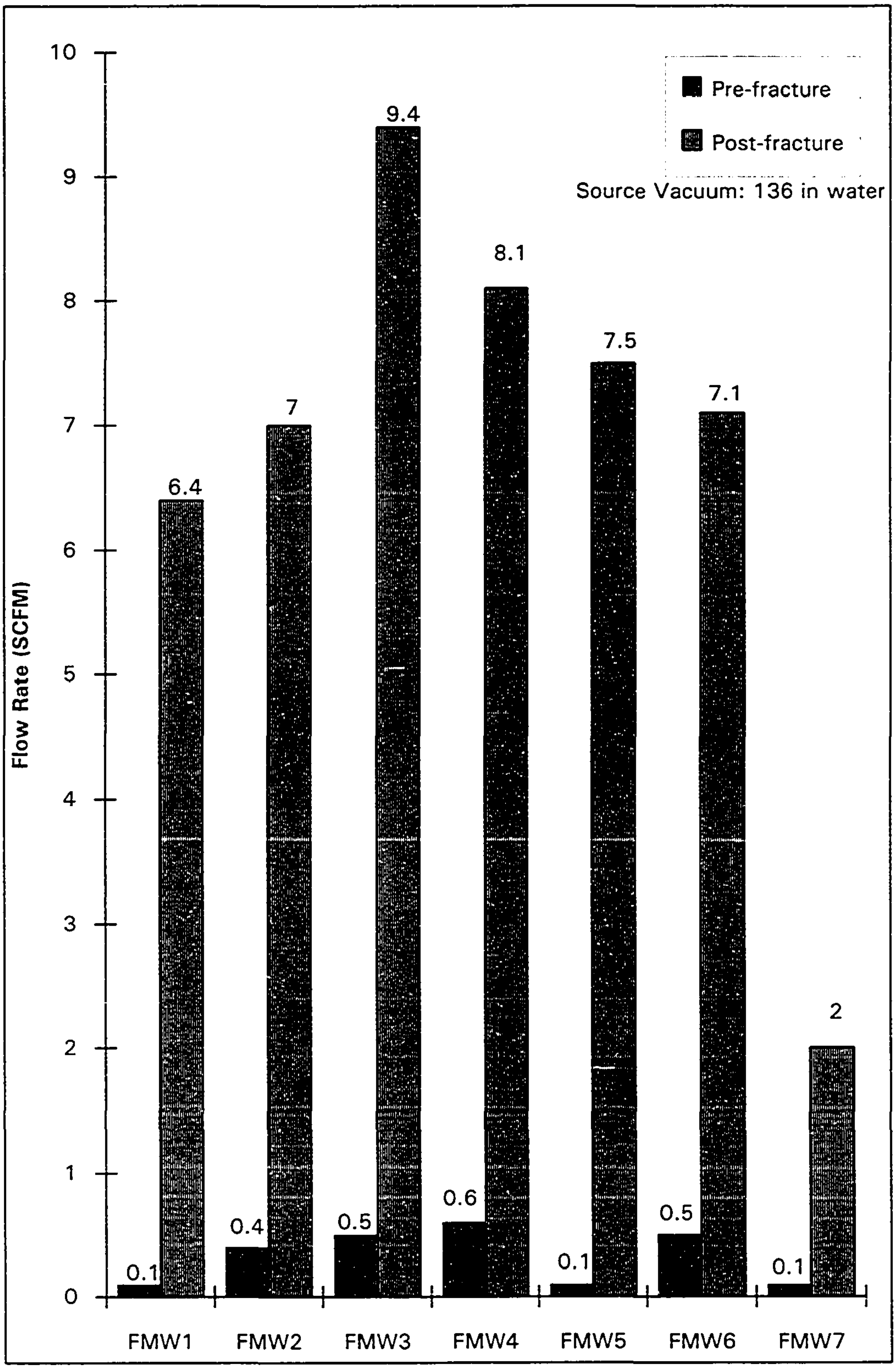

Figure 24 Air Flow enhancement for various MW's, H.T.S.

4.4 Analysis Of Case Study Data

4.4.1 Estimation of Fracture Aperture

An examination of the rock core samples and the video tape from the borehole camera confirmed that the primary permeability of the formation was negligible, and that the developed air flow was occurring within a network of discrete fractures. Since transport mechanisms within fractured media are dependent on the geometry of the fractures, a physical model of the fracture system around the extraction/ fracture well was developed. Specifically, the spacing and aperture of the pneumatically induced fractures were estimated based on available site data. Several different methods were used to confirm the physical model.

The first method was to analyze the pressure and flow data using the P.F. flow model to determine the magnitude of the fracture apertures in the siltstone formation. Apertures were calculated at each well location assuming that a single "equivalent" fracture intersected the well bore. Adjustments for multiple fracture intersections were also made, and are discussed in section 4.4.3, "Video Analysis of Fractures".

A summary of the calculated apertures is presented in Table 4. The apertures were estimated from eight different well locations for three general conditions: prefracture, postfracture and fracture injection. It is noted that multiple tests were available for some of these conditions. This existing data base allowed the aperture at any single well location to be cross-checked by at least seven or more independent calculations. Sample calculations for the Table 4 are contained in Appendix C.

A review of the data in Table 4 shows some very significant trends. First, the fracture aperture at all well locations increased substantially during the fracture event. The average prefracture aperture for the entire site, b_s, was 86 microns, which increased to 516 microns in the postfracture analysis. This represents a 6.0 times increase in average fracture aperture over the test site. Fig. 25 shows a contour plot of

Table 4 Single "equivalent" fracture aperture calculation summary
Hillsborough Test Site

Extraction Test From	Fracture Aperture (microns) at Locations								Avg. "b" (entire site)
	FW	MW1	MW2	MW3	MW4	MW5	MW6	MW7	
Prefracture									
FW-Base 1 (SW*)	69	65	65	70	67	68	76	68	
FW-Base 2 (SW)	94	89	90	95	93	93	103	93	
MW1 (SW)	74	74	72	76	77	79	75	78	
MW2 (SW)	87	85	87	85	91	93	90	89	
MW3 (SW)	68	70	67	68	70	72	71	68	
MW4 (SW)	104	109	109	107	105	104	106	110	
MW5 (SW)	68	69	69	68	64	64	68	69	
MW6 (SW)	119	113	116	117	114	118	115	118	
MW7 (SW) **	73	74	72	70	74	75	75	70	
FW (Passive) **	112	112	112	113	113	118	110	118	
Avg. "b"	**85**	**84**	**84**	**86**	**85**	**86**	**88**	**87**	*86*
Postfracture									
FW-Base 1 (SW*)	363	367	376	373	355	309	342	356	
FW-Base 2 (SW)	370	375	377	379	369	363	352	349	
MW1 (SW)	458	470	473	508	480	434	478	443	
MW2 (SW)	543	629	583	672	577	491	561	490	
MW3 (SW)	631	826	892	678	606	453	655	584	
MW4 (SW)	663	813	750	876	750	531	931	625	
MW5 (SW)	425	467	454	464	445	445	455	415	
MW6 (SW)	488	560	571	580	518	448	522	468	
MW7 (SW) **	200	207	201	196	207	207	209	196	
FW (Passive) **	771	774	774	774	774	813	757	813	
Avg. "b"	**493**	**563**	**560**	**566**	**512**	434	537	466	*516*
FW Injection									
9'-11'	1632	1531	1383	1448	1797	1452	2002	1349	*1574*
11'-13'	1422	1410	1410	1355	1410	1298	1528	1333	*1396*
13'-15'	2090	2207	2207	1937	2207	1406	1893	1406	*1919*

* SW ⇔ Sealed well extraction condition.

** Fracture aperture values calculated from these tests not included in the calculation of average fracture aperture.

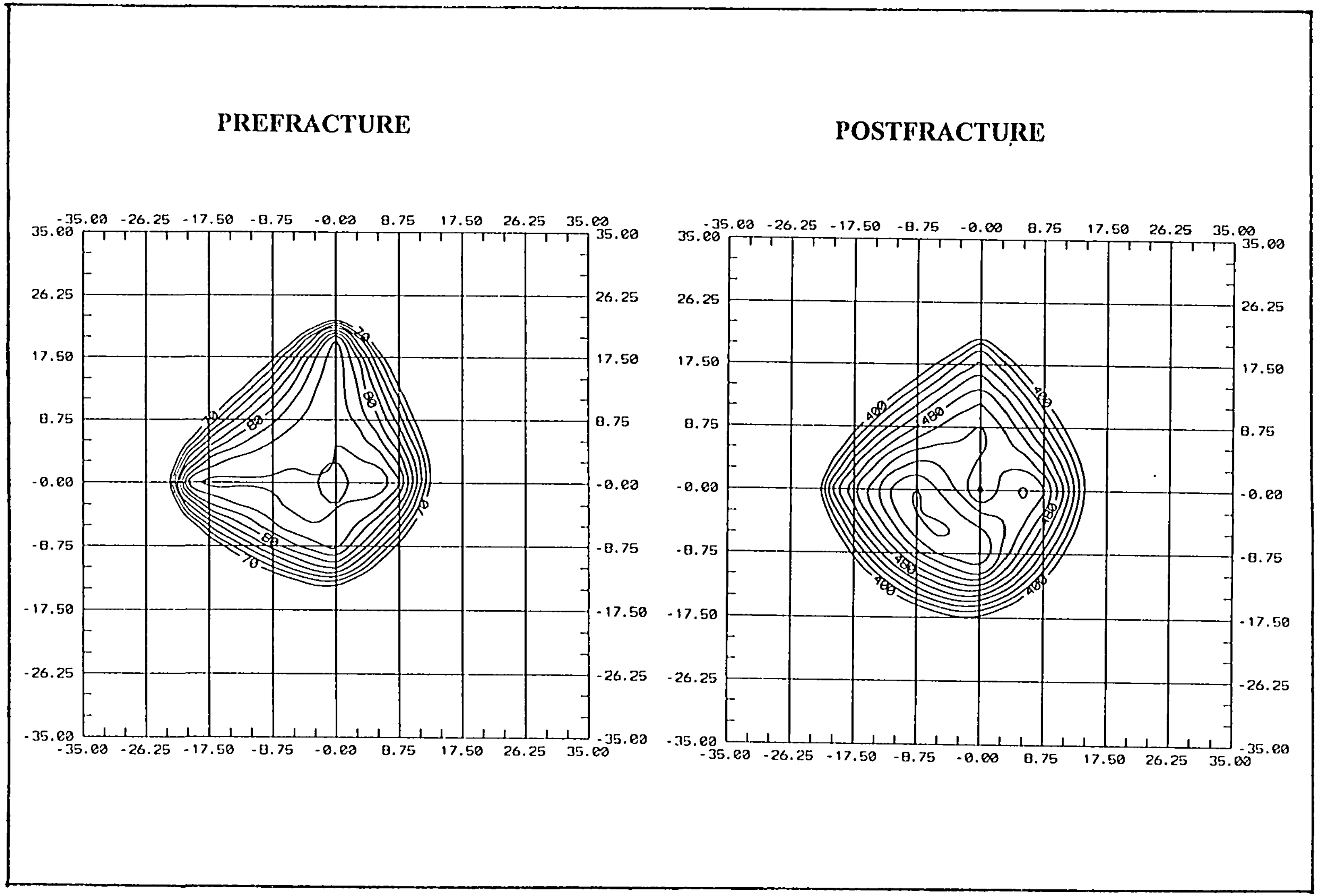

Figure 25 Contour plot of single "equivalent" fracture aperture

the estimated "equivalent" single fracture aperture under prefracture and postfracture conditions.

A second important trend in the data is the moderate degree of statistical variability of the calculated aperture. The computed variations from the average are presented in Table 5. As indicated, the maximum variation for the prefracture condition was +39.9 % to -25.6 %, and for the postfracture condition was +73.4 % to -36.4 %. These variations are considered modest compared with the complexity of the field test, i.e. geologic heterogenities, moisture effects, and pressure/ volume measurement precision. These statistical data also provide a general validation of the P.F. Flow Model.

Another remarkable trend of the data analysis is the constancy of estimated aperture across the test area. For the prefracture condition, all estimated average apertures at different well locations were within a range of ± 2.5%, and for the postfracture condition, the range was +10% to -16%. This demonstrates that the fracture aperture is relatively constant across the test area i.e., there is little evidence of fracture tapering. It is noted that the farthest monitoring well was 20 feet from the injection point, and tiltmeter data did show that fractures propagated in excess of a 30 foot radius.

Apertures calculated during the fracture injection events are also summarized in Table 4. As may be expected, the injection apertures are considerably larger than the postfracture apertures. This may be explained by the heaving and dilation of the formation during fracture injection. It is noted that these calculated fracture injection apertures are considerably less than the average surface heave observed during fracture injection which ranged from 0.246 to 0.375 inches (6248 to 9525 microns). This disparity is apparently due to the fact that the fracture injection event involves pseudo-static pressurization and dilation of the formation, and cannot be analyzed based solely on discrete fracture flow.

Table 5 Summary of variation from average fracture aperture "b"
Hillsborough Test Site

Extraction from	Percent variation from "b" at location								Stat.Cal.	
	FW	MW1	MW2	MW3	MW4	MW5	MW6	MW7	Avg.	Std. Dev.
Prefracture										
FW-Base 1 (SW*)	-19.7	-22.9	-22.8	-18.4	-21.7	-21.1	-13.7	-21.4	-20.2	2.9
FW-Base 2 (SW)	10.2	5.9	6.5	11.1	8.9	7.2	17.1	6.9	9.2	3.4
MW1 (SW)	-13.3	-12.7	-14.5	-11.8	-9.0	-8.2	-14.9	-9.9	-11.8	2.3
MW2 (SW)	2.0	0.8	2.8	-0.8	6.7	7.8	2.2	2.8	3.0	2.7
MW3 (SW)	-20.3	-17.0	-20.6	-20.5	-17.7	-16.5	-19.3	-21.5	-19.2	1.7
MW4 (SW)	21.9	29.2	29.3	24.5	23.6	20.4	20.3	27.0	24.5	3.4
MW5 (SW)	-20.7	-17.8	-17.9	-20.6	-24.3	-25.6	-22.9	-20.2	-21.3	2.6
MW6 (SW)	39.9	34.5	37.3	36.3	33.6	36.1	31.2	36.2	35.6	2.4
MW7 (SW) **	-14.0	-12.4	-14.6	-18.5	-13.1	-13.3	-14.9	-19.3	-15.0	2.4
FW (Passive) **	31.0	32.8	33.1	31.2	32.2	36.4	25.0	36.4	32.3	3.4
Postfracture										
FW-Base 1 (SW*)	-26.4	-34.8	-32.8	-34.2	-30.7	-28.9	-36.4	-23.7	-31.0	4.1
FW-Base 2 (SW)	-24.8	-33.4	-32.6	-33.0	-28.0	-16.5	-34.4	-25.1	-28.5	5.8
MW1 (SW)	-7.0	-16.7	-15.5	-10.3	-6.3	0.0	-11.0	-5.0	-9.0	5.2
MW2 (SW)	10.2	11.6	4.3	18.6	12.6	13.1	4.4	5.1	10.0	4.8
MW3 (SW)	28.1	46.6	59.4	19.7	18.1	4.3	22.0	25.3	27.9	16.2
MW4 (SW)	34.6	44.3	33.9	54.7	46.4	22.3	73.4	34.0	42.9	14.7
MW5 (SW)	-13.8	-17.1	-18.8	-18.0	-13.2	2.5	-15.3	-10.9	-13.1	6.4
MW6 (SW)	-0.9	-0.5	2.1	2.5	1.0	3.2	-2.7	0.3	0.6	1.9
MW7 (SW) **	-59.5	-63.3	-64.1	-65.4	-59.6	-52.2	-61.0	-57.9	-60.4	3.9
FW (Passive) **	56.4	37.4	38.3	36.7	51.0	87.2	41.0	74.4	52.8	17.7

* SW ⇔ Sealed well extraction condition.

** Fracture aperture values calculated from these tests not included in the calculation of average fracture aperture.

Notes:

A number of factors may have affected the variation in test results shown above. The following specific field observations were noted :

Prefracture

(1) MW6 showed the highest degree of connectivity with FW compared with the other monitoring wells.

(2) Some perched water accumulated in wells during FW baseline extraction which necessitated periodic dewatering

Postfracture

(1) MW4 showed the highest degree of connectivity with the FW compared with the other monitoring wells.

(2) Perched water continued to accumulate in wells during postfracture baseline extraction which necessitated periodic dewatering. Accumulation rate greater than for prefracture tests. MW5 had highest rate of perched water recharge.

(3) Surface heave data showed limit of fracture propagation to the west was 20 to 25 feet. This correlates with the reduced connectivity observed in MW7.

4.4.2 Assessment of Turbulence

For laminar flow conditions, the PF flow model assumes a cubic exponent for the aperture (the cubic law). In order to assess possible turbulence effects, the air velocities and associated Reynolds numbers were calculated for all the test conditions assuming that a single "equivalent" fracture intersected the borehole. Similar calculations were also performed for the case assuming six equal fractures intersected the borehole. These are presented in graphical form in Appendix D, and a sample plot is shown in Fig. 26. These data were compared with the transition values of laminar to turbulent flow determined by various investigators as described in section 3.4 "Investigation of Flow Through Fractured Formation : Chronological History". It is noted that transition values found by various investigators for fractures with rough surfaces ranged from 100 to 300.

It is clear from these data that laminar conditions existed during all prefracture testing since the Reynolds numbers are typically less than 100. For the postfracture tests, however, the higher flow velocities may have resulted in slight turbulence at some locations within the fracture zone. For the postfracture sealed well condition, Reynolds numbers as high as 1000 were recorded in immediate vicinity of the extraction well, although values dropped to below 100 at radii greater than 2 ft. This is not an unusual occurrence, as most higher capacity pumping wells experience some localized turbulence around the well bore. It is believed that the effects of turbulence for this test condition was minimal, since the calculated aperture does not vary significantly from the average value.

A review of the postfracture, passive inlet condition, however, indicates that the turbulence effects were more significant. As depicted in Fig. 26, the Reynolds number in the entire test zone ranged from approximately 100 to 20,000, which is clearly within the turbulent range. Given this degree of turbulence, it was speculated that the cubic law may not have been applicable for this test condition. It was also

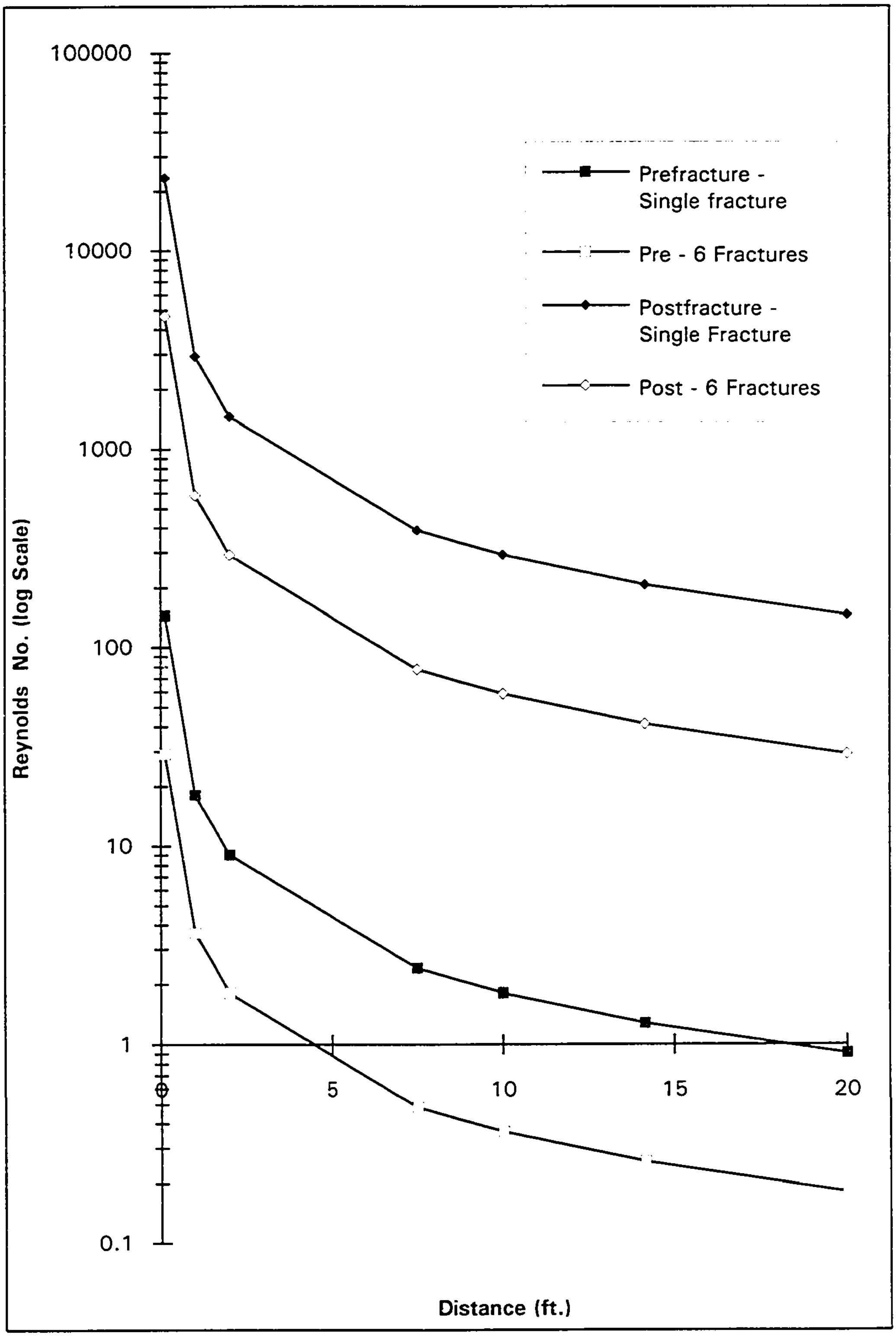

Figure 26 Reynolds number vs. radial distance (FW, passive inlet), H.T.S.

noted that the calculated aperture using the cubic law, for the test for postfracture condition did not correspond to the average aperture value.

The data from this test was therefore utilized to assess the effect of turbulence on the P.F. Flow Model. By using Eq. 4.28, the aperture exponent was regressed using the postfracture passive inlet condition, as shown below:

$$b^e = -\frac{12\nu Q \ln(R_2/R_1)}{\pi g} \frac{P_1}{(P_1^2 - P_2^2)} \tag{4.30}$$

Substituting the following values, corresponding to passive inlet test, in Eq. 4.30:

b = single "equivalent" fracture aperture = 516 microns = 0.0516 cm

b = six "equivalent" fracture aperture = 284 microns = 0.0284 cm

Q = 87.18 cfm = 41144.38 cm^3/sec;

P_1 = 70.5 "H2O = 0.8266 atm = 665938 cm of air

P_2 = 1 atm = 805635 cm of air

R_2 and R_1 as 10 ft. and 1.5 inches respectively

ν = 0.14987 cm^2/sec for air at 15 °C, and g = 981 cm/sec^2

the exponential power, e, is found equal to 2.7 for a single "equivalent" fracture and 2.75 for six "equivalent" fractures..

It is interesting to note that the reduced exponent values are an indication of slightly turbulent flow, and fall within the ranges given by Louis(1979) of 1.5 to 3.0, and by Sharp and Maini (1972) of 1.2 to 3.0. It was therefore concluded that pneumatically induced fractures have apertures which are sufficiently large so that the flow is no longer laminar for some extraction conditions.

It is noted that even higher levels of turbulence were developed during fracture injection conditions since Reynolds number ranged from 3,000 to 500,000 (see Appendix D). Regression analysis of this condition using Eq. 4.30 resulted in extremely large exponents (>100) which indicates that the model is not valid for pneumatic fracture injection. The result further suggests that the surface heave during injection is partly the result of "pseudo - static" pressurization and subsequent dilation of the formation, and cannot be represented by the continuous flow model used for the sealed and passive inlet extraction condition.

4.4.3 Video Analysis of Fractures :

As stated previously, the fracture aperture calculations in the previous two sections were based on the assumption of a single equivalent fracture. In order to evaluate the effects of multiple fractures intersecting the borehole, a detailed analysis of borehole video was conducted. Both prefracture and postfracture videos were recorded using 360^0 fish-eye lens, and with/without side scan mirror.

Based on this examination, fractures were mapped along the length of the borehole. Fractures were divided into three principal categories based on the video : major, medium, and minor. In addition, the continuity of the fracture around the borehole was noted. It is important to note that this assessment was based on the relative comparison of the aperture of the fracture visible at the fracture borehole walls only. An obvious limitation of the borehole mapping technique is the uncertainty of the fracture dimensions and continuity away from the borehole within the rock mass. It is also acknowledged that the drilling activity and packer inflation process may have locally altered the natural fractures present in the borehole. In spite of these limitations, the quantitative assessment of the borehole video is considered to be a general representation of the fracture aperture pattern.

The results of the video mapping are presented in Fig.27, which compares the prefracture and postfracture conditions. This figure illustrates the qualitative effects of the pneumatic fracture injection. Comparison of the prefracture and postfracture logs indicate that the most significant influence observed due to fracture injection are dilation of the existing fractures, and improvement of fracture connectivity and

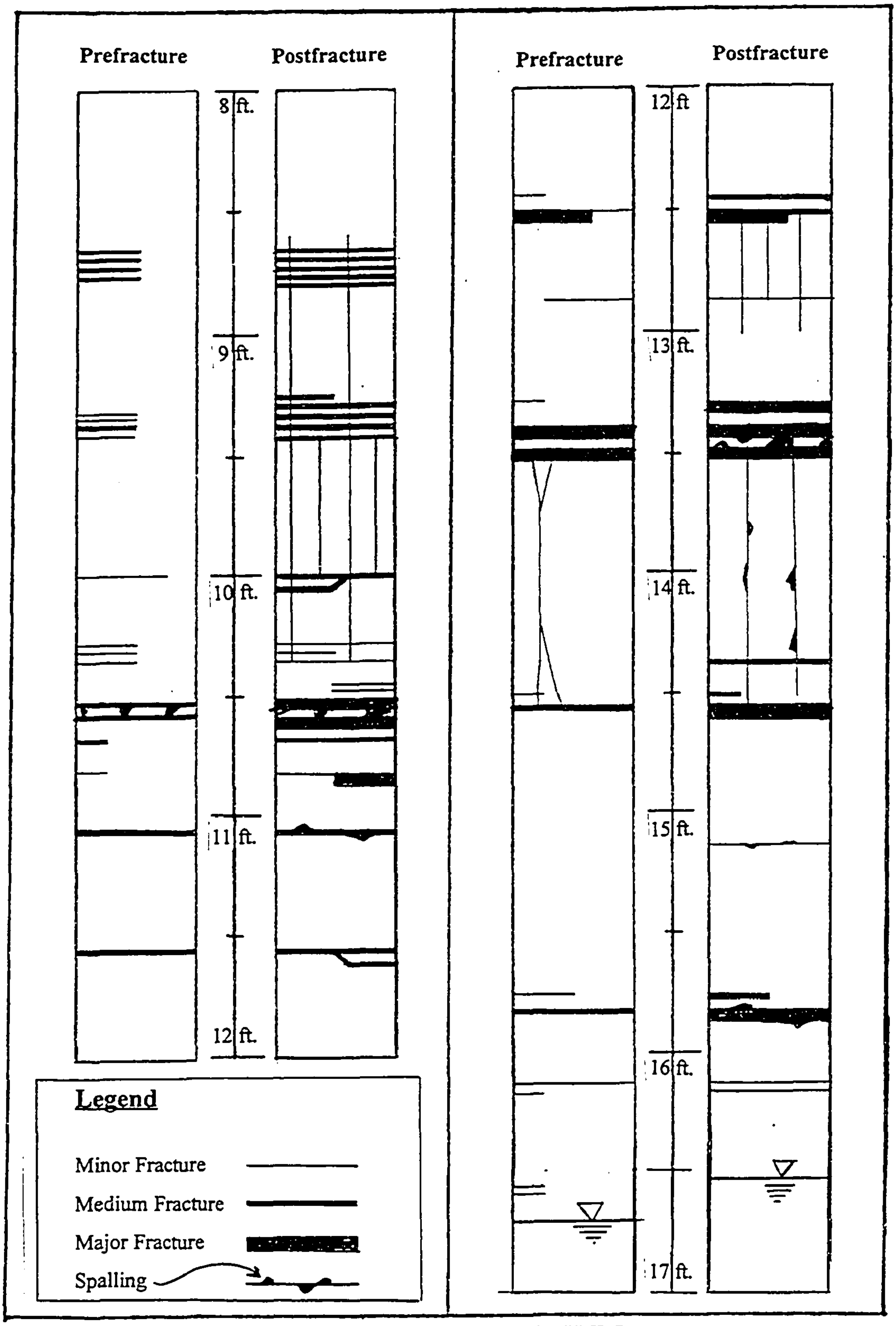

Figure 27 Fracture well profile from video analysis, H.T.S.

continuity. There also appears to be some minor amount of new fractures created both horizontally and vertically. It is noted that the "new" horizontal fractures tended to form along existing fracture zones, while the new vertical fracture tended to connect adjacent sets of horizontal fractures. However, no new vertical fractures were observed to extend beyond the injection interval.

In order to estimate the relative amount of air flow through different fracture zones, a scale was used to measure the fracture aperture. Based on the entire borehole profile, the following multiplier factors were established to quantify the aperture categories: minor (X), medium (3.7X), major (7.2X).

Utilizing this aperture scaling system, histograms were developed for one foot intervals along the entire borehole as shown in Fig. 28, Fig. 29 and Fig. 30. Fig. 28 and Fig. 29 summarizes the actual magnitude of air flow for each interval. Fig 28 is for the sealed well condition, and Fig. 29 is for the passive inlet condition. Substantial changes in most fracture zones are apparent.

Fig. 30 is a histogram showing the percentage of flow in each interval based on the total flow from the well. It is interesting to note the substantial improvement in flow uniformity for the various intervals. This is reflected in the reduction in standard deviation from 12.43 for the prefracture condition, to 7.74 for the postfracture condition. This "uniformization" of formation flow has been observed at other sites where pneumatic fracturing has been applied, and is considered paramount in the enhancement of contaminant mass removal from the fractures.

Based on the video analysis, an attempt was made to identify the major fracture zones, and to estimate the average fracture spacing. This information is essential for modeling contaminant mass removal by various mechanisms including molecular diffusion , heat transfer, and aerobic-anaerobic biodegradation processes. For this test interval, six major fracture zones, as presented in Table 6, were identified.

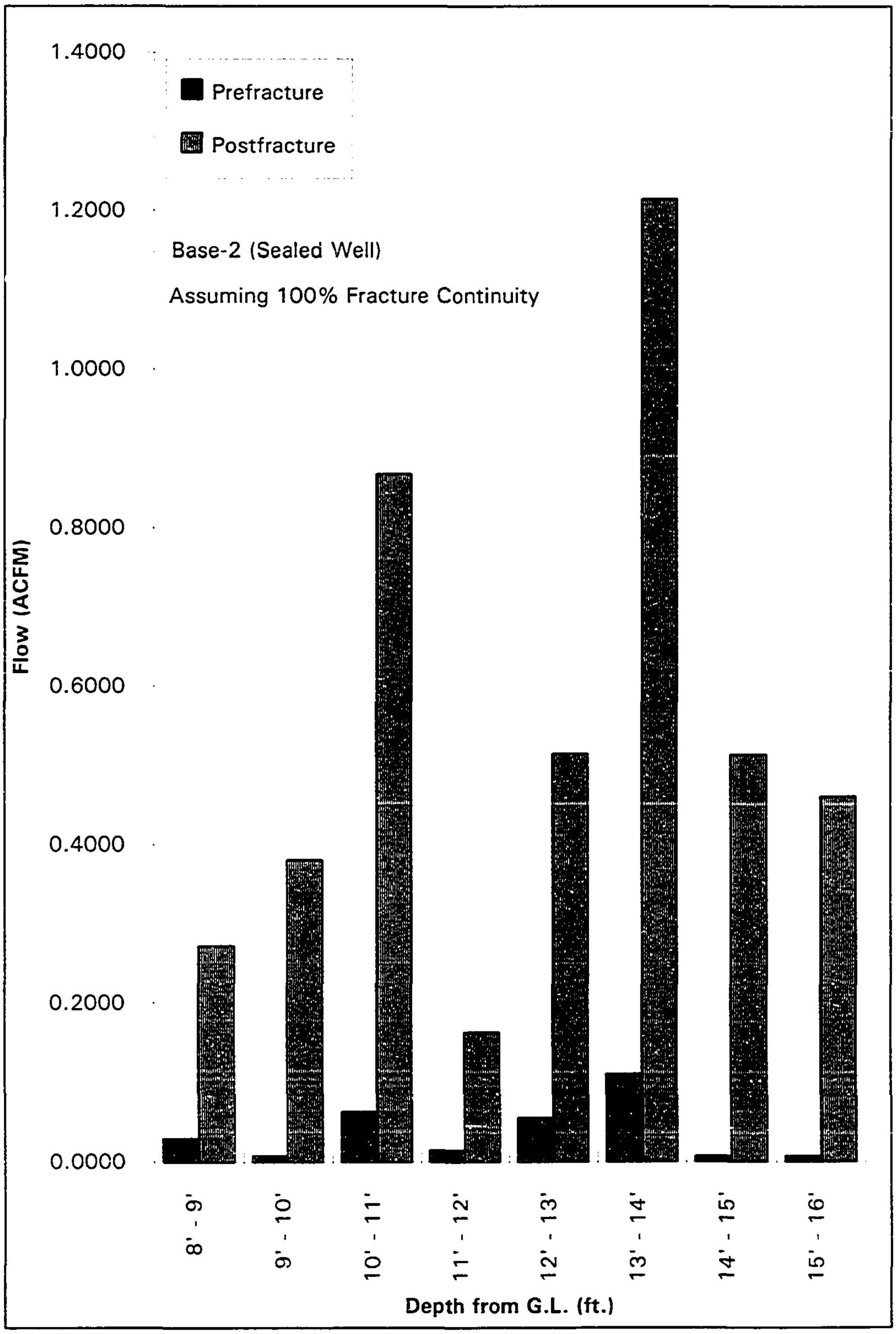

Figure 28 Distribution of flow for fracture well (sealed condition), H.T.S.

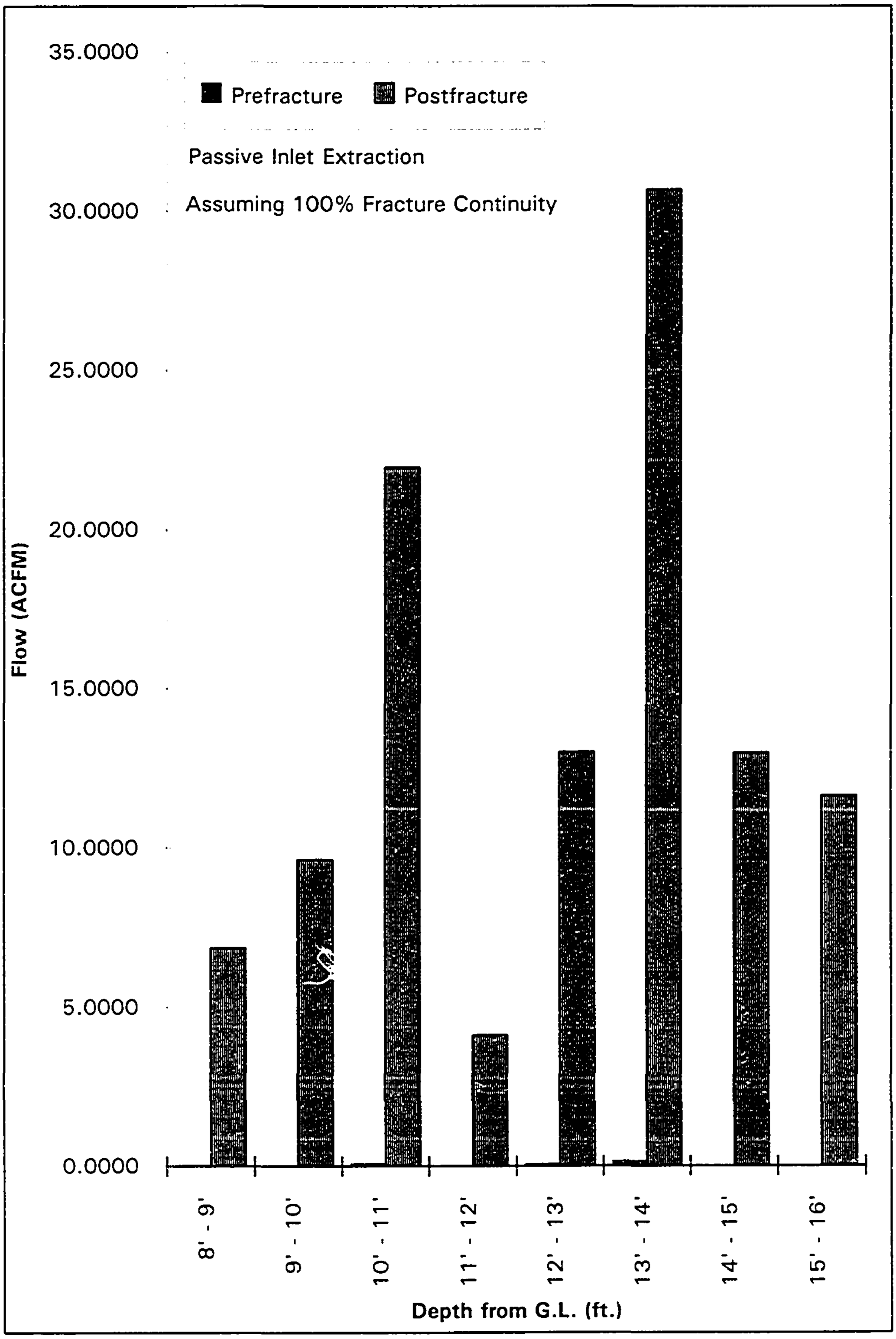

Figure 29 Distribution of flow for fracture well (passive inlet), H.T.S.

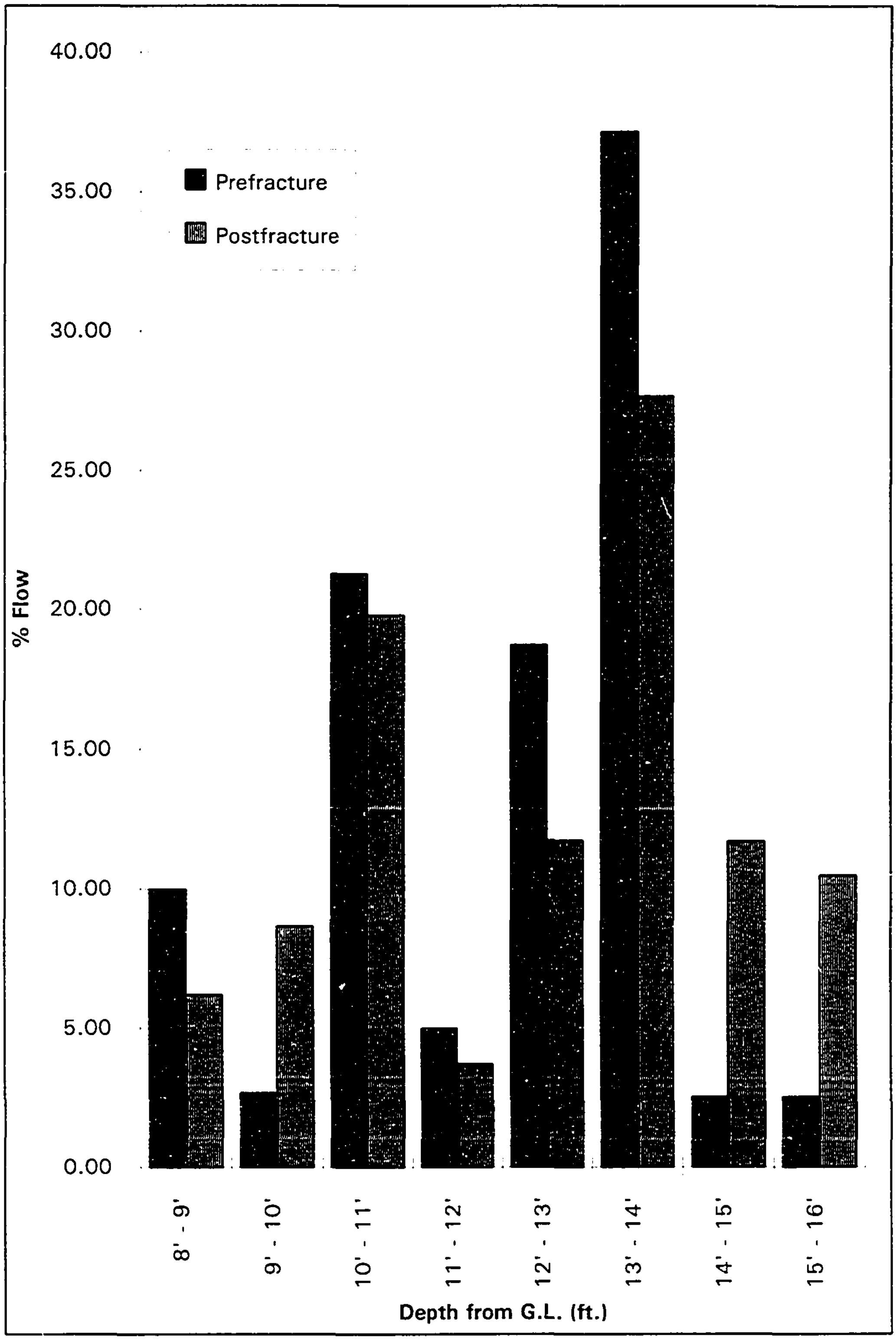

Figure 30 Histogram of flow percentage for various intervals of the F.W., H.T.S.

Table 6 Major fracture zones from video analysis, Hillsborough Test Site

Fracture Zone Number	**Depth From Ground Level (ft.)**
Zone 1	8.7
Zone 2	10.5
Zone 3	12.5
Zone 4	13.3
Zone 5	14.5
Zone 6	15.7

By incorporating this information into the P.F. fluid flow model, a physical model of fracture spacing and aperture was developed for the test section. The result is shown in Fig. 31. This is the recommended fracture geometry for modeling contaminant mass removal from the formation. It is noted that the average fracture spacing for the test interval assuming six equivalent fractures is 1.4 ft, and the average aperture is 284 microns.

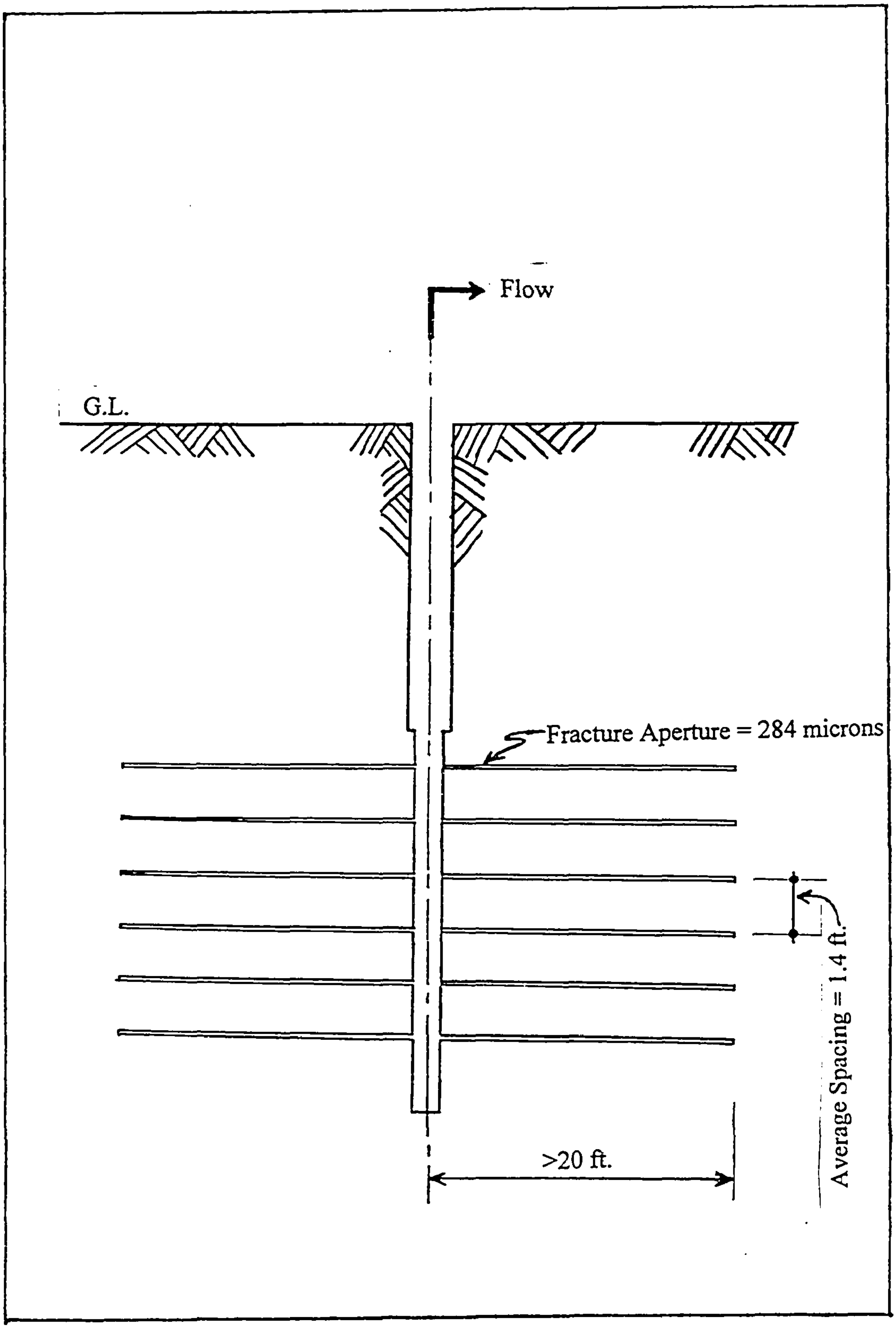

Figure 31 Physical model of pneumatically fractured formation, H.T.S.

Chapter 5

CONCLUSION AND RECOMMENDATIONS

5.1 General

1. A pneumatic fracturing (PF) flow model has been derived for radial flow of gases through a fractured formation. The model is based on the assumptions of viscous fluid flow through planar fractures. It also takes into account the non-linearity introduced by gas compressibility effects. Provisions has been made to extend the application of model to turbulent flow conditions arising from high flow velocities and/or surface roughness. The model presented in its general form is:

$$Q = -\frac{\pi g b^{e}(P_1^{1+m} - P_2^{1+m})}{6\nu \ln\left(R_2/R_1\right)(1+m)P_1^{m}} \tag{5.1}$$

where,

Q = volumetric flowrate (L^3/T)

b = fracture aperture (L)

ν = kinematic viscosity of the fluid (L^2/T) = 0.14987 cm^2/sec for air

g = acceleration due to gravity = 981 cm/ sec^2

P_1, P_2 = vacuum pressure at well in height of fluid (L)

R_1, R_2 = radial distance from extraction well ($R_1<R_2$) (L)

e = exponential power (e = 3 for laminar flow; e < 3 for turbulent flow)

m = 1 for isothermal conditions (for adiabatic conditions m < 1)

2. In order to validate the flow model, the data from a recent field study of pneumatic fracturing was analyzed. The research test site was located in Hillsborough, New Jersey, and the general stratigraphy can be described as three feet of soil fill overlying siltstone. Tests were conducted in the vadose zone at a depth range of 8.0 to 16.4 feet. As a result of pneumatic fracturing, an average flowrate enhancement of 13.3 to 177.5 times was achieved as compared with the prefracture baseline. It is also noted that surface heave data recorded by the electronic tiltmeters showed that the pneumatically induced fractures propagated up to 35 ft. from the injection point, but these larger radii could not be verified with flow and vacuum measurements since the farthest monitoring well was 20 feet.

3. Analysis of test site data using P.F. flow model showed some very significant trends. First, the average "equivalent" single fracture aperture increased from 86 microns in the prefracture condition, to 516 microns in the postfracture condition. Second, the variations of the calculated apertures at well locations for different test conditions were modest. Third, the fracture aperture is found quite constant across the test area, i.e. there was little evidence of fracture tapering.

4. By combining the results of the aperture calculations and the borehole video analysis, insight was gained into the mechanism of permeability enhancement by pneumatic fracturing. The most significant impact of pneumatic fracturing seems to be the dilation of existing natural fractures, and improvement of fracture connectivity and continuity. The process also creates some minor new horizontal and vertical fractures. The "new" horizontal fractures tend to form along existing fracture zones, while the "new" vertical fractures tend to connect adjacent sets of horizontal fractures, thereby improving fracture connectivity.

5. Air velocity and Reynolds number calculations showed that for all the prefracture test conditions and for postfracture sealed well extraction condition, laminar flow conditions existed. For the postfracture passive inlet extraction condition the flow became slightly turbulent, while for the pneumatic fracture injection condition a very high degree of turbulence was indicated. It was concluded that although laminar flow may be expected in natural fracture networks, some degree of turbulence may be encountered in pneumatically induced fractures owing to the enlarged apertures.

6. Study of prefracture and postfracture borehole videos resulted in identification of six major fracture zones intersecting the fracture well. A physical model of the fractures was established using the P.F. flow model to calculate "equivalent" apertures for these fracture zones. An average value of 284 microns was determined, separated by an average spacing of 1.4 ft. This physical model is useful for future analysis of contaminant mass removal by various mechanisms including molecular diffusion, heat transfer, and biodegradation processes.

5.2 Recommendations for Future Study

Based on the analysis in this thesis, and the experience from applying pneumatic fracturing at 10 sites, several valuable lessons have been learned. Although it is relatively easy to fracture a formation, it is more difficult to evaluate its effects. Careful evaluation of the effects of pneumatic fracturing are of course essential in the optimal design and application of pneumatic fracturing process.

In order to improve the quality of future data analysis and evaluation, the following recommendations are offered.

Level of Vacuum Application

Future site analysis and extraction testing with the P.F. flow model should be conducted at varying levels of vacuum pressure. In the present case study, variable pressures were provided by the sealed and passive inlet tests, at constant blower pressure of 10 inches of Hg vacuum. A better validation of the model could have had been established had these tests been conducted at different blower pressures.

Interval Extraction Tests

Due to the time constraint at the SITE program demonstration as well as the presence of perched water, it was not possible to conduct interval vacuum extraction tests. These tests could have been very useful in conforming flows and fracture apertures for various borehole intervals. It is also recommended that packer extraction tests be conducted for single, identifiable fractures when possible. Long packer elements should be used for interval tests to reduce potential leaks. It is acknowledged that a certain amount of error is inherent in interval testing due to vertical interconnectivity between adjacent fracture zones, especially for postfracture testing.

Video Mapping

Another important method emerging out from this study is the mapping of the fractures with a borehole video camera. Future video analysis should not only include the fracture well, but also the peripheral monitoring wells. By extending the video analysis to multiple borehole locations, the fracture continuity and orientation of the fracture network could be assessed more reliably.

Soil Moisture

At many sites, soil moisture has been a significant hindrance in evaluating the integrated process of pneumatic fracturing and vapor extraction. Water present in the fractures consumes much of the vacuum energy applied, thereby impeding the vapor extraction and contaminant mass removal process. At very high moisture contents, this problem can result in minimal gaseous flow from the formation. In consideration of this problem, it is desirable to dewater sites before evaluating the effects of pneumatic fracturing. However, in practice, pneumatic fracturing can be useful for dewatering enhancement of a site. Under such applications, it may be necessary to refracture the formation again after dewatering, to clear fractures of fines transported with water.

Long Term Residual Aperture

The results of this study indicated that the residual fracture aperture measured immediately after pneumatic injection may over estimate the long term residual aperture. That is, the formation probably settles or "relaxes" over a much longer period. It would therefore be desirable to monitor residual aperture for a extended period to confirm this effect. Possible approaches include tiltmeter measurements and / or laser leveling devices.

APPENDIX A

FUNDAMENTALS OF FLUID MOTION IN POROUS MEDIA

Newton's second law implies that the rate of change of momentum with respect to time (of an element of mass) is equal to the resulting force acting on the element (i.e., F = ma). For a fluid particle, Newton's law is written in the following analysis.

In this case, the only force acting on the particle, other than driving forces that act on static elements, is fluid shear. For any direction i, the Newton's law can be written as

$$\rho \frac{du_i}{dt} = \rho g_i - \frac{\partial P}{\partial x_i} + F_i(Shear) \qquad \text{(A.1)}$$

In the above equation the left side shows the product of mass and acceleration $\left(\frac{du_i}{dt}\right)$ and the right side is a summation of force components in the i direction.

A.1 Fluid Velocity

The component of velocity u_i refers to the motion of the center of mass of a specified volume (the fluid particle). It does not refer to the motion of individual molecules or ions, or to any species of molecule that constitute the fluid mass.

A.2 Fluid Acceleration

The derivative $\left(\frac{du_i}{dt}\right)$ is the "total" component of acceleration in the direction i. Noting that, in general, u_i is a function of orthogonal space coordinates, x_i, x_j, and x_k, as well as t,

$$du_i = \frac{\partial u_i}{\partial x_i} dx_i + \frac{\partial u_i}{\partial x_j} dx_j + \frac{\partial u_i}{\partial x_k} dx_k + \frac{\partial u_i}{\partial t} dt \tag{A.2}$$

Dividing Eq. A.2 by dt gives acceleration, as

$$\frac{du_i}{dt} = (u_i \frac{\partial u_i}{\partial x_i} + u_j \frac{\partial u_i}{\partial x_j} + u_k \frac{\partial u_i}{\partial x_k}) + \frac{\partial u_i}{\partial t} \tag{A.3}$$

in which u_i, u_j, and u_k are velocity components in the x_i, x_j, and x_k directions respectively.

Writing this with the summation convention results in

$$\frac{du_i}{dt} = u_j \frac{\partial u_i}{\partial x_j} + \frac{\partial u_i}{\partial t} \tag{A.4}$$

the repeated subscript j indicating a summation over three orthogonal coordinate directions, i, j, and k.

The first term on the right of Eq. A.4 is the convective acceleration which is due to velocity variations (direction as well as magnitude) with respect to position in space. The term $\frac{\partial u_i}{\partial t}$ refers to the variation of u_i (at a particular point in space) with respect to time. It is called local acceleration.

A.3 Fluid Shear :

Shear is a resisting force which acts tangential to the surface of moving particles. It is directly proportional to the area over which it acts, and also on the component of velocity gradient normal to the plane in which it acts. Shear on a particular face of a fluid element (say an element consisting of a cube) is a force in the direction of a faster moving adjacent element.

If the motion of the adjacent element is slower, the force of shear is in the opposite direction on the face under consideration. The force/area is called intensity of shear Γ. Γ_{ij} defines the intensity of shear (at a particular point) in a plane normal to direction i in the direction j.

The resultant of shear on a fluid particle of any shape in the direction i for the case of 3-dimensional flow is expressed as

$$F_i = \mu \frac{\partial^2 u_i}{\partial x_j \partial x_j} \tag{A.5}$$

where
$$\frac{\partial^2 u_i}{\partial x_j \partial x_j} = \frac{\partial^2 u_i}{\partial x_i^2} + \frac{\partial^2 u_i}{\partial x_j^2} + \frac{\partial^2 u_i}{\partial x_k^2} \tag{A6}$$

A.4 Equation Of Fluid Motion

Substituting Eq. A.4 and A.5 into Eq. A.1 we get

$$P(u_j \frac{\partial u_i}{\partial x_j} + \frac{\partial u_i}{\partial t}) = \rho g_i - \frac{\partial P}{\partial x_i} + \mu \frac{\partial^2 u_i}{\partial x_j \partial x_j} \tag{A.7}$$

Eq. A.7 is a special case of the Navier-Stokes equation of fluid motion, that is, the case for Newtonian viscous fluids undergoing negligible divergence.

This equation can be simplified further for application to flow in porous media. If the medium is homogenous, the convective acceleration term

$$u_j \frac{\partial u_i}{\partial x_j} \tag{A.8}$$

when integrated over a macroscopic volume, is zero for uniform rectilinear macroscopic flow, [Hubbert (1940)]. That is, the velocity is unchanged in respect to both magnitude and direction as a result of fluid passing through a macroscopic volume element of the medium. If ui is small, as is the usual case, $\frac{\partial u_i}{\partial t}$ is also small. It usually is assumed that both local and corrective terms of fluid velocity are small even for non-homogenous porous media and for flow that is not uniform or rectilinear.

Based upon these assumptions, the equation for motion of fluids in porous media becomes

$$\frac{\partial P}{\partial x_i} - \rho g_i = \mu \frac{\partial^2 u_i}{\partial x_j \partial x_j} \tag{A.9}$$

Both Eq. A.7 and A.9 are written in respect to fluid particles that are within one single fluid phase or another. Elements within mixed phase fluids are excluded.

APPENDIX B

SAMPLE CALCULATIONS

B.1. Fracture Aperture Estimation

B.1.1 *Sealed Well Extraction*

B.1.1.1 Calculation using kinematic viscosity

From Eq. 4.25 the fracture aperture, b, can be calculated as

$$b = \left(-\frac{12\nu Q \ln(R_2 / R_1) P_1}{\pi g (P_1^2 - P_2^2)} \right)^{1/3} \qquad \text{(B.1)}$$

here for example,

Q = 5.2 cubic ft./ min = 5.2 ×(12×2.54)^3/60 = 2455.07 cubic cm/ sec (L^3/T)

R_1 = 1.5 inch = 3.81 cm (L)

R_2 = 10 ft. =10×12×2.54 = 304.8 cm (L)

P_1 = 105 "H_2O

therefore, P_1absolute = (29.9×13.6)-105 = 301.64 "H_2O

= 301.64 ×(62.4/0.08) = 235279.2 inches of Air

= 235279.2×2.54 = 597609.17 cm of Air (L)

P_2 = 86 "H_2O

Similarly P_2 absolute =635251.97 cm of Air (L)

ν_{air} = 0.14987 cm^2/sec (L^2/T)

g = 981 cm/sec^2 (L/T^2)

Substituting these values in Eq. B.1 the aperture, b, is

b = 0.0432 cm = 432 microns

Dimensional analysis of Eq. B.1

$$\text{R.H.S.} = \left[\frac{\left(\frac{L^2}{T}\right)\left(\frac{L^3}{T}\right)\left(\frac{L}{L}\right)(L)}{\left(\frac{L}{T^2}\right)(L^2)} \right]^{1/3} = \left[L^3\right]^{1/3} = [L] = \text{L.H.S.}$$

B.1.1.2 *Calculation* using absolute or dynamic viscosity

When dynamic viscosity of a fluid is to be used for fracture aperture calculations Eq. B.1 reduces to the following form

$$b = \left(-\frac{12\mu Q \ln(R_2 / R_1) P_1}{\pi(P_1^2 - P_2^2)} \right)^{1/3} \tag{B.2}$$

for the same example as sited above in Case-1(a)

where,

Q = 5.2 cubic ft./ min = 5.2 ×(12×2.54)^3/60 = 2455.07 cubic cm/ sec (L^3/T)

R_1 = 1.5 inch = 3.81 cm (L)

R_2 = 10 ft. =10×12×2.54 = 304.8 cm (L)

P_1 = 105 "H_2O = 105 "H_2O × (3.61×10^{-2} psia per "H_2O) = 3.7905 psia

therefore, P_1absolute = 14.7 psia - 3.7905 psia

= 10.9095 psia × (6.9×10^4 gm/cm-s^2 per psia)

= 7.53 gm/cm-sec^2 (M/L-T^2)

P_2 = 86 "H_2O

Similarly P_2 absolute = 3.10 gm/cm-s^2 (M/L-T^2)

μ_{air} = absolute or dynamic viscosity of air = 1.8 × 10 -4 gm/cm-sec (M/L-T)

Substituting these values in Eq. B.2 the aperture, b, is

b = 0.042314 cm = <u>423</u> microns

Dimensional analysis of Eq. B.2

$$\text{R.H.S.}=\left[\frac{\left(\frac{M}{LT}\right)\left(\frac{L^3}{T}\right)\left(\frac{L}{L}\right)\left(\frac{M}{LT^2}\right)}{\left(\frac{M}{LT^2}\right)^2}\right]^{1/3}=\left[L^3\right]^{1/3}=\left[L\right]=\text{L.H.S.}$$

Case -2 ***Passive Inlet Condition***

here,

$Q = 87.18$ cubic ft./ min = $87.18 \times(12\times2.54)^3/60 = 41144.38$ cubic cm/ sec

$R_1 = 1.5$ inch = 3.81 cm

$R_2 = 10$ ft. $=10\times12\times2.54 = 304.8$ cm

$P_1 = 70.5$ "H_2O

therefore, P_1absolute = $(29.9\times13.6)-70.5 = 336.14$ "H_2O

$= 336.14 \times(62.4/0.08) = 262189.2$ inches of Air

$= 262189.2\times2.54 = 665960.568$ cm of Air

$P_2 = 0$ "H_2O

Similarly P_2 absolute =1atm. $=(29.9\times13.6)-0 = 406.64$ "H_2O

$= 406.64 \times(62.4/0.08) = 317179.2$ inches of Air

$= 317179.2\times2.54 = 805635.168$ cm of Air

$\nu_{air} = 0.14987$ cm^2/sec

$g = 981$ cm/sec^2

Substituting these values in Eq. 1 the aperture, b, is

$b = 0.069856$ cm = 698.56 microns

Case-3 *Pneumatic Fracturing Injection*

here,

Q = 1517 cubic ft./ min = 1517 ×$(12\times2.54)^3/60$ = 715944.27 cubic cm/ sec

R_1 = 1.5 inch = 3.81 cm

R_2 = 10 ft. =10×12×2.54 = 304.8 cm

P_1 = 21 psig

therefore, P_1absolute = 14.7 + 21 = 35.7 psig = (35.7/14.7) atms =2.43 atms

but since 1 atm = 805635.168 cm of air (as seen in Case2 sample calculation)

therefore, P_1absolute = 2.43×805635.168 = 1957693.458 cm of air

P_2 = 16 psig

Similarly P_2 absolute =14.7 + 16 = (30.7/14.7) = 2.09 atms = 1683777.5 cm of air

ν_{air} = 0.14987 cm^2/sec

g = 981 cm/sec^2

Substituting these values in Eq. 1 the aperture, b, is = 0.1532 cm = 1532microns

B.2 Air Velocity Calculations

the flow velocity, u, in a fracture of aperture, b,at any point at radial distance, R, from the extraction well is given as

$$u = \frac{Flow}{Area} = \frac{Q}{A} = \frac{Q}{2\pi Rb} \qquad \text{(B.3)}$$

here if,

Q = 4.0 cubic ft./min = 4.0×$(12\times2.54)^3/60$ = 1887.79 cubic cm/ sec

R = 10 ft = 10×12×2.54 = 304.8 cm, and

b = 432 microns = 0.0432 cm or 0.001417 ft.

therefore flow velocity, u = 22.82 cm/ sec = 44.92 ft./ min

B.3 Reynolds Number Calculation

the Reynolds number, R_e, in a fracture of aperture, b, at any point having a flow velocity, u, is given as

$$R_e = \frac{2bu}{\nu} \tag{B.4}$$

where, ν = kinematic viscosity of air = 0.14987 cm^2/ sec = 0.0016 ft^2/ sec

substituting in Eq. B.4,

u = 22.82 cm/sec, and

b = 432 microns = 0.0432 cm

the Reynolds number obtained is R_e = 13.16

APPENDIX C

FRACTURE APERTURE CALCULATIONS
Hillsborough Test Site

Table C1 Fracture Aperture Calculation Summary (FW, Base-1, Pre)

Hillsborough Test Site

Extraction Location : FW

Condition : Prefracture, Total Well/ Sealed, 1st 4hr. Baseline

Date: 08/18/1992

Assuming "Equivalent" Single Fracture

Time	T	Vacuum ("H2O) at well location								Flow	Aperture (microns) at well location						
		MW1	MW2	MW3	MW4	MW5	MW6	MW7	FW	"Q"	MW1	MW2	MW3	MW4	MW5	MW6	MW7
12:36	0	0	6	33.5	12	2.25	70	0		cfm							
12:41	5	2.5	9.5	33.75	12	1.75	63	0	105	0.52	110	113	126	114	115	149	114
12:46	10	4.5	5.5	32.5	12	1	60	0	107	0.49	108	108	121	111	112	140	111
12:51	15	4.75	3.5	30	11	0.5	55	0	107	0.37	98	97	109	100	101	123	101
13:06	30	2	2	23	9	0	44	0	107	0.16	73	73	80	75	76	87	76
13:21	45	1	1.5	18	7.5	0	39	0	107	0.12	67	67	72	69	70	77	70
13:36	60	1	1.5	17	7	0	38	0	107	0.09	59	60	63	61	62	68	62
13:51	75	0.5	1.5	16	7	0	38	0	107	0.09	59	60	63	61	62	68	62
14:06	90	0.25	1.5	15	6.5	0	37	0	107	0.09	59	60	63	61	62	68	62
14:21	105	0.25	1.5	14.5	6	0	36	0	107	0.06	53	53	56	54	56	60	56
14:36	120	0	1.25	12.25	5.75	0	33	0	107	0.09	59	60	62	61	62	67	62
14:51	135	0	1	11	5	0	30.5	0	107	0.06	53	53	55	54	56	59	56
15:06	150	0	1	10	4.5	0	28	0	107	0.07	56	56	58	57	59	62	59
15:21	165	0	1	8.25	4	0	26.5	0	109	0.07	56	56	57	57	59	61	59
15:36	180	0	0.5	7	3.75	0	25.5	0	107	0.06	53	53	54	54	56	57	56
15:51	195	0	0.25	6	3.5	0	23.5	0	107	0.06	53	53	54	54	56	57	56
16:06	210	0	0	5	2.5	0	22	0	107	0.06	53	53	54	53	56	56	56
16:21	225	0	0	4.5	2.5	0	20	0	107	0.06	53	53	54	53	56	56	56
16:44	248	0	0	2.75	2	0	18	0	107	0.05	51	51	51	51	53	53	53
							Average "b"				65	65	70	67	68	76	68

Table C2 Fracture Aperture Calculation Summary (FW, Base-2, Pre)

Hillsborough Test Site

Extraction Location : FW

Condition : Prefracture, Total Well/ Sealed, 2nd 4hr. Baseline

Date: 08/19/1992

Assuming "Equivalent" Single Fracture

Time	T	Vacuum ("H2O) at well location								Flow	Aperture (microns) at well location						
		MW1	MW2	MW3	MW4	MW5	MW6	MW7	FW	"Q"	MW1	MW2	MW3	MW4	MW5	MW6	MW7
9:21	0	0	0	0	2	0.25	30	0	106	0.43							
9:26	5	4	7.5	23	14	2.25	64	0	106	0.31	93	94	100	96	97	126	96
9:31	10	7.5	7	30.5	18	2.5	56	0	106	0.46	107	107	118	112	110	134	109
9:36	15	9	6	30	18	2.25	52	0	106	0.44	106	105	116	110	109	129	108
9:51	30	7.5	4.5	22	14	0	39	0	106	0.33	96	95	102	99	98	108	98
10:06	45	3.5	3	17.5	12	0	35	0	106	0.25	86	86	91	89	90	97	90
10:21	60	5.5	7.75	27.5	17	1	57	0	106	0.29	91	92	100	95	94	116	93
10:36	75	10.5	5.5	26	16	0	41.5	0	106	0.18	80	78	85	82	81	90	81
10:51	90	6	4	20	13.5	0	36	0	106	0.25	86	86	91	89	89	96	89
11:06	105	3.5	3.5	18.5	12.5	0	35	0	106	0.27	88	88	93	91	91	99	91
11:21	120	1.5	3.5	16.5	11	0	33	0	106	0.29	89	90	95	93	93	100	93
11:36	135	0.5	3.5	16	11.5	0	33	0	106	0.27	87	88	92	91	91	98	91
11:51	150	0.5	3.5	16	11.5	0	32.5	0	106	0.25	85	86	90	88	89	95	89
12:06	165	0.5	3.5	15.5	11	0	32	0	106	0.25	85	86	90	88	89	95	89
12:21	180	0.5	3.5	15	11	0	32	0	106	0.29	89	90	94	93	93	100	93
12:36	195	0.5	3.5	14.5	11	0	31	0	106	0.27	87	88	92	90	91	97	91
12:51	210	0.5	3	13	10	0	28	0	106	0.25	85	85	89	88	89	93	89
13:06	225	0.5	2.75	12	10	0	27	0	106	0.25	85	85	88	88	89	92	89
13:21	240	0.25	2.5	11	9	0	25.5	0	106	0.25	85	85	88	87	89	92	89
							Average "b"				89	90	95	93	93	103	93

Table C3 Fracture Aperture Calculation Summary (FW, Base-1, Post)

Hillsborough Test Site

Extraction Location : FW

Condition : Postfracture, Total Well/ Sealed, 1st 4hr. Baseline

Date: 08/25/1992

Assuming "Equivalent" Single Fracture

Time	T	Vacuum ("H2O) at well location								Flow	Aperture (microns) at well location						
		MW1	MW2	MW3	MW4	MW5	MW6	MW7	FW	"Q"	MW1	MW2	MW3	MW4	MW5	MW6	MW7
9:34	0	0	0	0	0	0	0	0		cfm							
9:39	5	97	98	98	96	80	97	86	105	5.19	580	607	607	557	413	567	454
9:44	10	100	100	100	100	84	100	89	106	5.18	639	639	639	639	431	624	471
9:49	15	94	94	94	94	78	91	82	110	4.76	445	445	445	445	368	410	386
10:04	30	92	93	92	92	77	90	81.5	110	4.03	405	413	405	405	344	381	362
10:19	45	89	92	90	90	75	88	80	96	4.81	592	714	623	623	428	553	469
10:34	60	86	90	87	89	74	86	78	110	4.6	383	408	389	401	349	374	364
10:49	75	81	82	80	82	68	80	72.5	109	4.57	362	367	358	367	333	350	347
11:04	90	80	80	83	80	67	77.5	74	109	4.39	353	353	367	353	325	335	347
11:19	105	78	78	82	74	62	72.5	74	102	3.89	362	362	386	343	318	330	361
11:34	120	75	74	76	67	56	64	69	109	3.66	314	311	318	292	282	278	312
11:49	135	72	71	73	62	52	60	66	109	3.66	305	302	308	280	275	270	304
12:04	150	68	66	68	55	47	54	62	105	3.32	295	290	295	265	264	258	294
12:19	165	66	64	65.5	52	44	52	59	105	2.95	279	274	277	250	249	244	276
12:34	180	65	64	65	50	43	50	58	106	2.95	274	271	274	245	246	239	272
12:49	195	63.5	62	63	48	41	51	56.5	106	2.95	270	267	269	242	244	241	269
13:04	210	62	60	61.5	47	39	51	55	106	2.75	261	257	260	235	235	235	260
13:19	225	59	58	59	44	37	51	53	108	2.75	251	249	251	228	230	232	253
13:34	240	58	57	57.5	42	35.5	51	52	108	2.56	243	242	242	220	223	227	245
							Average "b"				367	376	373	355	309	342	336

Table C4 Fracture Aperture Calculation Summary (FW, Base-2, Post)

Hillsborough Test Site

Extraction Location : FW

Condition : Postfracture, Total Well/ Sealed, 2nd 2hr. Baseline

Date: 08/25/1992

Assuming "Equivalent" Single Fracture

Time	T	Vacuum ("H2O) at well location								Flow	Aperture (microns) at well location						
		MW1	MW2	MW3	MW4	MW5	MW6	MW7	FW	"Q"	MW1	MW2	MW3	MW4	MW5	MW6	MW7
15:57	0	0	0	0	0	0	0	0	104	5.22							
16:02	5	86	86	86	86	69	85	76	105	5.2	432	432	432	432	364	415	392
16:07	10	88	88	88	87	71	86	76	105	5.1	446	446	446	438	369	420	390
16:12	15	89	88	89	88	72	87	77	105	5	453	443	453	443	370	425	392
16:27	30	86	89	88	88	72	87	76	106	4.52	409	433	424	424	356	407	372
16:42	45	81	82.5	80	82	66.5	79	72	106	4.25	368	376	363	373	329	350	347
16:57	60	79	79	77	79	64.5	77	69	106	4.25	358	358	349	358	323	341	337
17:12	75	77	77	82	78	63	75	70	107	4.13	342	342	364	346	314	327	334
17:27	90	76	77	80	71	58	68	70	108	4.04	332	335	348	315	297	300	328
17:42	105	73	73	74.5	64	53	61	66	109	3.81	314	314	318	290	281	277	309
17:57	120	70	69	71	59.5	48	56	63.5	110	3.5	292	290	295	269	262	257	291
							Average "b"				375	377	379	369	327	352	349

Table C5 Fracture Aperture Calculation Summary (FW, Passive Inlet)
Hillsborough Test Site

Extraction Location : FW
Condition : Prefracture, Total Well/ Well No. 1,3,4& 6 Unsealed
Date: 08/14/1992

Assuming "Equivalent" Single Fracture

Time	T	Vacuum ("H2O) FW	Q (cfm)	Aperture (microns) at well location MW1	MW2	MW3	MW4	MW5	MW6	MW7
9:06	0	105	0.67	118	118	118	118	124	115	124
9:08	5	105.5	0.62	115	115	115	115	121	112	121
9:10	10	105.5	0.58	113	113	113	113	118	110	118
9:12	15	105.5	0.53	109	109	109	109	115	107	115
9:14	20	105.5	0.58	113	113	113	113	118	110	118
9:16	25	105.5	0.55	111	111	111	111	116	108	116
9:16	45	105.5	0.55	111	111	111	111	116	108	116
9:16	57	105	0.55	111	111	111	111	116	108	116
		Average "b"		112	112	112	112	118	110	118

Condition : Postfracture, Total Well/ Well No. 1,3,4& 6 Unsealed
Date: 08/26/1992

Time	T	Vacuum ("H2O) FW	Q (cfm)	Aperture (microns) at well location MW1	MW2	MW3	MW4	MW5	MW6	MW7
9:06	0	70.5	107.12	748	748	748	748	786	732	786
9:08	15	65	112.16	783	783	783	783	822	766	822
9:10	30	65	111.85	782	782	782	782	822	765	822
9:12	35	65.5	112.5	782	782	782	782	821	764	821
		Average "b"		774	774	774	774	813	757	813

Table C6 Fracture Aperture Calculation Summary (MW Extraction)

Hillsborough Test site

Assuming "Equivalent" Single Fracture

Extraction Location: MW1

Prefracture Extraction Date: 08/17/1992 Total Well / Sealed Condition

Time	T	Vacuum ("H2O) at well location								Flow	Aperture (microns) at well location						
		MW1	MW2	MW3	MW4	MW5	MW6	MW7	FW	"Q"	FW	MW2	MW3	MW4	MW5	MW6	MW7
9:06	0	110	0	0	0	0	0	0	0	0.08							
9:08	2	110	0	0	0	0	0	0	0	0.23	82	80	84	86	88	83	86
9:10	4	110	0	0	0	0	0	0	0	0.13	68	66	70	71	73	69	72
9:12	6	110	0	0	0	0	0	0	0	0.17	73	72	75	77	79	74	77
9:14	8	110	0	0	0	0	0	0	0	0.17	73	72	75	77	79	74	77
9:16	10	110	0	0	0	0	0	0	0	0.17	73	72	75	77	79	74	77
										Average "b" =	74	72	76	77	79	75	78

Postfracture Extraction Date: 08/26/1992 Total Well/ Sealed Condition

Time	T	Vacuum ("H2O) at well location								Flow	Aperture (microns) at well location						
		MW1	MW2	MW3	MW4	MW5	MW6	MW7	FW	"Q"	FW	MW2	MW3	MW4	MW5	MW6	MW7
9:06	0	0	0	0	0	0	0	0		7							
9:08	2	76	56	58	58	47	57	48	54	8	478	481	522	535	465	508	462
9:10	4	83	65	67	63	52	62.5	56	60	7.25	452	482	526	499	440	479	453
9:12	6	85	68	70	66	54	65	58	65	6.25	454	468	512	483	419	460	431
9:14	8	87	70	71	67	55	67.5	59	67	6.25	449	468	500	475	414	464	426
9:16	10	87	72	71	60					5.5		468	480	410			
										Average "b" =	458	473	508	480	434	477	443

Extraction Location: MW2

Prefracture Extraction Date: 08/17/1992 Total Well / Sealed Condition

Time	T	Vacuum ("H2O) at well location								Flow	Aperture (microns) at well location						
		MW1	MW2	MW3	MW4	MW5	MW6	MW7	FW	"Q"	FW	MW1	MW3	MW4	MW5	MW6	MW7
12:05	0	0	108	0	0	0	0	0	0	0.45							
12:07	2	0	108	0	0	0	0	0	0	0.28	88	86	86	92	94	91	90
12:09	4	0	110	0	0	0	0	0	0	0.42	99	97	97	104	106	103	102
12:11	6	0	110	0	0	0	0	0	0	0.45	102	100	100	106	109	105	105
12:13	8	0	110	0	0	0	0	0	0	0.07	54	53	53	56	58	56	55
12:15	10	0	110	0	0	0	0	0	0	0.33	92	90	90	96	99	95	95
										Average "b" =	87	85	85	91	93	90	89

Postfracture Extraction Date: 08/26/1992 Total Well/ Sealed Condition

Time	T	Vacuum ("H2O) at well location								Flow	Aperture (microns) at well location						
		MW1	MW2	MW3	MW4	MW5	MW6	MW7	FW	"Q"	FW	MW1	MW3	MW4	MW5	MW6	MW7
9:24	0	0	62	0	0	0	0	0		9.5							
9:26	2	65	73	66	61	50	62.5	53	64	8	642	656	687	611	502	633	505
9:28	4	74	83	76	71	73	59	63	72	6.75	570	596	649	577	630	451	477
9:30	6	79	86	80	74	60	75	68	72	6.25	512	632	666	562	443	574	482
9:32	8	80	86	82	76	61	76	70	72	6	505	657	753	590	443	585	495
9:34	10	80	88	80	75	61	76	69	72	6.25	489	604	604	547	437	557	473
										Average "b" =	543	629	672	577	491	560	487

Table C6
(Continued)

Extraction Location: MW3

Prefracture Extraction Date: 08/17/1992 Total Well / Sealed Condition

Time	T	Vacuum ("H2O) at well location								Flow	Aperture (microns) at well location						
		MW1	MW2	MW3	MW4	MW5	MW6	MW7	FW	"Q"	FW	MW1	MW2	MW4	MW5	MW6	MW7
12:44	0	0	0	104	0	0	0	0	0	5							
12:46	2	0	0	104	0	0	0	0	0	0.17	75	77	73	77	79	78	75
12:48	4	0	0	111	0	0	0	0	0	0.15	70	72	69	72	74	73	70
12:50	6	0	0	110	0	0	0	0	0	0.16	72	74	70	74	76	75	72
12:52	8	0	0	110	0	0	0	0	0	0.15	71	72	69	72	75	73	71
12:54	10	0	0	110	0	0	0	0	0	0.07	54	55	53	55	57	56	54
										Average "b" =	68	70	67	70	72	71	68

Postfracture Extraction Date: 08/26/1992 Total Well/ Sealed Condition

Time	T	Vacuum ("H2O) at well location								Flow	Aperture (microns) at well location						
		MW1	MW2	MW3	MW4	MW5	MW6	MW7	FW	"Q"	FW	MW1	MW2	MW4	MW5	MW6	MW7
8:42	0	0	0	53	0	0	0	0	0	10.5							
8:44	2	81	84	93	80	59	85	70	84	9	678	623	656	606	449	725	486
8:46	4	92	94	95	87	68	90	86	90	7	739	914	1260	657	448	782	616
8:48	6	90	90	91	82	68	81	86	82	6.25	584	1271	1213	608	456	596	723
8:50	8	83	84	90	79	65	79	79	80	6.25	577	662	666	568	443	577	554
8:52	10	83	84	90	80	69	80	78	80	6.25	577	662	666	587	470	596	538
										Average "b" =	631	826	892	606	453	655	584

Extraction Location: MW4

Prefracture Extraction Date: 08/17/1992 Total Well / Sealed Condition

Time	T	Vacuum ("H2O) at well location								Flow	Aperture (microns) at well location						
		MW1	MW2	MW3	MW4	MW5	MW6	MW7	FW	"Q"	FW	MW1	MW2	MW3	MW5	MW6	MW7
13:54	0	0	0	0	106	0	0	0	0								
13:56	2	0	0	0	110	0	0	0	0	0.5	105	111	110	108	105	107	111
13:58	4	0	0	0	110	0	0	0	0	0.47	103	108	108	106	103	105	109
										Average "b" =	104	109	109	107	104	106	110

Postfracture Extraction Date: 08/26/1992 Total Well/ Sealed Condition

Time	T	Vacuum ("H2O) at well location								Flow	Aperture (microns) at well location						
		MW1	MW2	MW3	MW4	MW5	MW6	MW7	FW	"Q"	FW	MW1	MW2	MW3	MW5	MW6	MW7
10:02	0	0	0	0	53	0	0	0	0	10.5							
10:04	2	61	60	63	66	53	65	55	61	9	828	858	802	994	592	1422	662
10:06	4	70	68	71	74	60	71	64	68	8.5	754	907	787	975	566	967	671
10:08	6	78	77	79	83	67	76	71	72	7.25	584	798	747	840	513	690	598
10:10	8	80	79	81	86	69	78	73	75	6.75	565	733	692	761	490	644	568
10:12	10	81	80	82	86	70	79	74	76	6.5	583	769	720	810	494	665	577
										Average "b" =	663	813	750	876	531	878	615

Table C6
(Continued)

Extraction Location: MW5

Prefracture Extraction Date: 08/17/1992 Total Well / Sealed Condition

Time	T	Vacuum ("H2O) at well location								Flow	Aperture (microns) at well location						
		MW1	MW2	MW3	MW4	MW5	MW6	MW7	FW	"Q"	FW	MW1	MW2	MW3	MW4	MW6	MW7
14:15	0	0	0	0	0	109	0	0	0	0.08							
14:17	2	0	0	0	0	109	0	0	0	0.3	93.6	96.1	95.7	94.3	89.2	94	95.7
14:19	4	0	0	0	0	109	0	0	0	0.08	61.1	62.7	62.4	61.5	58.2	61.4	62.5
14:21	6	0	0	0	0	109	0	0	0	0.08	61.1	62.7	62.4	61.5	58.2	61.4	62.5
14:23	8	0	0	0	0	109	0	0	0	0.08	61.1	62.7	62.4	61.5	58.2	61.4	62.5
14:25	10	0	0	0	0	109	0	0	0	0.08	61.1	62.7	62.4	61.5	58.2	61.4	62.5
							Average "b" =				67.6	69.4	69.1	68.1	64.4	67.9	69.1

Postfracture Extraction Date: 08/26/1992 Total Well/ Sealed Condition

Time	T	Vacuum ("H2O) at well location								Flow	Aperture (microns) at well location						
		MW1	MW2	MW3	MW4	MW5	MW6	MW7	FW	"Q"	FW	MW1	MW2	MW3	MW4	MW6	MW7
10:22	0	0	0	0	0	66	0	0	0	10.3							
10:24	2	43	43	46	48	74	47.5	34	41	8.5	442	464	462	472	458	480	423
10:26	4	54	53	56	57	84	56	46	50	7.25	416	445	438	447	428	446	408
10:28	6	62	60	62	63	86	60	52	56	6.5	417	463	449	455	436	441	409
10:30	8	66	64	66	67	88	64	56	58	6.5	420	477	461	469	450	454	418
10:32	10	68	65	68	68	88	65	57.5	61	6.25	429	487	462	478	452	454	419
							Average "b" =				425	467	454	464	445	455	415

Extraction Location: MW6

Prefracture Extraction Date: 08/17/1992 Total Well / Sealed Condition

Time	T	Vacuum ("H2O) at well location								Flow	Aperture (microns) at well location						
		MW1	MW2	MW3	MW4	MW5	MW6	MW7	FW	"Q"	FW	MW1	MW2	MW3	MW4	MW5	MW7
14:33	0	0	0	0	0	0	109	0	0	0.5							
14:35	2	0	0	0	0	0	109	0	11	0.5	108	108	110	110	108	112	112
14:37	4	0	0	0	0.5	0	108	0	20	1	141	136	138	139	136	141	141
14:39	6	0	0	1.75	0.7	0	108	0	25	0.5	115	108	110	111	108	112	112
14:41	8	0	0	3.25	0.75	0	108	0	29	0.5	116	108	110	112	108	112	112
14:43	10	0	0	4.5	0.75	0	108	0	29	0.5	117	108	110	112	108	112	112
							Average "b" =				119	113	116	117	114	118	118

Postfracture Extraction Date: 08/26/1992 Total Well/ Sealed Condition

Time	T	Vacuum ("H2O) at well location								Flow	Aperture (microns) at well location						
		MW1	MW2	MW3	MW4	MW5	MW6	MW7	FW	"Q"	FW	MW1	MW2	MW3	MW4	MW5	MW7
10:42	0	0	0	0	0	0	73	0	0	9.5							
10:44	2	56	55	57	58	52	83	48	53	9.5	442	476	479	494	489	471	453
10:46	4	71	72	74	71	62	91	61	71	7.75	472	494	512	534	494	450	446
10:48	6	79	79	80	76	65	86	68	76	5.5	539	629	641	678	558	449	475
10:50	8	76	76	75	72	61	84	67	71	5.5	487	601	612	592	524	435	485
10:52	10	75	75	74.5	71	60	83	65.5	71	5.5	500	601	612	603	524	435	480
							Average "b" =				488	560	571	580	518	448	468

Table C6
(Continued)

Extraction Location: MW7

Prefracture Extraction Date: 08/17/1992 Total Well / Sealed Condition

Time	T	Vacuum ("H2O) at well location								Flow	Aperture (microns) at well location						
		MW1	MW2	MW3	MW4	MW5	MW6	MW7	FW	"Q"	FW	MW1	MW2	MW3	MW4	MW5	MW6
14:33	0	0	0	0	0	0	0	107	0	0.13							
14:35	2	0	0	0	0	0	0	110	0	0.13	71	72	70	68	72	73	73
14:37	4	0	0	0	0	0	0	110	0	0.08	61	61	60	58	61	62	62
14:39	6	0	0	0	0	0	0	110	0	0.17	77	77	75	73	77	78	78
14:41	8	0	0	0	0	0	0	110	0	0.17	77	77	75	73	77	78	78
14:43	10	0	0	0	0	0	0	110	0	0.2	82	82	80	78	82	83	83
								Average "b" =			73	74	72	70	74	75	75

Postfracture Extraction Date: 08/26/1992 Total Well/ Sealed Condition

Time	T	Vacuum ("H2O) at well location								Flow	Aperture (microns) at well location						
		MW1	MW2	MW3	MW4	MW5	MW6	MW7	FW	"Q"	FW	MW1	MW2	MW3	MW4	MW5	MW6
10:42	0	0	0	0	0	0	0	98	0	2.5							
10:44	2	11	11	12	13	10	12	100	0	2.4	194	204	198	194	206	206	208
10:46	4	15	15	16	15	12.5	15	100	11	2.35	201	206	200	196	206	207	209
10:48	6	16.5	16.5	17.5	16.5	14	17	100	11	2.35	201	208	202	197	208	208	211
10:50	8	18	18	19	18	15	18	100	12	2.3	201	207	202	197	207	208	210
10:52	10	18	18	19	18	15	18	100	14	2.3	202	207	202	197	207	208	210
								Average "b" =			200	207	201	196	207	207	209

Table C7 Six "Equivalent" Fracture Aperture Calculation Summary
Hillsborough Test Site

Extraction Test	Fracture Aperture (microns) at Locations								Avg. "b"
	FW	MW1	MW2	MW3	MW4	MW5	MW6	MW7	
Prefracture									
FW-Base 1 (SW*)	38	36	36	39	37	38	42	37	
FW-Base 2 (SW)	52	49	49	52	51	51	57	51	
MW1 (SW)	41	41	40	42	43	44	41	43	
MW2 (SW)	48	47	48	47	50	51	50	49	
MW3 (SW)	37	39	37	38	39	40	39	37	
MW4 (SW)	57	60	60	59	58	57	58	61	
MW5 (SW)	37	38	38	37	35	35	37	38	
MW6 (SW)	66	62	64	64	63	65	64	65	
MW7 (SW) **	40	41	40	38	41	41	41	38	
FW (Passive) **	62	62	62	62	62	65	61	65	
Avg. "b"	**47**	**46**	**46**	**47**	**47**	**48**	**48**	**48**	_47_
Postfracture									
FW-Base 1 (SW*)	200	202	207	205	195	170	188	196	
FW-Base 2 (SW)	204	206	207	209	203	199	194	192	
MW1 (SW)	252	258	260	280	264	239	263	244	
MW2 (SW)	299	346	321	370	318	270	309	270	
MW3 (SW)	347	455	491	373	333	249	361	321	
MW4 (SW)	365	447	413	482	413	292	512	344	
MW5 (SW)	234	257	250	255	245	245	250	229	
MW6 (SW)	269	308	314	319	285	247	287	257	
MW7 (SW) **	110	114	111	108	114	114	115	108	
FW (Passive) **	424	426	426	426	426	447	417	447	
Avg. "b"	**271**	**310**	**308**	**312**	**282**	**239**	**295**	**257**	_284_

* SW = Sealed well condition

** Fracture aperture values estimated from these tests not included in the calculation of average fracture aperture

APPENDIX D

REYNOLDS NUMBER & AIR VELOCITY PLOTS
Hillsborough Test Site

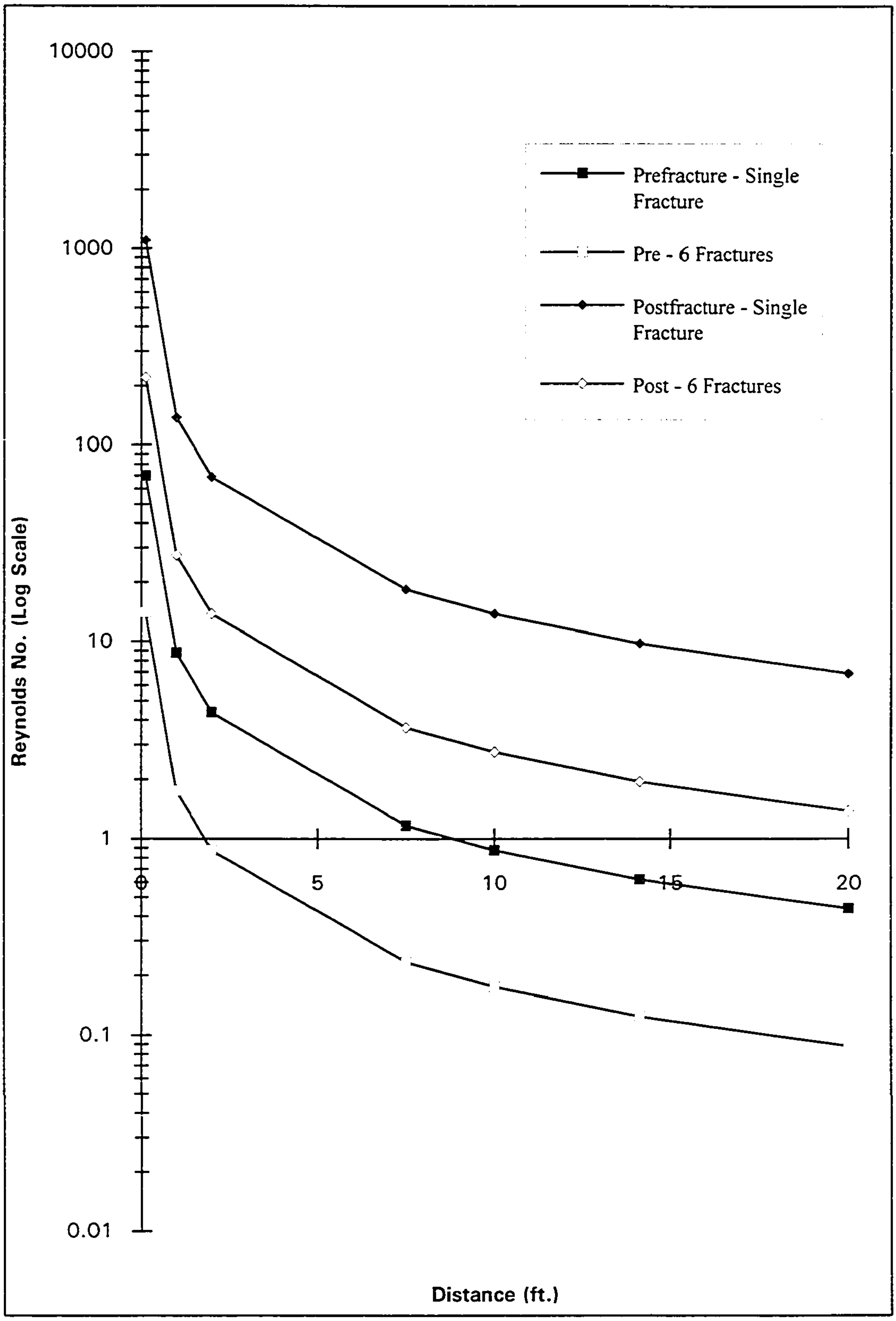

Figure D1 Reynolds number vs. radial distance (FW, Sealed, Base-2), H.T.S.

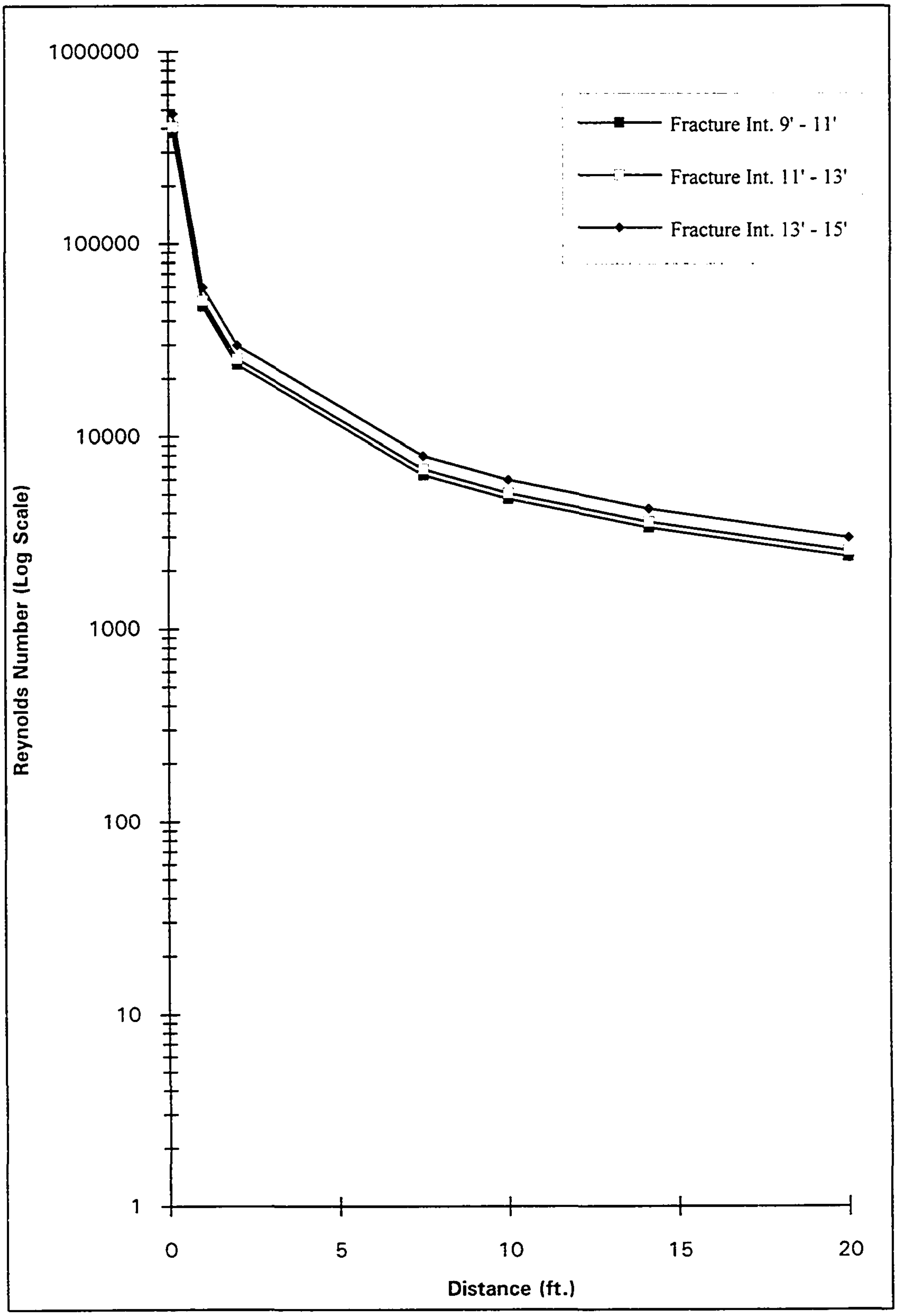

Figure D2 Reynolds number vs. radial distance (fracture injection), H.T.S.

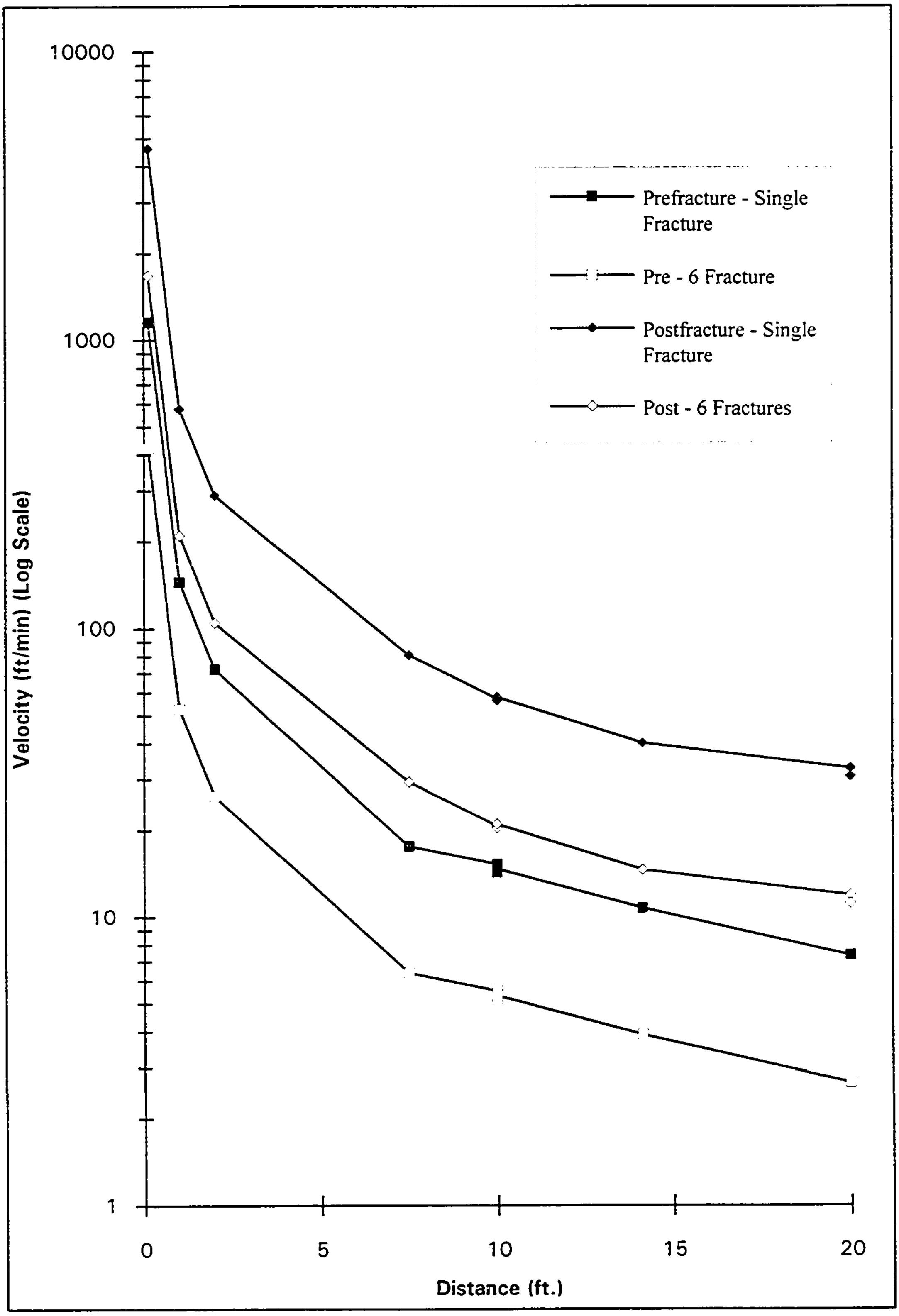

Figure D3 Air velocity vs. radial distance (FW, Sealed, Base-2), H.T.S.

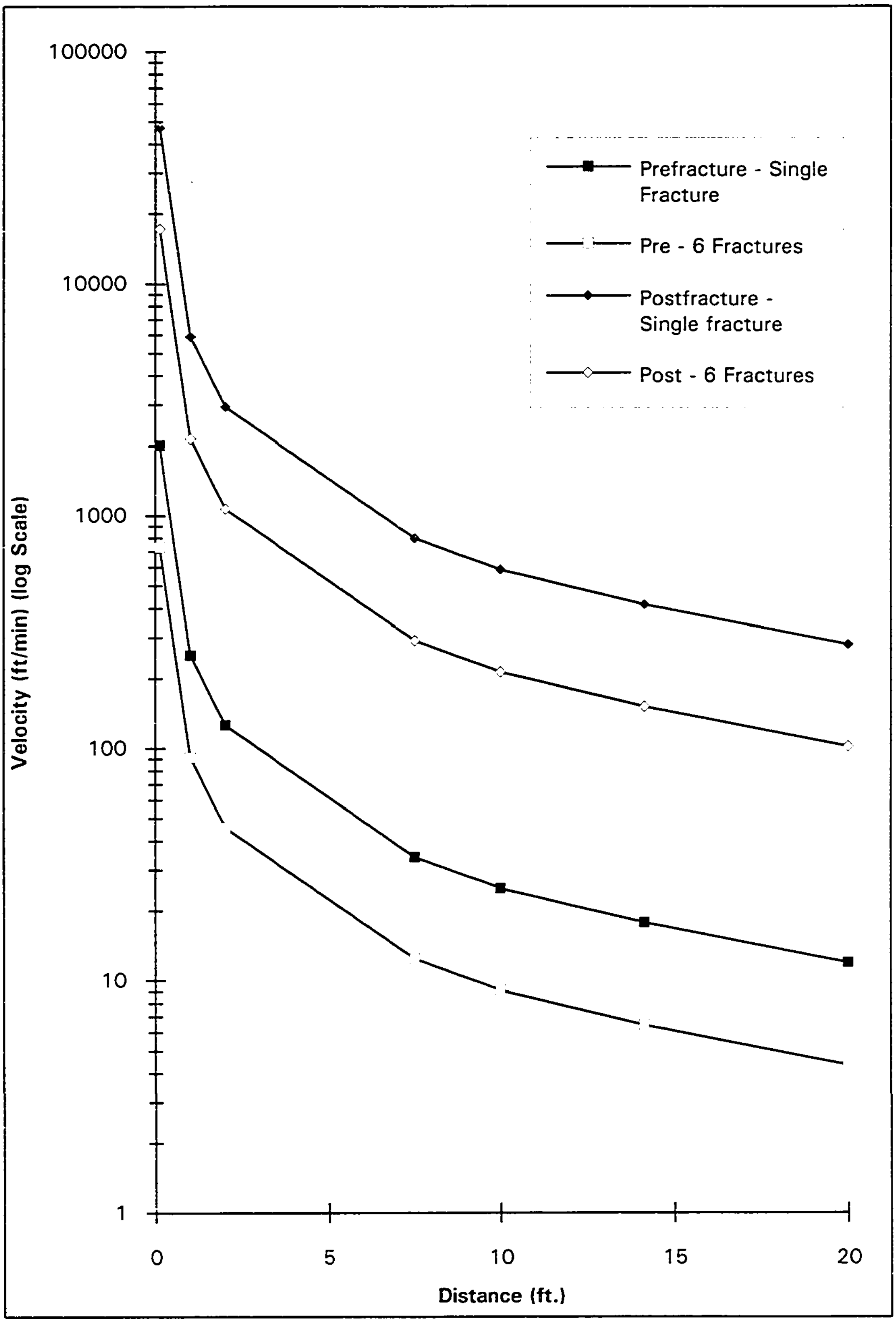

Figure D4 Air velocity vs. radial distance (FW, passive inlet), H.T.S.

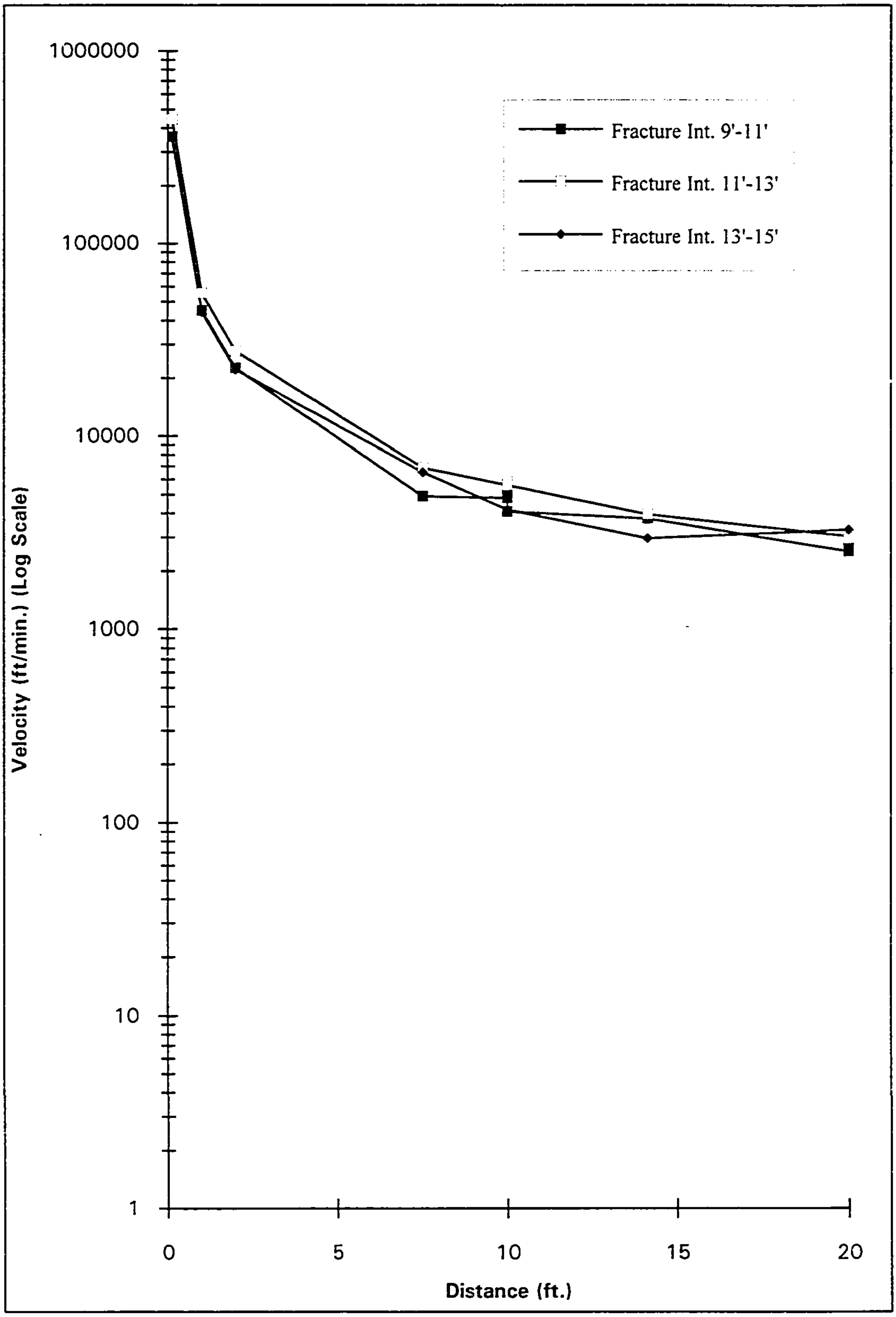

Figure D5 Air velocity vs. radial distance (fracture injection), H.T.S.

APPENDIX E

BOREHOLE VIDEO ANALYSIS RESULTS
Hillsborough Test Site

Table E1 Summary of Borehole Video Analysis Results

Table E1 Summary of Borehole Video Analysis Results

Hillsborough Test Site

Analyzed Borehole: FW

Pre-Fracture Flow

Assuming Fractures are 100% Continous

Borhole Interval	Interval Flow Contribution (*Q)	% Flow	Flow Base-1 (ACFM)	Flow Base-2 (ACFM)	Flow (passive inlet) (ACFM)
8' - 9'	202.6	9.98	0.0140	0.0300	0.0419
9' - 10'	54.65	2.69	0.0038	0.0081	0.0113
10' - 11'	431.35	21.26	0.0298	0.0638	0.0893
11' - 12'	101.3	4.99	0.0070	0.0150	0.0210
12' - 13'	379.7	18.71	0.0262	0.0561	0.0786
13' - 14'	754.4	37.18	0.0520	0.1115	0.1561
14' - 15'	51.65	2.55	0.0036	0.0076	0.0107
15' - 16'	51.65	2.55	0.0036	0.0076	0.0107
16' - 17'	2	0.10	0.0001	0.0003	0.0004
	2029.3				

Standard deviation for prefracture % flow = 12.43

Post-Fracture Flow

Assuming Fractures are 100% Continous

Borhole Interval	Interval Flow Contribution (*Q)	% Flow	Flow (Base-1) (ACFM)	Flow (Base-2) (ACFM)	Flow (passive inlet) (ACFM)
8' - 9'	253.25	6.20	0.2380	0.2721	6.88
9' - 10'	354.55	8.68	0.3333	0.3810	9.63
10' - 11'	808.05	19.78	0.7595	0.8683	21.94
11' - 12'	151.95	3.72	0.1428	0.1633	4.13
12' - 13'	479	11.73	0.4502	0.5147	13.01
13' - 14'	1130.1	27.66	1.0623	1.2144	30.68
14' - 15'	478	11.70	0.4493	0.5137	12.98
15' - 16'	428.35	10.49	0.4026	0.4603	11.63
16' - 17'	2	0.05	0.0019	0.0021	0.05
	4085.25				

Standard deviation for postfracture % flow = 7.74

REFERENCES

Baehr, A.L., and M.F. Hult, "Evaluation of unsaturated zone air permeability through pneumatic tests," *Water Resour. Res.*, **27**(10), 2605-2617, 1991.

Bandis, S.C., N.R. Barton, and M. Christianson, "Application of a new numerical model of joint behavior to rock mechanics problems," *Proc. Int. Symp. on Fundamentals of Rock Joints*, Bjorkliden, 1985.

Barton, N.R., "Review of new shear strength criterion for rock joints," *Engineering Geol.*, 8, 287-332, 1973.

Bianchi, L. and D.T. Snow, "Permeability of crystalline rock interpreted from measured orientations and apertures of fractures," *Annals of the Arid Zone*, 8(2), 231-245, 1968.

Darcy, H.P.G., *Les Fountaines de la Ville de Dvon*, Victor Dalmont, Paris, 1856.

Fitzgerald, C.D., "Integration of Pneumatic Fracturing to Enhance In Situ Bioremediation," M.S. Thesis, Department of Civil and Environmental Engineering, New Jersey Institute of Technology, Newark, NJ, 1993.

Gale, J.E. and K.G. Raven, "Effect of sample size on stress-permeability relationship for natural fractures," Technical Information Report No. 48, LBL-11865, SAC-48, UC-70, 1980.

Gale, J.E., "Assessing the permeability haracteristics of ractured rock," *Geological Society of America*, Special Paper 189, 1982.

Gidley, J.L., S.A. Holditch, D.E. Nierdoe, and R.W. Veatch, *Recent Advances in Hydraulic Fracturing*, SPE, Richardson, TX, 1989.

Harr, M.E., *Groundwater and Seepage*, McGraw-Hill Book Company, 1962.

Howard, G.C. and C.R. Fast, *Hydraulic Fracturing*, Monograph Series, SPE, Richardson, TX, 1970.

Hubbert, M.K. and G. Willis, "Mechanics of hydraulic fracturing," *Trans. AIME*, Vol. 210, 1957: 153-166.

Huitt, J.L., "Fluid flow in simulated fractures," *AIChE J.*, 2,259,1956.

REFERENCES
(Continued)

Johnson, P.C., C.C. Stanely, M.W. Kemblowski, D.L. Byers, and J.D. Colhart, "A practical approach to the design, operation, and monitoring of in situ soil-venting systems," *Ground Water Monit. Rev.*, 10(2), 159-178, 1990.

King, T.C., "Mechanism of Pneumatic Fracturing," M.S. Thesis, Department of Civil and Environmental Engineering, New Jersey Institute of Technology, Newark, NJ, 1992.

Klinkenberg, L.J., "The permeability of porous media to liquids and gases," in *Drilling and Production Practice*, pp. 200-213, American Petroleum Institute, Washington, D.C., 1941.

Lamb, H., *Hydrodynamics* Cambridge University Press, New York, 1945.

Langfelder, L.J., C.F. Chen, and J.A. Justice, "Air permeability of compacted cohesive soils," *Journal of the Soil Mechanics and Foundations Division*, ASCE, No. SM4, July 1968, pp. 981-1001.

Lomize, G.M., *Fluid Flow in Fractured Rocks* (in Russian), Gosenergoizdat, Moscow , 1951.

Louis, C.A., "A study of groundwater flow in jointed rock and its influence on the stability of rock mases," *Rock Mechanics* Research report No. 10, Imperial College, London, 1969.

Louis, C.A., "Rock hydraulics," in *Rock Mechanics* (ed. L. Muller), Springer Verlag, Vienna, 1974, pp. 299-382.

Maini, Y.N.T, "In Situ Hydraulic Parameters in Jointed Rock - Their Measurement and Interpretation," [Ph.D. Dissertation] : Imperial College, University of London, 1971, 136 p.

Massmann, J.W., "Applying groundwater flow models in vapor extraction system design," *J. Environ. Eng.*, 115(1), 129-149, 1989.

McWhorter, D.B., "Unsteady radial flow of gas in the vadose zone," *J. Contam. Hydrol.*, 5, 297-314, 1990.

REFERENCES
(Continued)

Mises, R.V., *Elemente der Technischen Hydrodynamik*, S.G. Teuber, Leipzig, 1914

Muskat, M., *The Flow of Homogeneous Fluids Through Porous Media*, J.W. Edwards, Inc., Ann Arbor, Michigan, 1946

Ng. N., "Enhancement of Air Flow and Contaminant Removal in Fractured Soil," M.S. Project, Department of Civil and Environmental Engineering, New Jersey Institute of Technology, Newark, NJ, 1991.

Nikurdase, J., "Forsch. gebiete ingenieurw forschungsheft," (Sept.-Oct., (1932); reprinted in *Petroleum Eng.*, No. 6,164; No. 8,75; No.11,38; No.12,83 (1940)

Papanicolaou, P., "Laboratory Model Studies of Pneumatic Fracturing of Soils to Remove Volatile Organic Compounds," M.S. Thesis, Department of Civil and Environmental Engineering, New Jersey Institute of Technology, Newark, NJ, 1989.

Schuring, J., V. Jurka,and P. Chan, "Pneumatic fracturing of a clay formation to enhance removal of VOC's," Proceedings Fourteenth Annual Madison Waste Conference, Univ. of Wisconsin-Madison, September 1991.

Schuring, J. and P. Chan, "Removal of contaminants from the vadose zone by pneumatic fracturing," U.S. Geological Survey, Dept. of Interior, U.S.G.S. Award 14-08-0001-G1739, January 1992.

Shah, N.P., "Study of Pneumatic Fracturing to Enhance Vapor Extraction of the Vadose Zone," M.S. Thesis, Department of Civil and Environmental Engineering, New Jersey Institute of Technology, Newark, NJ,1991.

Sharp, J.S., and Y.N.T. Maini, "Fundamental consideration on the hydraulic characteristics of joints in rock," *Proc. Symp. on Percolation Through Fissured Rock*, Int. Soc. for Rock mech. and Int. Assoc. of Eng. Geology, T1-F, 1972.

Snow, D.T., "A Parallel Plate Model of Permeable Fractured Media," Ph.D. Thesis, University of California, Berkeley, 1965.

Snow, D.T. (1968), "Rock fractures spacings, openings and porosities," *J. Soil Mech. Found. Div.*, ASCE, 94 (SM1), 73-91.

REFERENCES
(Continued)

Snow, D.T., "Anisotropic permeability of fractured media," *Wat. Resour. Res.* 5, 1969, pp. 1273-1289.

Stokes, G.G., 1898, "Mathematical proof of the identity of the stream lines obtained by means of a viscous film with those of a perfect fluid moving in two dimensions," *Report of the British Association*, 1989, pp. 143-147

Streltsova-Adams, T.D., "Fluid flow in naturally fractured reservoirs," in Proceedings, Second Invitational Well Testing Symposium, Berkely, California : Berkely, Lawrence Berkely laboratory, LBL-8883, October 25-27, 1978.

Sullivan, R.R., and K.L. Hertel, "The flow of air through porous media," *Journal of Applied Physics*, Vol. 11, 761-765, 1940.

Sutera, S.P., and R. Skalak, "The history of Poiseuille's law," *Annu. Rev. Fluid Mech.*, 1993, 25: 1-19.

Tsang, Y.W. and P.A. Witherspoon, "The dependence of fracture mechanical and fluid flow properties on fracture roughness and sample size," *J. Geophys. Res.*, 88(B3), 1983, pp. 2359-66.

Wilson, C.R., and P.A. Witherspoon, "An investigation of laminar flow in fractured porous rocks," Berkely, University of California, Department of Civil Engineering, Pub. 70-6, 1970.

Wilson, C.R., and P.A. Witherspoon, "Steady state flow in rigid networks of fractures," *Water Resour. Res.*, **10**(2):328-335, 1985.

Witherspoon, P.A., J.S.Y. Wang, K. Iwai, and J.E. Gale, "Validity of cubic law for fluid flow in a deformable rock fracture," *Water Resour. Res.*, **16**(6), 1980, pp. 1016-24.

Ziegler, T.W., "Determination of rock mass permeability," Technical Report S-76-2, US Army Corps of Engineer, Waterway Experiment Station, Vicksburg. MS, 1976.